APPENDIX I

Fig. A

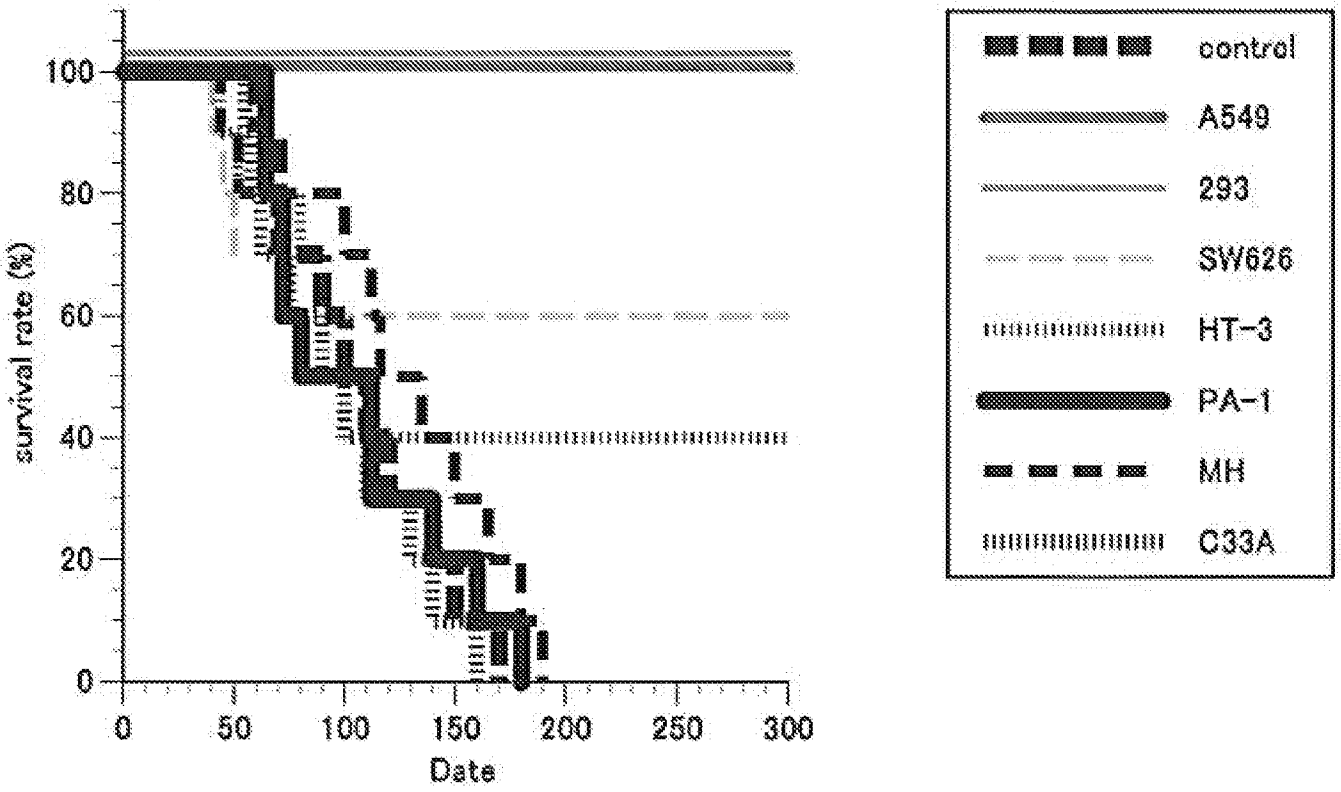
100
80
60
40
20
0
survival rate (%)
0
50
100
150
200
250
300
Date
control
A549
293
SW626
HT-3
PA-1
MH
C33A

APPENDIX II

Use of Carrier Cells to Deliver a Replication-selective Herpes Simplex Virus-1 Mutant for the Intraperitoneal Therapy of Epithelial Ovarian Cancer[1]

George Coukos, Antonis Makrigiannakis, Eugene H. Kang, David Caparelli, Ivor Benjamin, Larry R. Kaiser, Stephen C. Rubin, Steven M. Albelda, and Katherine L. Molnar-Kimber[2]

Divisions of Gynecologic Oncology [G. C., I. B., S. C. R.] and Reproductive Biology [A. M.], Department of Obstetrics and Gynecology; Division of Pulmonary Medicine/Critical Care, Department of Medicine [S. M. A.]; and the Thoracic Oncology Laboratory, Department of Surgery [E. H. K., D. C., L. R. K., K. L. M-K.], University of Pennsylvania Medical Center, Philadelphia, Pennsylvania 19104

ABSTRACT

Epithelial ovarian cancer (EOC) remains localized within the peritoneal cavity in a large number of patients, lending itself to i.p. approaches of therapy. In the present study, we investigated the effect of replication-selective herpes simplex virus-1 (HSV-1) used as an oncolytic agent against EOC and the use of human teratocarcinoma PA-1 as carrier cells for i.p. therapy. HSV-1716, a replication-competent attenuated strain lacking ICP34.5, caused a direct dose-dependent oncolytic effect on EOC cells *in vitro*. A single i.p. administration of 5×10^6 plaque-forming units resulted in a significant reduction of tumor volume and tumor spread and an increase in survival in a mouse xenograft model. PA-1 cells supported HSV replication *in vitro* and bound preferentially to human ovarian carcinoma surfaces compared with mesothelial surfaces *in vitro* and *in vivo*. In comparison with the administration of HSV-1716 alone, irradiated PA-1 cells, infected at two multiplicities of infection with HSV-1716 and injected i.p. at 5×10^6 cells/animal, led to a significant tumor reduction in the two models tested and the significant prolongation of mean survival in one model. Histological evaluation revealed extensive necrosis in tumor areas infected by HSV-1716. Immunohistochemistry against HSV-1 revealed areas of viral infection within tumor nodules, which persisted for several weeks after treatment. Administration of HSV-infected PA-1 carrier cells resulted in larger areas of tumor infected by the virus. Our results indicate that replication-competent attenuated HSV-1 exerts a potent oncolytic effect on EOC, which may be further enhanced by the utilization of a delivery system with carrier cells, based on amplification of the viral load and possibly on preferential binding of carrier cells to tumor surfaces.

INTRODUCTION

Despite the aggressive surgical approaches and combination chemotherapeutic regimens implemented over the past 2 decades, EOC[3] still remains a disease with a grim prognosis. Recent statistics indicate that 25,000 new patients with EOC are diagnosed yearly in the United States; 15,000 deaths occur from this disease yearly (1). Unfortunately, because of the lack of symptoms, the majority of patients are diagnosed at a late stage (2). In addition, although 70% of the patients initially respond to cisplatin-based chemotherapy, the majority of them relapse and develop chemotherapy-resistant disease (3). As a result, the overall 5-year survival is approximately 20% for advanced-stage disease. New therapeutic approaches are, therefore, warranted.

EOC remains localized within the peritoneal cavity in a large proportion of patients, ultimately causing local morbidity and lethal complications (4). Because of its localized nature, EOC lends itself to i.p. approaches of therapy. One such approach is gene therapy. Gene therapy using the HSV*tk* suicide gene followed by ganciclovir (5, 6) or targeting tumor suppressor genes and oncogenes (7, 8) has been tested on experimental ovarian cancer *in vitro* and *in vivo*. Sufficient encouraging preclinical results have been obtained to justify initiation of clinical Phase I trials (9, 10). However, results from a recent clinical trial using a HSV*tk*-carrying adenoviral vector applied to mesothelioma localized in the pleural space indicate that gene delivery is restricted to a few superficial cell layers, and treatment of larger three-dimensional tumors may still be inadequate (11).

Replication-competent viral agents may provide a feasible alternative for cancer therapy. Recombinant attenuated forms of HSV-1 represent one family of such agents, which are replication-restricted (12–17). HSV-1 mutants have been generated

Received 11/9/98; revised 2/25/99; accepted 2/26/99.

The costs of publication of this article were defrayed in part by the payment of page charges. This article must therefore be hereby marked *advertisement* in accordance with 18 U.S.C. Section 1734 solely to indicate this fact.

[1] This study was supported by Grant PO-66726-S1 from National Cancer Institute (to S. M. A. and K. L. M-K.), the Samuel H. Lunenfeld Charitable Foundation (to L. R. K.), and the A. Onassis Foundation (to A. M.).

[2] To whom requests for reprints should be addressed, at Department of Surgery, University of Pennsylvania, 351 Stemmler Hall, 36th and Hamilton Walk, Philadelphia, PA 19104-6070. Phone: (215) 662-7898; Fax: (215) 573-2001; E-mail: molnark@mail.med.upenn.edu.

[3] The abbreviations used are: EOC, epithelial ovarian cancer; pfu, plaque-forming unit(s); MOI, multiplicities of infection; HSV, herpes simplex virus; HSV*tk*, HSV-1 thymidine kinase; CNS, central nervous system; SCID, severe combined immunodeficient; CPE, cytopathic effect; FCS, fetal calf-serum; PCR, polymerase chain reaction; OR, odds ratio.

that harbor alterations in genes such as *thymidine kinase* (*tk*) or *ribonucleotide reductase* (*RR*), exhibiting decreased viral replication in nondividing neuronal cells (13, 17–20). The specificity of the RR^- mutants has been shown to be up to 1000-fold higher for malignant rodent cells than endogenous neural cells (21). Another series of HSV-1 mutants has been produced by alterations in both copies of the *RL1* gene, a diploid fragment of the HSV-1 genome (12, 16, 19, 22, 23). Its product, the ICP34.5 protein, has been implicated in neurovirulence (24–26) and is responsible for preventing apoptosis related to premature shutoff of protein synthesis in the infected host cells (27). ICP34.5-null HSV-1 mutants have been shown to replicate preferentially in tumor cells, causing a direct oncolytic effect but appear to spare normal differentiated tissues (28, 29). These strains have been successfully used to reduce or cure tumors of the CNS in experimental models (12, 13, 15–23, 30, 31).

Previous studies in our laboratories (32) demonstrated the efficacy of HSV-1716, an ICP34.5-null mutant, in reducing tumor burden and conferring survival advantage in an i.p. model of malignant mesothelioma in the SCID mouse. Moreover, these studies suggested that extra-CNS administration of replication-restricted HSV-1 might be safe. HSV-1716 administered i.p. to SCID mice was found to be completely avirulent (32). In fact, there was no viral spread outside the tumors, as was documented by immnunohistochemistry and PCR analysis of multiple murine tissues, including i.p. and retroperitoneal organs as well as distant organs and the brain. This was not true for wild-type HSV-1, to which SCID mice were found to be extremely sensitive. In fact, i.p. administration of wild-type HSV-1 to SCID mice led to rapid systemic spread of the virus and death of the animals within 1 week (32). Further supporting the safety of HSV-1 mutants, the administration of HSV-1716 to normal human skin in a murine xenograft model was accompanied by no toxicity, whereas administration of a wild-type HSV-1 led to rapid destruction of the xenograft (28). Application of replication-restricted HSV-1 for extra-CNS malignancies was recently extended to other tumors; a RNase reductase-deleted mutant was used in an experimental animal model of metastatic colorectal carcinoma in the liver (33), and a replication-restricted ICP34.5 mutant was used to treat experimental metastatic and s.c. melanoma (23, 34). Moreover, a multiattenuated mutant, HSV-G207, was efficacious in the treatment of breast cancer (35).

In the present study, we sought to define the applicability of HSV-1716 in the treatment of human EOC *in vivo*. Moreover, we investigated the suitability of PA-1 human teratocarcinoma cells as a carrier system for the delivery of HSV-1716 *in vivo*. We report that attenuated HSV-1716 exerts a potent oncolytic effect on EOC, which may be enhanced by the utilization of a carrier cell line for the *in vivo* administration of replication-restricted HSV-1.

MATERIALS AND METHODS

Virus. HSV-1716 was originally isolated in the laboratory of S. M. Brown (Glasgow University, United Kingdom; Ref. 24). The genome of this virus contains a 759-bp deletion located within each copy of the *Bam*HI fragment of the long repeat region of the genome. These deletions remove most of the gene encoding ICP34.5, and the mutant fails to make the protein. The virus used in this study was passed in our laboratory, as originally described (24, 32).

Cells. EOC cell lines SKOV3, NIH:OVCAR3, CaOV3, and human ovarian teratocarcinoma line PA-1 (36) were obtained from the American Type Culture Collection (Manassas, VA). The A2780 EOC line was a kind gift of Dr. Tom Hamilton (Fox Chase Cancer Center, Philadelphia, PA). Primary ovarian cultures were obtained from patients with advanced EOC stage III or IV, according to the criteria set by the International Federation of Gynecologists and Obstetricians (FIGO) (4). Malignant effusions, obtained at the time of exploratory laparotomy or diagnostic/therapeutic paracentesis, were centrifuged at $300 \times g$ for 10 min at room temperature, and the cell pellets were collected and seeded in standard tissue culture media (see below). These cells assumed an epithelial phenotype, and their malignant nature was confirmed by a rapid doubling time (average, 18 h) and their immortalized behavior *in vitro*. EOC cells were passaged 4–5 times before using them in experiments. Normal peritoneal mesothelial cells were obtained from intraoperative pelvic peritoneal lavages carried out with normal saline in patients undergoing laparotomy for benign pelvic pathology (pelvic relaxation, uterine myomata). Lavage fluids were centrifuged at $300 \times g$ for 10 min at room temperature, and the cell pellets were collected and seeded in standard media (see below). These cells assumed an epithelial-like phenotype and grew in a cobblestone pattern. Their doubling time was longer than that of primary EOC cultures (average, 36 h) and their nonmalignant nature was confirmed by the fact that they propagated for only a few (4–5) passages even in the presence of growth factors. To eliminate macrophages from primary cultures, culture media were aspirated 30 min after plating, and suspended cells were reseeded in new culture flasks. All of the cell lines and EOC primary isolates were cultured under standard conditions (37°C in a 5% CO_2 atmosphere) and media of RPMI 1640 with 10% heat-inactivated FCS and antibiotics. For normal mesothelial cells, media were supplemented with a mixture of growth factors (SerXtend, Irvine Scientific, Santa Anna, CA) at 0.1% dilution. Institutional Review Board approval had been obtained for the retrieval and utilization of primary cultures.

Assessment of Cytotoxicity *in Vitro*. Cells were plated at a density of 3×10^3 cells/well in 96-well plates and incubated with HSV-1716 at 0.1 and 1 MOI in serum-free media for one h. Serum-enriched media were added subsequently and cultures were followed for 4 days. Cell proliferation assays were performed using a chromogenic kit (CellTiter AQueous96, Promega, Madison, WI) and colorimetric assays were carried out in a microplate ELISA reader (Bio-Tek Instruments, Winooski, VT). CPEs were documented by phase microscopy.

Flow Cytometry Analysis of HSV Antigens. PA-1 cells were cultured in T25 flasks until they reached 60% confluence. They were then infected with 0.5–2.5 MOI of HSV-1716, as above. Cells were harvested at 16 h with a 0.05% trypsin solution, washed once with PBS, and fixed/permeabilized with 70% methanol at -20°C for 20 min. A polyclonal antibody against HSV-1 proteins (American Qualex, La Mirada, CA) was used at a dilution of 1:250, and a secondary antirabbit FITC (FITC)-conjugated antibody (Jackson Immunoresearch Labora-

tories Inc., West Grove, PA) was used at a dilution of 1:250. Flow cytometry analysis was performed using an EPICS XL flow cytometer (Coulter Corporation, Hialeah, FL).

One-Step Growth Curves. PA-1 teratocarcinoma cells were plated in 6-well plates at a density of 4×10^5 cells/well under standard conditions overnight and subsequently infected with HSV-1716 at 0.3 MOI. In parallel experiments, PA-1 cells were subjected to a single 2000-cGy dose of ionizing radiation 1 h before exposure to HSV-1716. Cells were harvested in their media by mechanical scraping 1 h after exposure to the virus (0 h) as well as 6, 20, 24, and 48 h later and stored at −80°C. One-step growth curves were carried out as described previously (32).

***In Vivo* Adhesion Assays.** PA-1 teratocarcinoma cells were labeled with a rhodamine fluorescent dye (PKH26 Red Fluorescent Cell Linker Kit, Sigma, St. Louis, MO) as recommended by the manufacturer. Briefly, cells were harvested with a 0.05% trypsin solution, resuspended in PBS and incubated with the dye at 1:250 dilution for 8 min. The reaction was interrupted with the addition of 100% FCS. Cells were then washed, suspended in RPMI containing 10% FCS, and injected i.p. (5×10^6 cells/animal) into SCID mice bearing i.p. SKOV3 tumor (see below). Eight h later, animals were sacrificed, the parietal peritoneum was entirely dissected, and four specimens were prepared containing almost entirely the four different segments of the parietal peritoneum (diaphragmatic, ventral, lateral left, and lateral right). In addition, random biopsies were obtained from the mesentery and the visceral peritoneum. Six-μm sections were prepared, mounted in Fluoromount medium (Fisher, Pittsburgh, PA) containing 2.5% 1,4-diazabicyclo-(2,2,2)octane (DABCO, Polyscience, Warrington, PA), to prevent quenching, and examined under a Zeiss microscope.

For quantitative analysis of *in vivo* adhesion, 20 random fields/slide (×40) were inspected on five slides cut 18 μm apart from each other from the four different segments of the parietal peritoneum and from two sections of mesenteric areas. Fields were selected in such a way to contain only tumor surface or only tumor-free normal peritoneum. The number of fields containing SKOV3 tumor with or without adhering fluorescent PA-1 cells and those containing normal peritoneum with or without adhering fluorescent PA-1 cells were counted. This experiment was repeated twice.

***In Vitro* Adhesion Assays.** Normal peritoneal mesothelial cells, PA-1 teratocarcinoma cells, and EOC SKOV3, CaOV3, NIH:OVCAR3, and A2780 cells were plated in 48-well plates at a density of $3–4 \times 10^4$ cells/well and allowed to form 100% confluent monolayers. Teratocarcinoma PA-1 cells cultured in T25 flasks were starved with methionine-free media for 2 h and subsequently incubated with [^{35}S]methionine media (50 μCi/ml) containing 1% dialyzed FCS overnight. Radiolabeled PA-1 cells were harvested by short exposure to 0.05% trypsin solution, washed with serum-free media once, centrifuged at $300 \times g$ for 5 min at room temperature, and resuspended in media containing 1% FCS. PA-1 cells were then seeded at 5×10^3/well on the different monolayers and allowed to interact with adherent mesothelial or ovarian cancer cells for 30 min. Subsequently, cells were washed three times with PBS to remove nonadherent cells. Adherent cells were harvested with 0.1% trypsin solution, transferred to scintillation vials and counted in a scintillation counter (LS 6500, Beckman Instruments, Fullerton, CA). In separate experiments, PA-1 teratocarcinoma cells were radiolabeled with [^{35}S]methionine, as described above, and subsequently subjected to ionizing radiation (2000 cGy) and/or infection with HSV-1716 (2 MOI). Cells subjected to different treatments were subsequently plated on the different monolayer substrates, as described above. Adhesion was measured as described above.

***In Vivo* Xenograft Model of EOC.** Six-to-eight-week-old female CB17 SCID mice (Charles River, Wilmington, MA) were housed in an isolation unit at the Wistar Institute (Philadelphia, PA). Animals were cared for according to protocols approved by the Animal Use Committees of the Wistar Institute and the University of Pennsylvania, in compliance with the Guide for the Care and Use of Laboratory Animals (NIH 85–23, revised 1985). A2780 and SKOV3 cells were cultured under standard conditions until they reached confluence of 70%, were harvested with 0.05% trypsin solution, were washed with serum-enriched media, and centrifuged at $300 \times g$ for 5 min at 4°C. Cells were injected i.p. (SKOV3, 5×10^6 cells/animal; A2780, 1×10^6 cells/animal) in 0.5 ml of RPMI containing 10% FCS and 1% SerXtend® (Irvine Scientific). Five mice were killed at selected times to confirm the presence of i.p. tumors before administering treatment in each experiment. At the end of the experiments, animals were killed, and i.p. tumors were assessed for spread and volume. A semiquantitative scoring system was devised to grade tumor spread. Five areas were screened for the presence of tumor: (*a*) the injection site; (*b*) the parietal peritoneum and diaphragm; (*c*) the small bowel mesentery and omentum; (*d*) the lesser omentum and hepatic hilum; and (*e*) the retroperitoneum. Each site received a score of 0–3 as follows:

(*a*) 0, if no microscopic tumor was seen;

(*b*) 1, if microscopic tumor was visible with the aid of a dissecting microscope at ×2.5;

(*c*) 2, if tumor nodules less than 5 mm were visible; and

(d) 3, if tumor nodules equal to or more than 5 mm were present.

Moreover, the presence of ascites added one additional point in the scoring system. Thus, the maximum score accumulated in this scale was 16. Subsequently, all of the visible nodules of the tumor were dissected from surrounding normal peritoneum and viscera, and total intra-abdominal tumor was weighed for each animal individually.

Utilization of PA-1 Teratocarcinoma Cells as HSV-1716 Carrier Cells. PA-1 human teratocarcinoma cells were exposed to ionizing radiation at a single dose of 2000 cGy and then infected with HSV-1716 at 2 MOI. Two h after infection, cells were washed with PBS and harvested with 0.05% trypsin solution. Cells were then washed twice in media containing 10% heat-inactivated FCS, centrifuged at $300 \times g$ for 5 min, and resuspended in RPMI containing 1% heat-inactivated FCS. Five $\times 10^6$ cells were injected i.p. into tumor-bearing animals. Control tumor-bearing animals received PA-1 teratocarcinoma cells that had been previously exposed to the same amount of radiation but not infected with HSV-1716. To confirm the lack of tumorigenicity of irradiated PA-1 cells, non- tumor-bearing mice received a flank ($n = 10$) or an i.p. administration ($n = 10$)

of 5×10^6 irradiated PA-1 cells and were followed for 16 weeks.

Application of HSV-1716 *in Vivo*. At selected times, animals received a single i.p. dose of HSV-1716 at 5×10^6 pfu in 500 μl of serum-free RPMI, a dose found effective in our previous studies with mesothelioma (32). Control animals received a similar volume of media. A separate group of animals received an i.p. injection of 5×10^6 irradiated PA-1 teratocarcinoma cells infected with HSV-1716 at 2 MOI as described above, and a second control group received irradiated noninfected PA-1 cells. Animals were killed at selected times, and i.p. tumors were assessed in the different groups. For survival experiments, animals were injected with tumor and treated as above. Animals were followed daily and were removed from the cages if found dead, or were killed if they seemed severely ill. Tumor weight was estimated in killed animals as described above. Survival experiments were repeated twice for each EOC cell line. Kaplan-Meier survival curves were computed using the StatView computer program.

Histology and Immunohistochemistry. Tumors obtained from treated and control animals were immediately fixed in formalin (3.7% formaldehyde-PBS) and subsequently embedded in paraffin. Six-μm-thick sections were deparaffinized and stained with H&E. For immunohistochemistry, slides were subjected to antigen retrieval at 105°C for 10 min in 0.1 N citric acid and incubated with a monoclonal antibody against HSV-1 (DAKO, Carpenteria, CA) at a dilution of 1:4 for 30 min at 47°C. A horseradish peroxidase-conjugated antimouse antibody (Vectastain, Vector Laboratories, Burlingane, CA) was used at a dilution of 1:400. Slides were then processed according to the manufacturer's instruction using the ABC kit (Vector Laboratories). A mouse preimmune serum was used at a dilution of 1:4 as a negative control (DAKO).

Statistical Analysis. Differences in values obtained during *in vitro* adhesion assays and differences in tumor weights in the animal experiments were determined with one-way ANOVA. *Post-hoc* comparisons of specific paired groups were done with the *t* test. The differences in the *in vivo* adhesion assays were computed with the χ^2 test for 2×2 contingency tables. ORs were computed with the formula $OR = a \times d/b \times c$ from the 2×2 contingency tables. Survival curves were analyzed with the Mantel-Cox log-rank test. Statistical significance was set at $P < 0.05$. Results are expressed as the mean ± SE.

RESULTS

HSV-1716 Exerts an Oncolytic Effect on EOC *in Vitro*. To assess the oncolytic effect of HSV-1716 on EOC *in vitro*, primary EOC cultures and established EOC cell lines were exposed to HSV-1716 at 0.1 and 1 MOI. Cell survival was assessed by proliferation colorimetric assays and evaluation of CPEs under phase microscopy. HSV-1716 exerted a direct dose-dependent cytolytic effect on all of the EOC cell lines and on human teratocarcinoma PA-1 cell line (Fig. 1). Primary EOC cultures obtained from patients with advanced disease displayed 10- to 20-fold higher sensitivity compared with established EOC cell lines. A2780 appeared to be the most sensitive EOC cell line, and SKOV3 was the least sensitive. Moreover, teratocarcinoma PA-1 cells displayed a remarkable sensitivity, which

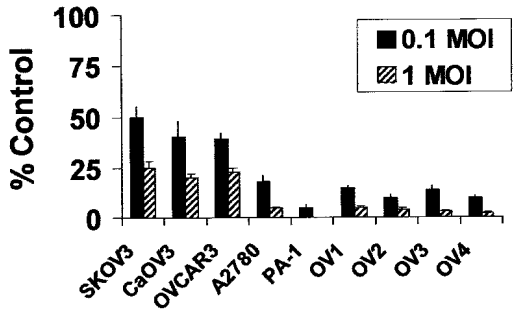

Fig. 1 *In vitro* cytolytic effect of HSV-1716 on established EOC cell lines, human teratocarcinoma line PA-1, and primary epithelial ovarian cultures (*OV1*, *OV2*, *OV3*, and *OV4*). The effect of HSV-1716 was assessed by a colorimetric proliferation assay performed 4 days after exposure to the virus. Values are expressed as a percentage of noninfected control cells. A clear dose-dependent cytotoxic effect is noted. Data represent the results of three experiments and are expressed in mean ± SE. *Black columns*, 0.1 MOI; *striped columns*, 1 MOI.

was comparable to primary EOC cultures. The above results were also confirmed by phase microscopy: 100% of primary EOC cells, A2780 cells and teratocarcinoma PA-1 cells displayed CPEs within 24–48 h at 1 MOI, whereas 95–99% of NIH:OVCAR3, SKOV3 and CaOV3 cells displayed CPEs by day 4 of culture (data not shown).

HSV-1716 Exerts an Oncolytic Effect on EOC *in Vivo*. To assess the efficacy of HSV-1716 in treating established i.p. EOC, a murine xenograft model was used with two well-characterized EOC cell lines, SKOV3 and A2780, which displayed the lowest and highest sensitivity, respectively, to HSV-1716 *in vitro*. The oncolytic effect of HSV-1716 was evaluated on different tumor burdens by varying the time of treatment and by using the two aforementioned cell lines, which yield i.p. tumors of different volume.

To assess the effect of HSV-1716 in minimally spread EOC, the virus was administered 1 week after the injection of SKOV3 ovarian cancer cells. Injection i.p. of 5×10^6 SKOV3 cells resulted in microscopic tumor at the diaphragm and occasionally the omentum, mesentery, or lesser omentum within 1 week (tumor score, 2/16; tumor weight, 202 ± 7.1 mg; $n = 5$). At that time, a group of animals received a single dose of HSV-1716 ($n = 10$), whereas a group of control animals received media only ($n = 10$). Animals were then sacrificed at 6 weeks (5 weeks later) to evaluate tumors. Animals that received virus displayed significantly smaller tumors compared with control animals ($P < 0.001$; Table 1). Moreover, HSV-treated animals displayed tumors similar to their pretreatment counterparts ($P = 0.78$). Tumor spread was advanced in untreated animals (15.5/16), whereas it remained similar to pretreatment in the HSV-treated animals (2.2/16).

To assess the role of HSV-1716 in more advanced disease, SKOV3 tumors were allowed to grow for 3 weeks before they were treated with virus. At 3 weeks, larger i.p. tumors were observed (tumor score, 3.5/16; tumor weight, 837 ± 9.1 mg; $n = 5$; Table 1). Treated animals received a single dose of i.p. virus, whereas control animals received media only. Animals were then killed at 6 weeks (3 weeks later) to evaluate tumors. Animals that received HSV-1716 ($n = 10$) displayed signifi-

Table 1 Effect of HSV-1716 on tumor burden

To assess the efficacy of HSV-1716 in treating EOC *in vivo*, HSV-1716 was administered directly i.p. to SCID mice (n = 10/group) at 1 or 3 weeks after a single i.p. injection of 5×10^6 SKOV3 cells or 1×10^6 A2780 cells. Control animals received media only. Animals from each group were killed at 6 weeks after tumor injection. Separate groups of control animals were killed before viral administration at 1 and 3 weeks. Tumors were dissected and weighed. Weights are expressed in mg and values are expressed as the mean ± SE.

Tumors	Pretreatment weight	Wk of treatment	Weight of tumor at 6 wk	
			Untreated	HSV-1716
SKOV3	202 ± 7	1	1,147 ± 11	191 ± 1[a,b]
	837 ± 9	3	1,249 ± 13.2	732 ± 3[a,b]
A2780	1,860 ± 532	1	18,705 ± 2,120	2,870 ± 923[a,b]
	8,150 ± 912	3	19,100 ± 1,115	10,032 ± 1,812[b,c]

[a] $P < 0.001$ *versus* untreated.
[b] Nonsignificant *versus* pretreatment.
[c] $P < 0.05$.

cantly smaller tumors compared with control animals (n = 10; $P < 0.001$). Moreover, HSV-treated animals displayed tumors similar to their pretreatment counterparts (P = 0.86). Tumor spread was again advanced in untreated animals (score, 16/16), whereas it remained similar to tumor spread at pretreatment in the HSV-treated animals (3.7/16).

To assess the role of HSV-1716 in bulky EOC, we used the A2780 model. Administration of 1×10^6 A2780 cells resulted in bulky i.p. tumors with 0.5–2 mm tumor nodules spread throughout the abdominal cavity within 1 week (score, 16/16; tumor weight, 1860 ± 532 mg; n = 5; Table 1). At that time, a group of animals received a single dose of HSV-1716 (n = 10), and a group of control animals received media only (n = 10). Animals were then killed at 6 weeks (5 weeks later) to evaluate tumors. HSV-treated animals displayed significantly smaller tumors compared with control animals that received saline at week one ($P < 0.001$; n = 10; Table 1). In addition, no difference in tumor weight was detected between the HSV-treated animals and their pretreatment counterparts (P = 0.86; n = 10).

To assess the role of HSV-1716 in more bulky i.p. disease, A2780 tumors were allowed to grow for 3 weeks after cell injection. At that time, wide-spread tumor nodules, 4–14 mm in size (score 16/16; tumor weight, 8150 ± 912 mg; n = 5), were noted (Table 1). Administration of a single dose of HSV-1716 at 3 weeks resulted in the arrest of tumor growth at 6 weeks (3 weeks later) compared with their pretreatment counterparts (Table 1). HSV-treated animals displayed significantly smaller tumors at 6 weeks, compared with control animals that received media ($P < 0.05$; n = 10). In addition, no significant differences in tumor weight were observed between the animals treated with HSV-1716 on week 3 compared with their pretreatment counterparts (P = 0.66; n = 10).

HSV-1716 Efficiently Infects and Replicates in Irradiated PA-1 Cells. One of the hypotheses of the present study was that i.p. administration of PA-1 cells previously infected with HSV mutant might effectively deliver virus to the tumor *in vivo*. One of the difficulties of comparing the effect of virus administered alone *versus* carrier cells administered after being infected *in vitro* with HSV lies in the different amounts of particles potentially inoculated. To minimize the difference in the amount of viral load initially administered, we determined the lowest MOI at which 100% of PA-1 cells were infected with

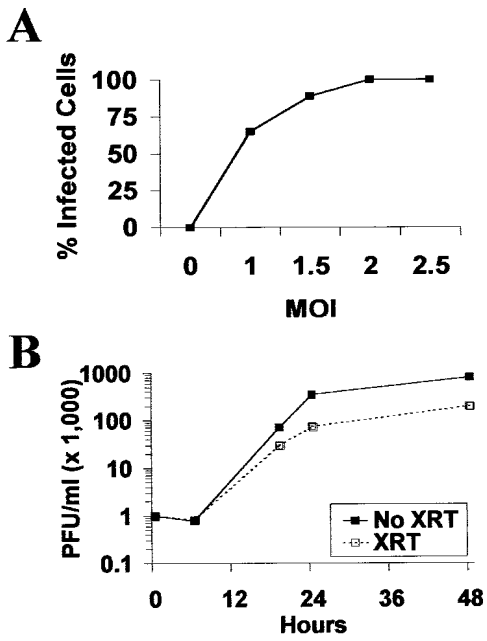

Fig. 2 HSV-1716 infection of PA-1 cells. *A*, infection rate of PA-1 teratocarcinoma cells 16 h after exposure to increasing MOI of HSV-1716. Analysis was carried out by flow cytometry using a polyclonal antibody against HSV-1 antigens. *B*, single step-growth curve of HSV-1716 in control nonirradiated human teratocarcinoma PA-1 cells (■) and cells exposed to ionizing radiation (20 Gy) before the infection (□). PA-1 cells support viral replication even after exposure to a lethal dose of radiation. Cells were incubated with 0.3 MOI, which was 1000 pfu of virus.

HSV-1716. PA-1 cells were incubated with increasing doses of the virus, and the rate of infection of the cells was determined by flow cytometry (Fig. 2*A*). These experiments indicated that approximately 100% of PA-1 cells were infected at an MOI of 2. At this MOI, each PA-1 cell presumably was initially infected by one or, at most, two viral particles.

We hypothesized that carrier cells would lead to significant amplification of the viral load delivered i.p. to the animals *in vivo*. To assess the magnitude of viral replication in PA-1 cells *in vitro*, we determined the viral burst size (Fig. 2*B*). The burst size of HSV-1716 in PA-1 teratocarcinoma cells was 200 in the

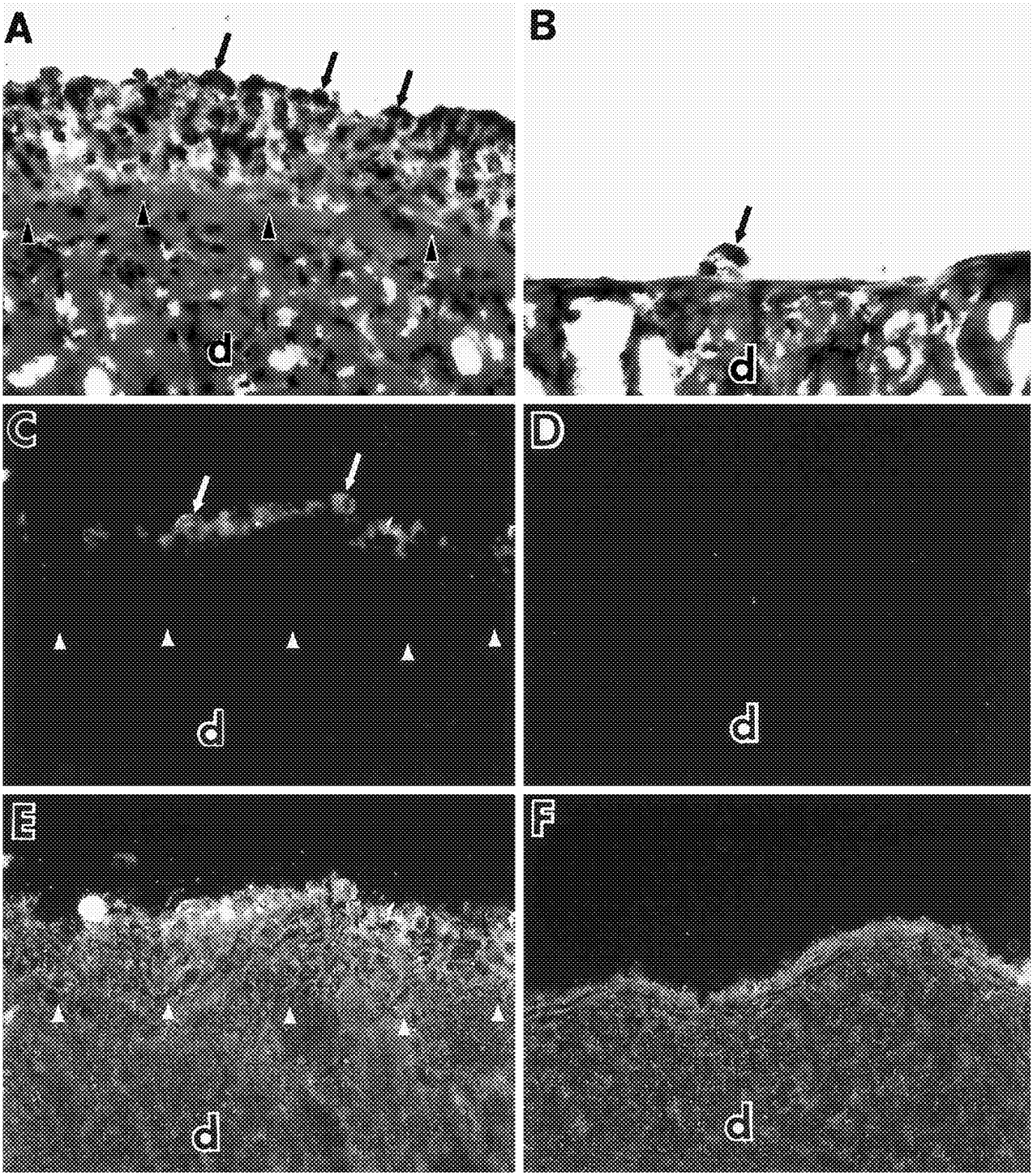

Fig. 3 PA-1 producer cells adhere preferentially to tumor nodules rather than to normal peritoneum. PA-1 cells were labeled with fluorescent dye, and 5×10^6 cells were injected i.p. in SKOV3 tumor-bearing mice. Animals were killed 8 h later, and multiple biopsies were obtained from tumor-bearing areas and normal peritoneum. Representative areas of the abdomen covered by tumor and diaphragm are shown. *A*, H&E staining of a diaphragmatic area demonstrates the presence of several layers of SKOV3 tumor cells adhering on the surface (*arrowheads*) of the diaphragm (*d*). A layer of cells with darker nuclei on the surface represent PA-1 cells (*arrows*); ×60. *B*, H&E staining of an area of the diaphragm (*d*) that is not covered by tumor. The peritoneum is free of tumor; two cells are noted on the peritoneal surface, probably representing PA-1 cells (*arrow*). *C*, a continuous layer of fluorescent PA-1 cells (*arrows*) is adherent to the tumor cells coating the diaphragm (rhodamine). *Arrowheads,* the margin of the diaphragm; ×40. *D*, examination of an adjacent area of the diaphragm (*d*) that is not covered by tumor. Fluorescent PA-1 cells are absent from the peritoneum. *E*, in the same section as *C*, tissue autofluorescence (*blue filter*) reveals several layers of SKOV3 tumor cells covering the diaphragm under the PA-1 layer. *Arrowheads,* the margin of the diaphragm; ×40. *F*, in the same section as *D*, no SKOV3 tumor cells are detected in this area of the diaphragm by tissue autofluorescence; ×40.

Table 2 Preferential binding of PA-1 cells to EOC *in vivo*

To assess the behavior of PA-1 carrier cells in our murine xenograft model, we injected fluorescent PA-1 cells i.p. into SKOV3-tumor-bearing mice. Eight h later, animals were killed, the parietal peritoneum was entirely dissected, and four specimens were prepared containing almost entirely the four different segments of the parietal peritoneum (diaphragmatic, ventral, lateral left, and lateral right). In addition, random biopsies were obtained from the mesentery and the visceral peritoneum. Twenty random fields/slide (×40) were inspected on five slides cut 18 μm apart from each other from the four different segments of the parietal peritoneum and from two sections of mesenteric areas. Fields were selected in such a way to contain only tumor surface or tumor-free normal peritoneum. The number of fields containing SKOV3 tumor with or without adhering fluorescent PA-1 cells and those containing normal peritoneum with or without adhering fluorescent PA-1 cells were counted. *P*s were computed with the χ^2 test for 2 × 2 contingency table.

	Tumor present *n* (%)[a]	Tumor absent *n* (%)	Total
Diaphragmatic peritoneum			
PA-1 present	82 (91.1)	20 (18.2)	102
PA-1 absent	8 (8.9)	90 (81.8)	98
Total	90 (100)	110 (100)	200
Nondiaphragmatic peritoneum			
PA-1 present	67 (75.3)	34 (14.1)	101
PA-1 absent	22 (24.7)	207 (85.9)	229
Total	89 (100)	241 (100)	330

[a] Percentages represent number of observations over total for each column.

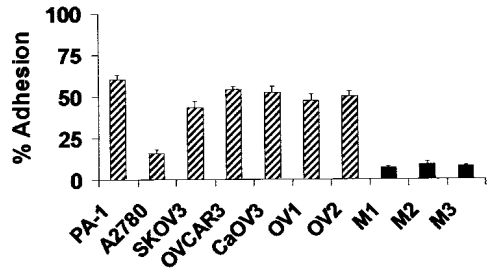

Fig. 4 *In vitro* adhesion of PA-1 cells on human normal mesothelium or ovarian cancer. PA-1 cells were radiolabeled and plated on monolayers of normal mesothelium obtained from three women with benign pelvic pathology (*M1*, *M2*, and *M3*) or on monolayers of established ovarian cancer cell lines (*PA-1*, *A2780*, *SKOV3*, *OVCAR3*, and *CaOV3*) or primary EOC cultures obtained from two patients with advanced EOC (*OV1* and *OV2*). Results are expressed as percentage of cells that were adherent 30 min after the plating. With the exception of A2780 cells, a 5- to 8-fold higher affinity of PA-1 cells is noted for ovarian cancer monolayers (*striped columns*) compared with normal human mesothelial cells (*black columns*).

absence of ionizing radiation. The administration of the HSV-1 infected carrier cells into humans will most likely require a safeguard such as radiation to eliminate risks from the administration of potentially uninfected carrier cells. Therefore, PA-1 cells were subjected to a single (lethal) dose of 20 Gy 1 h before infection, and viral replication was assessed. Burst size experiments indicated that irradiated PA-1 cells supported viral replication with a burst size of 70.

PA-1 Carrier Cells Preferentially Bind to EOC Surface Compared with Normal Peritoneum *in Vivo*. To assess the behavior of the carrier cells in our murine xenograft model, we injected fluorescent PA-1 cells i.p into SKOV3-tumor-bearing mice. Overall, we observed that a large number of fluorescent PA-1 cells adhered to areas of the diaphragm or other peritoneal surfaces that were covered by tumor. In some areas, PA-1 cells almost formed a monolayer covering the SKOV3 preexisting tumors (Fig. 3, *A*, *C*, and *E*). In contrast, in the absence of tumor nodules, there were few and isolated fluorescent PA-1 cells attaching to normal peritoneal surfaces (Fig. 3, *B*, *D*, and *F*).

When the number of tumor fields containing adherent PA-1 cells were compared with the normal peritoneum fields containing adherent PA-1 cells, we found a significantly higher frequency of binding of PA-1 cells to tumor surfaces compared with normal peritoneum. Specifically, 90 random diaphragmatic areas harboring SKOV3 tumor were examined, and 91.1% displayed adherent PA-1 cells, whereas among 110 diaphragmatic areas with no tumor examined, only 18.1% displayed PA-1 adherent cells ($P < 0.0001$; OR, 49.9; Table 2). If only the areas displaying more than 3 PA-1 cells were considered, 91.1% of tumor-positive and 6.3% of tumor-negative areas had bound PA-1 cells ($P < 0.0001$; OR, 158.4; not shown). Similar results were obtained analyzing lateral or ventral parietal peritoneum and mesenteric peritoneum. Among 89 areas examined that harbored SKOV3 tumor, 75.3% displayed adherent PA-1 cells, whereas among 241 areas with no tumor inspected, only 14.1% displayed PA-1 adherent cells ($P < 0.0001$; OR, 18.6; Table 2). If only the areas displaying more than three PA-1 cells were considered, 79.8% of tumor-positive and 9.9% of tumor-negative areas displayed PA-1 cells ($P < 0.0001$; OR, 36.1; not shown).

PA-1 Carrier Cells Preferentially Bind to EOC Surface Compared with Normal Peritoneum *in Vitro*. The observed differences may have been related to molecular factors controlling cell-cell interactions between PA-1 cells and murine mesothelial cells. Alternatively, they may have been related to physical forces governing peritoneal fluid circulation, which might direct both SKOV3 tumor cells and PA-1 cells toward the same peritoneal sites. In addition, they may have been caused by decreased affinity of PA-1 teratocarcinoma cells to murine tissues as compared with human tissues. To analyze the interaction of PA-1 cells with human EOC and normal peritoneal cells, we performed *in vitro* adhesion assays comparing the adhesion of PA-1 teratocarcinoma cells with normal human peritoneum mesothelial cells, several EOC cell lines, and primary EOC cultures (Fig. 4). These experiments indicated that PA-1 teratocarcinoma cells displayed significantly higher binding to ovarian cancer cells compared with normal human mesothelium ($P < 0.001$ for each mesothelial culture *versus* each ovarian cancer primary culture or cell line except A2780). To assess the effect of radiation or HSV infection on PA-1 adhesion, we compared the adhesion of PA-1 teratocarcinoma cells with different ovarian cancer cell lines after radiation, after infection with HSV-1716, or after both treatments. No significant effects of these treatments were observed on PA-1 adhesion (data not shown).

PA-1 Carrier Cells Effectively Deliver HSV-1716 *in Vivo*. To assess the suitability of carrier cells for the delivery of HSV-1716 *in vivo*, we compared the effects of HSV-1716 administered directly with the effects of HSV-1716 delivered via PA-1 cells. One week after the administration of A2780 tumor cells, SCID mice received a single i.p. administration of

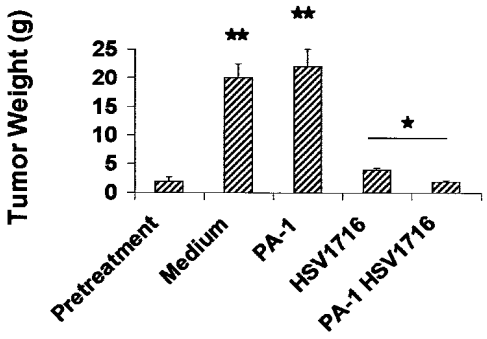

Fig. 5 *In vivo* effect of HSV-1716 on A2780 tumor growth. SCID mice received injections of 1×10^6 A2780 cells i.p., and control animals were killed 1 week later to assess i.p. tumors (*Pretreatment*, *black bar*; $n = 5$). At that time, animals received treatment with i.p. HSV-1716 at 5×10^6 pfu/animal (*HSV1716*; $n = 10$) or with radiated PA-1 cells infected with HSV-1716 [5×10^6 cells/animal, infected at 2 MOI (*PA-1 HSV1716*); $n = 10$]. Control animals received i.p. media (*Medium*; $n = 10$) or radiated PA-1 cells (*PA-1*; $n = 10$). There was a significant reduction in tumor growth 4 weeks after a single i.p. administration of the virus compared with controls treated with media ($P < 0.01$) and an even larger reduction after the administration of PA-1 cells infected with HSV-1716 compared with their respective controls ($P < 0.001$). The progression of disease was completely stabilized 4 weeks after a single administration of HSV-infected PA-1 cells. (*, $P < 0.01$; **, $P < 0.001$).

virus alone or HSV-infected PA-1 cells (Fig. 5). Control animals received media or uninfected/irradiated PA-1 cells, respectively. Four weeks later, a significant increase in tumor weight was noted in control animals receiving media (20 ± 2.5 g; $n = 20$) or irradiated PA-1 cells (22.3 ± 3 g; $n = 20$) compared with pretreatment animals (1.9 ± 0.1 g; $n = 5$; $P < 0.001$, both). The administration of HSV-1716 alone ($n = 20$) allowed for a small increase in tumor weight (3.4 ± 0.2 g) compared with pretreatment animals ($P < 0.05$), whereas the injection of PA-1 infected with HSV-1716 ($n = 20$) resulted in the stabilization of disease (2 ± 0.2 g) compared with pretreatment animals ($P = 0.198$). Tumors in HSV-treated animals or in those treated with HSV-infected carrier cells were significantly smaller compared with those of their control counterparts receiving media ($P < 0.01$) or receiving uninfected PA-1 cells ($P < 0.001$), respectively. Moreover, tumors in animals treated with HSV-infected carrier cells were significantly smaller compared with those receiving HSV-1716 alone ($P < 0.05$).

Similar results were obtained in experiments carried out with SKOV3 cells injected i.p. (5×10^6/animal) into SCID mice (Fig. 6). One week after the injection of tumor cells, control animals received media (group 1, $n = 20$) or irradiated PA-1 cells (group 2, $n = 20$), whereas treated animals received a single i.p. injection of virus (group 3, $n = 20$) or HSV-infected PA-1 carrier cells (group 4, $n = 20$), respectively (Table 3). Animals from each group were killed at 4 and 7 weeks after treatment. Control animals from group 1 receiving media alone ($n = 10$) displayed a 6-fold increase in tumor weight ($P < 0.01$) and an extensive spread of disease at 4 weeks (score, 15.5/16) compared with pretreatment animals killed at 1 week ($n = 5$; tumor score, 2.5/16). A 10-fold increase in tumor weight ($P < 0.001$ *versus* pretreatment) and further tumor spread (score, 16/16) was noted at 7 weeks ($n = 10$). Control animals from group 2, receiving irradiated PA-1 cells ($n = 10$), displayed a 6.5-fold increase in tumor weight ($P < 0.001$ *versus* pretreatment) and extensive tumor spread (score, 15.9/16) at 4 weeks (Table 3). A 12-fold increase in tumor weight ($P < 0.001$ *versus* pretreatment) and diffuse spread (score, 16/16) were noted at 7 weeks ($n = 10$). There was no significant difference in tumor growth or tumor spread between the control groups receiving media or irradiated PA-1 cells. Animals treated with HSV-1716 (group 3, $n = 10$) displayed significantly less tumor growth ($P < 0.001$) and spread (score, 2.5/16) at 4 or 7 weeks compared with control group 1 (Table 3). Group 3 displayed no difference in tumor weight at 7 weeks from pretreatment animals ($P = 0.61$), which suggests a stabilization of disease. Animals receiving HSV-infected carrier cells (group 4) also had significantly smaller tumors ($P < 0.001$) and less tumor spread (score, 2/16) at 4 and 7 weeks than their control group 2 (Table 3). Group 4 showed no tumor progression at 4 weeks ($P = 0.43$) and significant tumor regression by week 7 ($P < 0.05$ *versus* pretreatment). In addition, group 4 had a significantly smaller tumor burden at 7 weeks than HSV-1716-treated animals (group 3, $P < 0.05$; Table 3). Remarkably, in the group receiving HSV-infected PA-1 producer cells, 20% of the animals displayed no detectable disease either grossly or under the dissecting microscope at 4 weeks ($n = 4$ of 20) or at 7 weeks ($n = 4$ of 20).

To assess the carcinogenic potential of PA-1 carrier cells, 6–8-week-old SCID mice ($n = 10$) were given i.p. injections of 5×10^6 irradiated PA-1 cells infected with HSV-1716 at 2 MOI. Animals were followed for 16 weeks and then killed to evaluate the presence of i.p. tumors. No microscopic or gross tumor was detected. In addition, 10 animals were given injections in the flank with 5×10^6 PA-1 cells, which were prepared in a similar manner. Similarly, no tumor was detected over 16 weeks.

The Use of HSV-infected Carrier Cells Prolongs the Survival of SKOV3 Tumor-bearing Animals. Survival experiments carried out in animals bearing SKOV3 tumors confirmed the oncolytic activity of HSV-1716 on EOC (Fig. 7). A single dose of HSV-1716 was administered 4 weeks after the injection of tumor cells, a time in which there would be a sizable i.p. tumor burden (Table 3). This resulted in the approximate doubling of the mean survival time (17 weeks; $n = 20$) compared with that for control animals receiving media alone (9 weeks; $n = 20$; $P < 0.001$). Moreover, the administration of HSV-infected PA-1 cells ($n = 20$) allowed for a slightly longer mean survival time compared with the administration of HSV-1716 (20 weeks; $P < 0.01$ *versus* HSV-1716 alone).

Similar experiments were performed in animals bearing A2780 tumors: the injection of a single dose of HSV-1716 4 weeks after the injection of tumor cells, a time in which there would be extensive i.p. tumor, also led to the doubling of animal survival (13 weeks, $n = 20$) compared with controls (6 weeks, $n = 20$; not shown). PA-1 cells infected with HSV-1716 did not result in any further increase in mean animal survival time (13.5 weeks, $n = 20$) compared with the administration of HSV-1716 alone ($P = 0.987$). However, when some of the moribund animals in the treated groups were killed, the amount of i.p. tumor encountered was minimal in HSV-treated animals (1.9 ± 0.4 g; $n = 4$) and even smaller in PA-1/HSV-treated animals

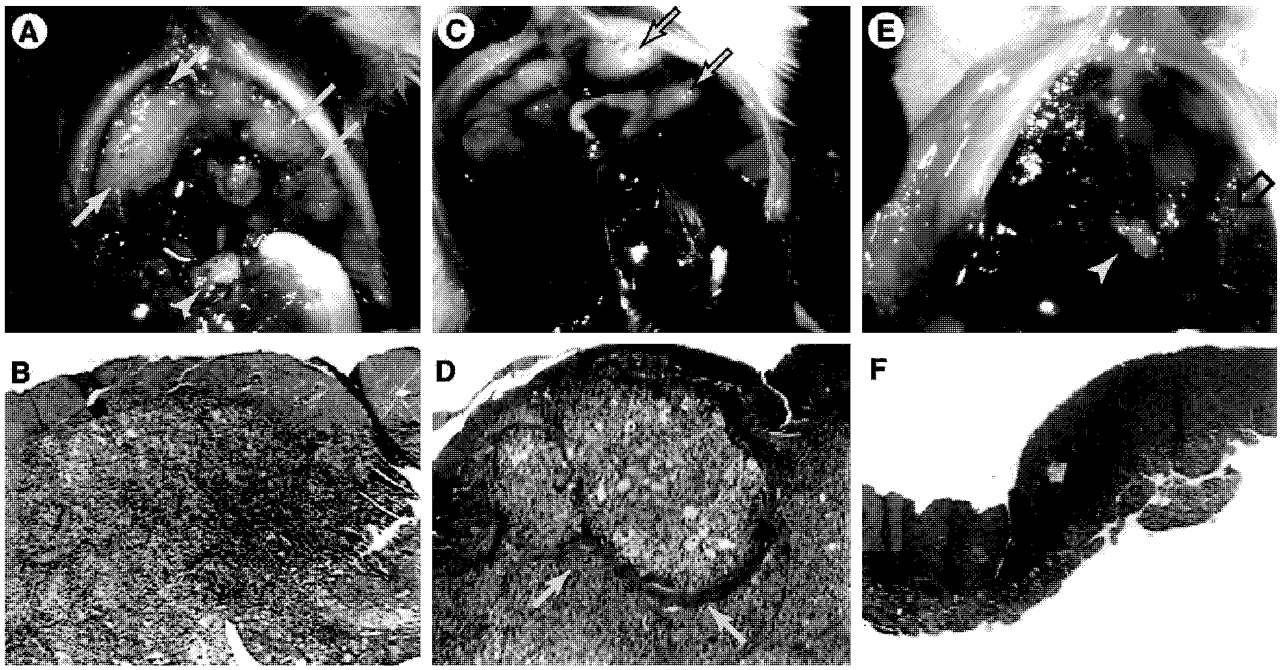

Fig. 6 *In vivo* effect of HSV-1716 on SKOV3 tumor growth. SCID mice were given i.p. injections of 5×10^6 SKOV3 cells and 1 week later received treatment with i.p. HSV-1716 (5×10^6 pfu) or PA-1 cells (5×10^6 cells) previously radiated and infected with HSV-1716 (2 MOI). Control animals received i.p. media or radiated PA-1 cells. Animals were killed 4 weeks later. *A*, large tumor nodules extend throughout the entire surface of the diaphragm in control animals (*yellow arrows*) after ascites was removed. *Arrowhead*, nodule at the hepatic hilum. *B*, microscopic evaluation reveals solid tumor sheets. *C*, a significant reduction in tumor growth is seen after a single i.p. administration of HSV-1716; only a few tumor nodules are present on the diaphragm (*yellow arrows*) and in other peritoneal areas. *D*, microscopic evaluation reveals tumor nodules with necrosis and cell vacuolization surrounded by connective tissue (*yellow arrows*), which suggests a desmoplastic reaction to HSV-infected tumor. Solid tumor sheets have grown around this nodule. *E*, a more pronounced tumor reduction is documented after the administration of HSV-infected PA-1 cells. No large tumor nodules are noted. Occasional miliary nodules are seen on the diaphragm (*open arrow*); a nodule at the hepatic hilum is also noted (*arrowhead*). Similar reduction was observed in other areas of the peritoneal cavity. *F*, microscopic evaluation reveals few layers of tumor cells on the diaphragm in areas with miliary nodules.

Table 3 Enhancement of HSV-1716 treatment by carrier cells *in vivo*

To assess the efficacy of HSV-1716 to treat EOC and the suitability of carrier cells for the delivery of HSV-1716 *in vivo*, we compared the effects of HSV-1716 administered directly i.p. with the effects of HSV-1716 delivered via PA-1 carrier cells injected i.p. after radiation and *in vitro* infection. All of the animals (SCID mice) received a single i.p. injection of 5×10^6 SKOV3 cells. Control animals received media (group 1, $n = 20$) or irradiated PA-1 cells (group 2, $n = 20$) 1 week later. Treated animals received a single i.p. injection of virus (group 3, $n = 20$) or HSV-infected PA-1 carrier cells (group 4, $n = 20$) 1 week later. Animals from each group were killed at 4 and 7 weeks after treatment. Tumors were dissected and weighed. Weights are expressed in mg and values are expressed as the mean ± SE. Pretreatment weight = 0.214 ± 0.032 mg.

Group No.	Treatment	Weight at posttreatment	
		4 wk	7 wk
1	Media	1.225 ± 0.09^a	2.256 ± 0.06^b
2	Irradiated PA-1	1.412 ± 0.01^b	2.494 ± 0.16^b
3	HSV-1716	0.225 ± 0.03^c	0.380 ± 0.06^d
4	PA-1/HSV-1716	0.185 ± 0.04^e	0.131 ± 0.09^f

[a] $P < 0.01$ *versus* pretreatment.
[b] $P < 0.001$ *versus* pretreatment.
[c] $P < 0.001$ *versus* control group 1 at 4 weeks.
[d] $P < 0.01$ *versus* control group 1 at 7 weeks.
[e] $P < 0.01$ *versus* control group 2 at 4 weeks.
[f] $P < 0.001$ *versus* control group 2 at 7 weeks; $P < 0.05$ *versus* pretreatment; $P < 0.05$ *versus* group 3 (HSV-1716 alone) at 7 weeks.

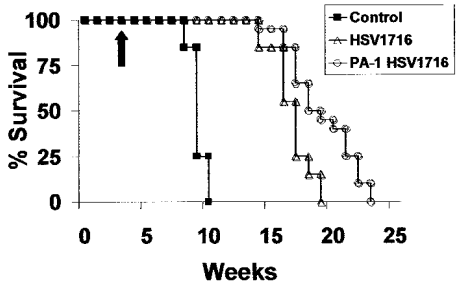

Fig. 7 *In vivo* effect of HSV-1716 on the survival of SCID mice bearing SKOV3 tumors. SKOV3 cells (5×10^6) were injected i.p., and 4 weeks later, animals received treatment (*arrow*) with HSV-1716 (5×10^6 pfu/SCID mouse, $n = 20$, △) or PA-1 cells infected with HSV-1716 at 2 MOI (5×10^6/SCID mouse, $n = 20$, ○). Control animals ($n = 20$, ■) received media alone. Curves represent the sum of two experiments carried out under identical conditions. A significant prolongation of survival is noted after i.p. injection of HSV-1716 ($P < 0.001$ *versus* controls). An even more dramatic prolongation is noted after the administration of HSV-infected PA-1 cells ($P < 0.001$ *versus* control; $P < 0.01$ *versus* HSV-1716 alone).

(0.9 ± 0.4, $n = 3$). Of note, these animals displayed large tumors at the abdominal injection site, which were ulcerated and necrotic. These findings suggested that death may have ensued because of infectious or tumor-related complications stemming

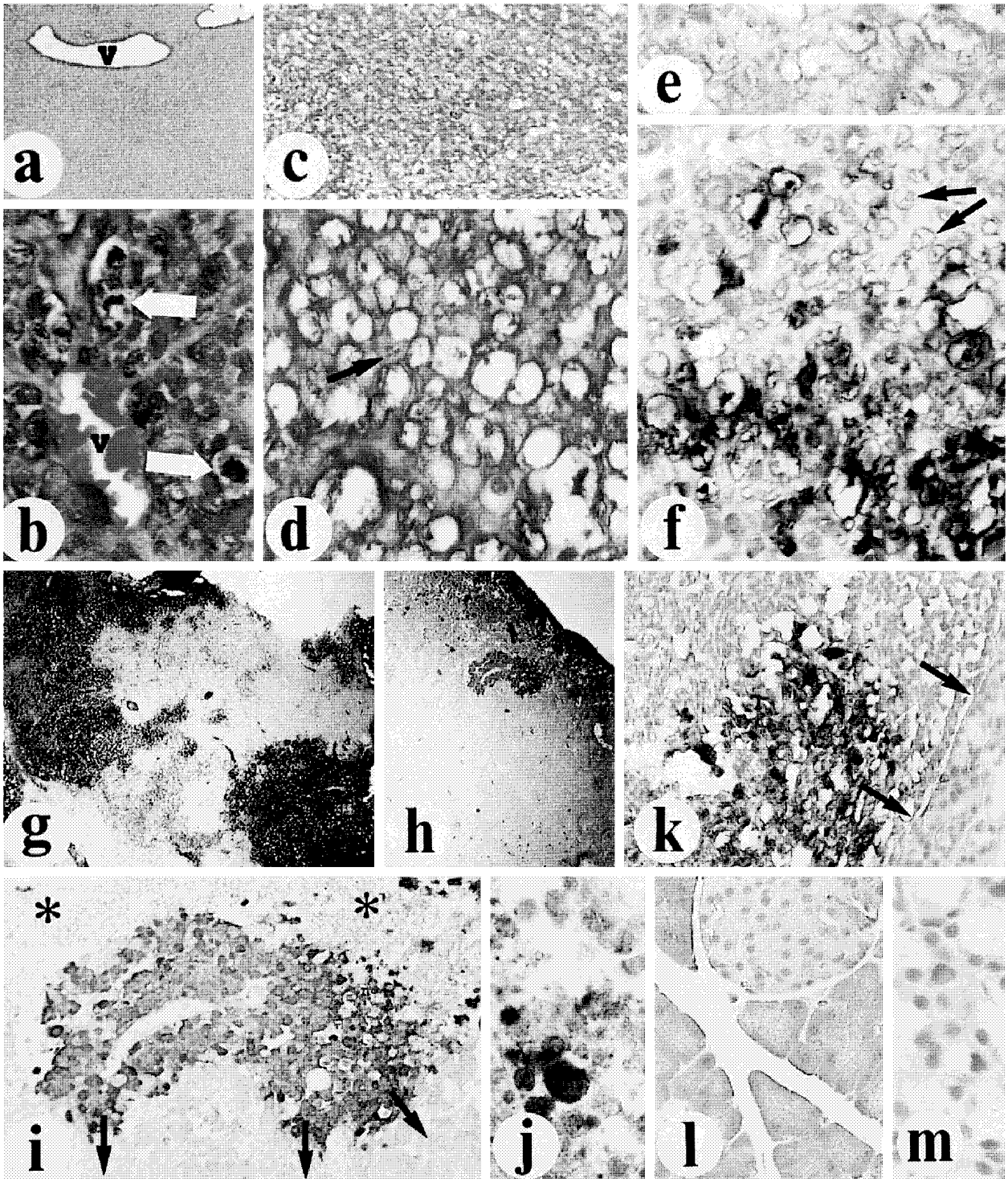

Fig. 8 Microscopic features of tumor infected by HSV-1716. *a*, H&E staining of control untreated A2780 tumor reveals solid sheets of tumor cells with well-established vascularization (*v*); ×10. *b*, higher magnification (×100) reveals numerous mitoses (*white arrows*) and capillaries (*v*). *c*, H&E staining of SKOV3 tumor treated with HSV-1716—delivered i.p. directly or via PA-1 producer cells—results in extensive tumor necrosis; ×10. *d*, higher magnification (×100) reveals marked cell vacuolization, suggestive of HSV-induced cytopathic effects. Occasional polymorphonucleates are seen in the tumor (*black arrow*). *e*, HSV-treated tumor with extensive vacuolization incubated with preimmune rabbit serum (negative control); ×100. *f*, HSV-treated tumor displaying extensive vacuolization incubated with a polyclonal antibody against HSV-1 antigens (×100). Intense HSV staining is noted in most cells displaying vacuolization. Some cells show features of necrosis but do not stain for HSV (*arrows*), which suggests possible bystander killing mechanisms. *g*, low-power view of SKOV3 tumor treated with a single i.p. dose of PA-1 cells (5×10^6 pfu/SCID mouse) infected with HSV-1716 at 2 MOI; ×6. Extensive areas of the tumor show strong staining for HSV, indicating deep penetration of the virus within the nodule. *h*, low-power view of SKOV3 tumor treated with a single i.p. dose of HSV-1716 (5×10^6 pfu/SCID mouse); ×6. Immunohistochemistry for HSV-1 antigens reveals areas of viral infection penetrating deep in the nodule. Application of HSV-1716 alone is followed by less extensive tumor infection

from the injection-site tumors. This was in sharp contrast to the untreated animals, which carried very bulky i.p. tumors (22.7 ± 3.1 g, $n = 4$), most of which were associated with hemorrhagic ascites.

HSV-1716 Penetrates Deeply in Tumor Nodules and Causes Extensive Necrosis in a Dose-dependent Manner. Microscopic examination of control untreated tumors revealed solid sheets of tumor with well-established vascularization (Fig. 8*a*), and examination under higher magnification revealed numerous mitoses (which indicated rapid tumor growth), many capillaries, and no inflammatory infiltrate (Fig. 8*b*). On the contrary, tumors collected from animals treated with HSV-1716 or with HSV-infected producer cells revealed extensive necrosis (Fig. 8*c*). Examination at high power revealed extensive cell vacuolization, suggestive of HSV-induced CPE (Fig. 8*d*). Occasional polymorphonucleate leukocytes were also visible within the necrotic areas of the tumor. Immunohistochemistry against HSV-1 revealed the presence of virus within the necrotic areas, in which many vacuolized cells stained strongly for HSV-1 (Fig. 8*f*). Interestingly, some nearby cells displaying features of cell death did not stain for HSV-1, which suggests the existence of bystander killing mechanisms. In treated animals, the virus invaded deeply in solid tumor nodules, within which distinct areas of viral spread were noted several weeks after a single i.p. injection (Fig. 8, *g* and *h*). Immunohistochemistry evaluation of tumors obtained from animals treated with HSV-infected PA-1 cells revealed even larger areas of viral infection penetrating deeply within the tumor nodules (Fig. 8*g*) compared with animals treated with HSV-1716 alone (Fig. 8*h*). Areas of viral infection were primarily found in the interface between uninfected tumor and areas of necrosis, which suggests that, by virtue of its replication, the virus advanced into the tumor leaving behind an area of necrosis (Fig. 8*i*). In keeping with data reported previously with HSV-1716 (32), no HSV-1 staining was detected in normal murine tissues (Fig. 8, *k*, *l*, and *m*) such as liver, pancreas, kidney, adrenal, spleen, small bowel myenteric plexus, or brain of treated animals.

DISCUSSION

In this study, we sought to determine the efficacy of attenuated HSV-1716 in treating human EOC. ICP34.5 mutants such as HSV-1716 have proven effective in treating experimental CNS malignancies (12, 15, 16, 19, 20, 22, 30, 31), s.c. melanoma, and metastatic melanoma to the brain (23, 34). Moreover, it was previously shown to exert an oncolytic effect on malignant mesothelioma, a localized peritoneal tumor (32). In the present study, we show that i.p. administration of HSV-1716 to tumor-bearing animals resulted in significant reduction or arrest of tumor growth. The effect of a single i.p. dose to stabilize i.p. disease was noted even with bulky tumors and with different cell lines. Further confirming the effect of the virus, a single administration of HSV-1716 resulted in significant survival advantage in both of the models studied.

The mechanism by which HSV stabilized tumor growth in the SCID model is attributable to its direct oncolytic effect. *In vitro*, this virus was shown to exert a direct lytic effect on EOC cell lines and primary cultures. i.p. tumors in treated animals displayed large areas of necrosis, which were related to infection by the replication-competent HSV-1 mutant. Our immunohistochemistry studies confirmed that the virus penetrated deeply into the tumor tissue and was present within, or adjacent to, areas of necrosis. In those areas, tumor cells displaying fragmentation, necrosis, or CPE, stained positive for HSV. Of note, within the areas of necrosis, many necrotic-appearing cells did not display immunopositivity for HSV-1 antigens. Although HSV antigens may have degraded, another interpretation is that cell death may have been caused by different mechanisms than direct HSV-1 infection. Recently, Brandt *et al.* (37) reported that the antitumor effect of a recombinant-attenuated HSV-1/HSV-2 strain was disproportionately extensive compared with viral spread in the tumor. Taken together, these data suggest that bystander killing mechanisms may also mediate the oncolytic effects of HSV-1 mutants. Similar bystander mechanisms inducing apoptosis *in vitro* and *in vivo* were recently reported for wild-type HSV-1 (38, 39).

HSV-1716 actively infected tumor nodules, but there was no evidence of viral spread within normal murine tissues by immunohistochemistry. Although there is no current mechanistic explanation for the tumor selectivity of ICP34.5-deficient HSV mutants, this selectivity has been documented in multiple models *in vitro* and *in vivo* (15, 18–20, 23, 26, 28, 30–32, 34). Brown *et al.* (40), reported that HSV-1716 replication is severely restricted in terminally differentiated cells compared with tumor cells, whereas wild-type HSV-1 can usually replicate equally well in both cell types. Moreover, human keratinocytes were shown to support HSV-1716 replication much less than wild-type HSV *in vitro* and in normal human skin xenografts (28). Our group previously reported that i.p. inoculation of HSV-1716 into SCID mice did not result in viral spread to normal murine tissues by immunohistochemistry and PCR analysis (32). It is possible that different susceptibility to HSV infection between murine and human cells might have partly affected these results. Nevertheless, the SCID mouse is very sensitive to wild-type HSV-1 (32), suggesting that the lack of spread of HSV-1716 is due to its attenuation. Additional experiments may be needed to confirm the tumor selectivity of these mutants in the human.

Our *in vitro* results indicated that there was a clear dose-related effect of the virus. Because large-scale production of mutant HSV may offer significant technical difficulties, meth-

and necrosis compared with the application of HSV-infected PA-1 cells. *i*, higher magnification of viral infection area from *h*; ×40. The viral plaque is located in the interface of a large area of necrosis (*asterisks*) and normal uninfected tumor, which suggests that the virus, by virtue of its replication, advances within the tumor nodule (*arrows*), leaving behind an area of necrosis. *j*, detail from an area of necrosis lying peripherally to the viral plaque in *h*; ×100. Cellular debris and necrotic cells staining for HSV are noted. *k*, HSV immunohistochemistry in a SKOV3 tumor nodule adjacent to the liver capsule (*arrows*). Note a viral plaque extending throughout the tumor nodule but not to the liver parenchyma; ×40. *l* and *m*, detail from pancreas (*l*) and liver (*m*) parenchyma demonstrating the absence of viral staining at high magnification; ×100.

odologies to amplify the viral load delivered to the animals will be very useful. We hypothesized that the use of carrier cells could represent one such methodology. With this approach, appropriate cells supporting HSV replication (carrier cells) would be infected *in vitro* with HSV virions and subsequently injected in proximity of the tumor, where they would eventually burst, releasing a large amount of active viral particles. Cell-based therapies using homologous or heterologous cells have been designed previously for tumor vaccines (41–44). In the present work, we elected to use the human teratocarcinoma PA-1, a well-characterized cell line (36), as an HSV carrier cell line. This line has been approved by the Food and Drug Administration for i.p. use in humans and is already being used in a Phase 1 clinical trial for vaccine therapy of ovarian cancer (45). *In vitro,* we observed a 70-fold amplification of the virus in irradiated PA-1 cells within 24 h. The efficacy of PA-1 cells to deliver HSV was then tested *in vivo*. To minimize the artifact potentially produced by the administration of different viral loads between animals receiving virus alone and animals receiving infected carrier cells, the minimal amount of viral particles capable of infecting 100% of PA-1 cells was estimated by flow cytometry. Our results indicated that 100% of PA-1 cells were infected at two MOI. Theoretically, carrier cells were initially infected on average by one or at most two viral particles at two MOI. Therefore, inoculation of an equal number of HSV particles or PA-1 cells infected at two MOI should represent comparable amounts of viral loads initially administered to the animals. HSV-1716 administered via carrier PA-1 cells led to a reduction in tumor volume and tumor spread that was significant compared with virus alone in both of the models used. In the SKOV3 model, the carrier cell strategy also led to a significant prolongation of animal survival compared with virus alone. In the A2780 model, mean animal survival was not significantly prolonged by the utilization of the carrier cells. However, survival may not have been the best end point to assess the effect of the i.p. treatment in this model. In our experiments, moribund A2780-bearing animals that had been treated with virus harbored minimal i.p tumors, and animals treated with carrier cells harbored even smaller tumors, whereas untreated animals carried large i.p. tumors. On the other hand, all of the A2780-bearing animals carried large s.c. tumors that were not affected by the i.p. treatment and may have impacted survival (32). It is possible that survival would have been different in the absence of these s.c. tumors. Nevertheless, it is impossible to exclude other reasons for the failure of HSV-infected carrier cells to improve survival in comparison with virus treatment alone in A2780 tumors.

Although additional studies are needed to fully explore the benefits of using carrier cells, the present study supports the concept that the utilization of carrier cells may have a role in HSV-based oncolytic therapies. Our results indicate that carrier cells successfully deliver the virus i.p. and result in tumor reduction that is at least equivalent to, or better than, virus alone in the immunodeficient host. Our immunohistochemistry studies showed that the utilization of carrier cells resulted in larger areas of i.p. tumors being infected by the virus and in deeper penetration of the virus within tumor nodules compared with virus administered directly. Two possible mechanisms may account for this: (*a*) based on our *in vitro* observations, the lysis of infected carrier cells within the peritoneal cavity may have released high amounts of viral particles within the peritoneal fluid; and (b) because HSV is known to propagate also by direct cell-to-cell spread (46, 47), carrier cells may have promoted direct cell-to-cell viral infection of the tumor by directly binding to EOC cells. It is attractive to speculate that by virtue of viral amplification and through direct adhesion of carrier cells to tumor cells, a significantly larger amount of virus actually infected the i.p. tumors. Although immune neutralization of HSV was not an issue with the SCID model, this may occur in the peritoneal cavity of an immunocompetent host by complement or by neutralizing antibodies (48) that may be present in the peritoneal fluid. In fact, antiherpes antibodies are highly prevalent in the adult population (49). The utilization of a cell carrier system to deliver the virus may partly circumvent this barrier because cell-to-cell spread is less affected by neutralizing antibodies than infection by free virus (46, 47).

The *in vivo* distribution of carrier cells after i.p. administration is intriguing. PA-1 cells seemed to adhere predominantly to areas of peritoneum that were covered by established tumor and not to close-by areas of normal peritoneum. There was a close correlation between the presence of tumor and PA-1 cells as calculated by ORs. It is possible that the physical forces governing fluid migration within the peritoneal cavity were partially responsible for this effect or that species-related differences in the affinity of interaction may have influenced these findings. However, our *in vitro* studies performed with human normal mesothelial cells showed that PA-1 cells bound predominantly to EOC surfaces compared with normal human mesothelium. This finally suggests that cell-cell interactions may also play a role in promoting the adhesion of PA-1 producer cells to tumor compared with normal mesothelium. The molecular mechanisms underlying these interactions were beyond the focus of the present study. Other cell lines may support HSV replication well and also display high affinity of interaction with ovarian cancer cells. These issues are currently being investigated.

The ultimate fate of carrier cells after i.p. inoculation may pose some safety concerns. In a clinical context, there must be certainty that carrier cells will not survive. In the present study, we "sterilized" carrier cells with lethal ionizing radiation. An argument could be made that this extra step was not necessary inasmuch as these cells are very sensitive to HSV-induced killing. In fact, radiation decreased viral amplification and may have adversely affected efficacy. However, the possibility of clinical applications of carrier cells warrants that safety be ensured. If few carrier cells escape infection by HSV *in vitro*, a carcinogenic potential would emerge. Recently, Advani *et al.* (50) reported that malignant glioma cells displayed higher viral replication of HSV R3616, another ICP34.5$^-$ mutant, after exposure to similar amounts of ionizing radiation. Although the molecular mechanisms underlying this enhancement are unknown, the authors speculated that ionizing radiation may induce specific cellular genes, complementing the defects resulting from the deletion of ICP34.5 in the virus and leading to an increased ability of the virus to replicate in the host cells. Although radiation-induced enhancement may not occur in the case of PA-1 cells infected with HSV-1716, there may be other cell lines that respond to radiation in a manner similar to glioma

cells and may become more suitable for HSV-1716 carrier strategies. It should be noted, also, that R3616 and 1716 are derived from two different wild-type prototypes, namely HSV(F) and Glasgow HSV17$^+$ strains, respectively, which differ in several genes including *ICP4* (51, 52). These intrinsic differences between the two viruses may account for the observed different response to radiation.

A potential advantage offered by the utilization of a carrier cell line in HSV-based oncolytic therapy relates to the possibility of manipulating these cells as follows:

(*a*) the identification of molecules mediating the interaction between carrier cells and tumor cells or normal human mesothelial cells may allow for the engineering of carrier cells that exhibit enhanced preferential binding to tumor cells (but not to normal mesothelium) or that promote greater cell-to-cell viral spread;

(*b*) molecular engineering of carrier cells may increase their ability to support viral replication;

(*c*) molecular manipulation of carrier cells could aid in circumventing natural or acquired host immune mechanisms. For example, carrier cells could be manufactured to secrete truncated HSV-like glycoproteins that inactivate complement (gC) or antibodies (gE) (53–55). Carrier cells could also be engineered to secrete immunomodulatory cytokines. Interleukin-12 (IL-12) and IL-4 were recently shown to enhance the efficacy of HSV-based oncolysis (56, 57); and

(d) a vaccine antitumor response in selective patients might be generated. It is interesting to note that an antitumor vaccine clinical trial for the treatment of advanced EOC has been initiated using HSV*tk*-enriched PA-1 cells (45). The lysis of PA-1 cells after the administration of ganciclovir is anticipated to trigger an antitumor immune response. Similarly, HSV-infected carrier cells may lyse on the surface of i.p. tumors, increasing the recruitment of antigen-presenting cells and mononuclear cells to the site of injection (58). This may augment the immediate oncolytic effect of the virus and, by unmasking tumor antigens, possibly lead to a sustained vaccine effect.

In conclusion, the present study demonstrates that EOC is extremely sensitive to attenuated HSV-1. These findings may have significant implications for both oncolytic as well as gene therapy of EOC. In fact, attenuated HSV-1 mutants may be used as gene therapy vectors with significant advantages over replication-incompetent adenoviral or retroviral vectors (21). In addition, oncolytic attenuated HSV-1 strains are being engineered with progressively increased specificity (59, 60), and the insertion of immunomodulatory (56, 57) or corrective genes (59, 60) may further increase the efficacy of these agents. The present study also investigated the use of carrier cells and showed that this methodology may be useful in viral-based i.p. therapies. Theoretical advantages offered by a carrier-cell approach include amplification of the viral load and possibly enhanced local delivery afforded by carrier cells binding to the tumor and mediating direct cell-to-cell viral delivery. Additional potential advantages of a carrier cell system may relate to the possibility of manipulating the cells to maximize viral replication, to enhance binding to tumor surfaces, and to mediate evasion from immune-mediated viral inactivation as well as to possibly generate an antitumor vaccine effect.

ACKNOWLEDGMENTS

We thank Carmen Lord for the editorial help in the preparation of this article.

REFERENCES

1. Ries, L. Survival and treatment differences by age. Cancer (Phila.), *71:* 524–529, 1993.

2. Benjamin, I., and Rubin, S. C. Modern treatment options in epithelial ovarian carcinoma. Curr. Opin. Obstet. Gynecol., *10:* 29–32, 1998.

3. Coukos, G., and Rubin, S. Chemotherapy resistance in ovarian cancer; new molecular perspectives. Obstet. Gynecol., *9:* 783–792, 1998.

4. DiSaia, P. J., and Creasman, W. T. Epithelial ovarian cancer. *In:* Clinical Gynecologic Oncology. St. Louis, MO; Mosby-Year Book, Inc., 1993.

5. Tong, X., Block, A., Chen, S., Contant, C., Agoulnik, I., Blankenburg, K., Kaufman, R., Woo, S., and Kieback, D. *In vivo* gene therapy of ovarian cancer by adenovirus-mediated thymidine kinase gene transduction and ganciclovir administration. Gynecol. Oncol., *61:* 175–179, 1996.

6. Behbakht, K., Benjamin, I., Chiu, H., Eck, S., Van Deerlin, P., Rubin, S., and Boyd, J. Adenovirus-mediated gene therapy of ovarian cancer in a mouse model. Am. J. Obstet. Gynecol., *175:* 1260–1265, 1996.

7. Deshane, J., Siegal, G. P., Alvarez, R. D., Wang, M. H., Feng, M., Cabrera, G., Liu, T., Kay, M., and Curiel, D. T. Targeted tumor killing via an intracellular antibody against erbB-2. J. Clin. Invest., *96:* 2980–2989, 1995.

8. Mujoo, K., Maneval, D., Anderson, S., and Gutterman, J. Adenoviral-mediated p53 tumor suppressor gene therapy of human ovarian carcinoma. Oncogene, *12:* 1617–1623, 1996.

9. Link, C. J., Moorman, D., Seregina, T., Levy, J., and Schabold, K. A Phase I trial of *in vivo* gene therapy with the herpes simplex thymidine kinase/ganciclovir system for the treatment of refractory or recurrent ovarian cancer. Hum. Gene Ther., *7:* 1161–1179, 1996.

10. Alvarez, R. D., and Curiel, D. T. A Phase I study of recombinant adenovirus vector-mediated intraperitoneal delivery of herpes simplex virus thymidine kinase (HSV-*tk*) gene and intravenous ganciclovir for previously treated ovarian and extraovarian cancer patients. Hum. Gene Ther., *8:* 597–613, 1997.

11. Sterman, D. H., Treat, J., Elshami, A. A., Amin, K., Molnar-Kimber, K., Coonrod, L., Recio, A., Wilson, J. M., Roberts, J. R., Litzky, L. A., Albelda, S. M., and Kaiser, L. R. Adenovirus mediated herpes simplex virus thymidine kinase/ganciclovir gene therapy in patients with localized malignancy: results of a Phase I clinical trial in malignant mesothelioma. Hum. Gene Ther., *9:* 1083–1092, 1998.

12. Chambers, R., Gillespie, G. Y., Soroceanu, L., Andreansky, S., Chatterjee, S., Chou, J., Roizman, B., and Whitley, R. J. Comparison of genetically engineered herpes simplex viruses for the treatment of brain tumors in a SCID mouse model of human malignant glioma. Proc. Natl. Acad. Sci. USA, *92:* 1411–1415, 1995.

13. Jia, W. W-G., McDermott, M., Goldie, J., Cynader, M., Tan, J., and Tufaro, F. Selective destruction of gliomas in immunocompetent rats by thymidine kinase defective herpes simplex virus type 1. J. Natl. Cancer Inst., *86:* 1209–1215, 1994.

14. Glorioso, J. C., DeLuca, N. A., and Fink, D. J. Development and application of herpes simplex virus vectors for human gene therapy. Annu. Rev. Microbiol., *49:* 675–710, 1995.

15. Kesari, S., Randazzo, B., Valyi-Nagy, T., Huang, Q., Brown, S., MacLean, A., Lee, V., Trojanowski, J., and Fraser, N. Therapy of experimental human brain tumors using a neuroattenuated herpes simplex virus mutant. Lab. Invest., *73:* 636–648, 1995.

16. Kramm, C. M., Chase, M., Herrlinger, U., Jacobs, A., Pechan, P. A., Rainov, N. G., Sena-Esteves, M., Aghi, M., Barnett, F. H., Chiocca, E. A., and Breakefield, X. O. Therapeutic efficiency and safety of a second-generation replication-conditional HSV 1 vector for brain tumor gene therapy. Hum. Gene Ther., *8:* 2057–2068, 1997.

17. Nilaver, G., Muldoon, L. L., Kroll, R. A., Pagel, M. A., Breakefield, X. O., Davidson, B. L., and Neuwelt, E. A. Delivery of herpes virus and adenovirus to nude rat intracerebral tumors after osmotic blood-brain barrier disruption. Proc. Natl. Acad. Sci. USA, *92:* 9829–9833, 1995.

18. Martuza, R., Malick, A., Markert, J., Ruffner, K., and Coen, D. Experimental therapy of human glioma by means of a genetically engineered virus mutant. Science (Washington DC), *252:* 854–856, 1991.

19. Mineta, T., Rabkin, S., and Martuza, R. Treatment of malignant gliomas using ganciclovir-hypersensitive, ribonucleotide reductase-deficient herpes simplex viral mutant. Cancer Res., *54:* 3963–3966, 1994.

20. Mineta, T., Rabkin, S., Yazaki, T., Hunter, W., and Martuza, R. Attenuated multi-mutated herpes simplex virus-1 for the treatment of malignant gliomas. Nat. Med., *1:* 938–943, 1995.

21. Boviatsis, E., Chase, M., Wei, M., Tamiya, T., Hurford, R. J., Kowall, N., Tepper, R., Breakefield, X., and Chiocca, E. Gene transfer into experimental brain tumors mediated by adenovirus, herpes simplex virus, and retrovirus vectors. Hum. Gene Ther., *5:* 183–191, 1994.

22. Pyles, R. B., Warnick, R. E., Chalk, C., Szanti, B. E., and Parysek, L. A novel multiply mutated HSV-1 strain for the treatment of human brain tumors. Hum. Gene Ther., *8:* 533–544, 1997.

23. Randazzo, B., Kesari, S., Gesser, R., Alsop, D., Ford, J., Brown, S., MacLean, A., and Fraser, N. Treatment of experimental intracranial murine melanoma with a neuroattenuated herpes simplex virus 1 mutant. Virology, *211:* 94–101, 1995.

24. MacLean, M., Ul-Fareed, M., Roberson, L., Harland, J., and Brown, S. Herpes simplex virus type 1 deletion variant 1714 and 1716 pinpoint neurovirulence-related sequences in Glasgow strain 17^+ between immediate early gene 1 and the 'a' sequence. J. Gen. Virol., *72:* 631–639, 1991.

25. Taha, M., SM, B., Clements, G., and Graham, D. The JH2604 deletion variant of herpes simplex virus type 2 (HG52) fails to produce necrotizing encephalitis following intracranial inoculation of mice. J. Gen. Virol., *71:* 1597–1601, 1990.

26. Valyi-Nagy, T., Fareed, M., O'Keefe, J., Gesser, R., MacLean, A., Brown, S., Spivak, J., and Fraser, N. The herpes simplex virus type 1 strain 17^+ γ-34.5 deletion mutant 1716 is avirulent in SCID mice. J. Gen. Virol., *75:* 2059–2063, 1994.

27. Poon, A. P., and Roizman, B. Differentiation of the shutoff of protein synthesis by virion host shutoff and mutant γ (1)34.5 genes of herpes simplex virus 1. Virology, *229:* 98–105, 1997.

28. Randazzo, B. P., Kucharczuk, J. C., Litzky, L. A., Kaiser, L. R., Brown, S. M., MacLean, A., Albelda, S. M., and Fraser, N. W. Herpes simplex 1716—an ICP 34.5 mutant—is severely replication-restricted in human skin xenografts *in vivo*. Virology, *223:* 392–395, 1996.

29. Brown, S., MacLean, A., Aitken, J., and Harland, J. ICP34.5 influences herpes simplex virus type I maturation and egress from infected cells *in vitro*. J. Gen. Virol., *75:* 3767–3686, 1994.

30. Andreansky, S., Soroceanu, L., Flotte, E., Chou, J., Markert, J., Gillespie, G., Roizman, B., and Whitley, R. Evaluation of genetically engineered herpes simplex viruses as oncolytic agents for human malignant brain tumors. Cancer Res., *57:* 1502–1509, 1997.

31. Yazaki, T., Manz, H., Rabkin, S., and Martuza, R. Treatment of human malignant meningiomas by G207, a replication-competent multimutated herpes simplex virus 1. Cancer Res., *55:* 4752–4756, 1995.

32. Kucharczuk, J. C., Randazzo, B., Elshami, A. A., Sterman, D. H., Amin, K. A., Molnar-Kimber, K. L., Brown, M. S., Litzky, L. A., Fraser, N. W., Albelda, S. M., and Kaiser, L. R. Use of a replication-restricted, recombinant herpes virus to treat localized human malignancy. Cancer Res., *57:* 466–471, 1997.

33. Carroll, N., Chiocca, E., Takahashi, K., and Tanabe, K. Enhancement of gene therapy specificity for diffuse colon carcinoma liver metastases with recombinant herpes simplex virus. Ann. Surg., *224:* 323–329, 1996.

34. Randazzo, B., Bhat, M., Kesari, S., Fraser, N., and Brown, S. Treatment of experimental subcutaneous human melanoma with a replication-restricted herpes simplex virus mutant. J. Invest. Dermatol., *108:* 933–937, 1997.

35. Toda, M., Rabkin, S. D., and Martuza, R. L. Treatment of human breast cancer in a brain metastatic model by G207, a replication-competent multimutated herpes simplex virus 1. Hum. Gene Ther., *9:* 2173–2185, 1998.

36. Tainsky, M. A., Krizman, D. B., Chiao, P. J., Yim, S. O., and Giovanella, B. C. PA-1, a human cell model for multistage carcinogenesis: oncogenes and other factors. Anticancer Res., *8:* 899–913, 1988.

37. Brandt, C., Imesch, P., Robinson, N., Syed, N., Untawale, S., Darjatmoko, S., Chappell, R., Heinzelman, P., and Albert, D. Treatment of spontaneously arising retinoblastoma tumors in transgenic mice with an attenuated herpes simplex virus mutant. Virology, *229:* 283–291, 1997.

38. Ito, M., Watanabe, M., Kamiya, H., and Sakurai, M. Herpes simplex virus type 1 induces apoptosis in peripheral blood T lymphocytes. J. Infect. Dis., *175:* 1220–1224, 1997.

39. Wilson, S., Pedroza, L., Beuerman, R., and Hill, J. M. Herpes simplex virus type-1 infection of corneal epithelial cells induces apoptosis of the underlying keratocytes. Exp. Eye Res., *64:* 775–779, 1997.

40. Brown, S. M., Harland, J., MacLean, A. R., Podlech, J., and Clements, J. B. Cell type and cell state determine differential *in vitro* growth of non- neurovirulent ICP34.5-negative herpes simplex virus types 1 and 2. J. Gen. Virol, *75:* 2367–2377, 1994.

41. McLaughlin, J. P., Abrams, S., Kantor, J., Dobrzanski, M. J., Greenbaum, J., Schlom, J., and Greiner, J. W. Immunization with a syngeneic tumor infected with recombinant vaccinia virus expressing granulocyte-macrophage colony-stimulating factor (GM-CSF) induces tumor regression and long-lasting systemic immunity. J. Immunother., *20:* 449–459, 1997.

42. Simons, J., Jaffee, E., Weber, C., Levitsky, H., Nelson, W., Carducci, M., Lazenby, A., Cohen, L., Finn, C., Clift, S., Hauda, K., Beck, L., Leiferman, K., Owens, A. J., Piantadosi, S., Dranoff, G., Mulligan, R., Pardoll, D., and Marshall, F. Bioactivity of autologous irradiated renal cell carcinoma vaccines generated by *ex vivo* granulocyte-macrophage colony-stimulating factor gene transfer. Cancer Res., *57:* 1537–1546, 1997.

43. Ram, Z., Walbridge, S., EM, O., Vila, J., Yawen, C., Mueller, S., Blaese, M., and Oldfield, E. Intrathecal gene therapy for malignant leptomeningeal neoplasia. Cancer Res., *54:* 2141–2145, 1994.

44. Abdel-Wahab, Z., Weltz, C., Hester, D., Pickett, N., Vervaert, C., Barber, J. R., Jolly, D., and Seigler, H. F. A Phase I clinical trial of immunotherapy with interferon-γ gene-modified autologous melanoma cells: monitoring the humoral immune response. Cancer (Phila.), *80:* 401–412, 1997.

45. Freeman, S. M., McCune, C., Robinson, W., Abboud, C. N., Abraham, G. N., Angel, C., and Marrogi, A. The treatment of ovarian cancer with a gene modified cancer vaccine: a Phase I study. Hum. Gene Ther., *6:* 927–939, 1995.

46. Dingwell, K. S., Brunetti, C. R., Hendricks, R. L., Tang, Q., Tang, M., Rainbow, A. J., and Johnson, D. C. Herpes simplex virus glycoproteins E and I facilitate cell-to-cell spread *in vivo* and across junctions of cultured cells. J. Virol., *68:* 834–845, 1994.

47. Weeks, B. S., Sundaresan, P., Nagashunmugam, T., Kang, E., and Friedman, H. M. The herpes simplex virus-1 glycoprotein E (gE) mediates IgG binding and cell-to-cell spread through distinct gE domains. Biochem. Biophys. Res. Commun., *235:* 31–35, 1997.

48. Gange, R. W., de Bats, A., Park, J. R., Bradstreet, C. M., and Rhodes, E. L. Cellular immunity and circulating antibody to herpes simplex virus in subjects with recurrent herpes simplex lesions and controls as measured by the mixed leukocyte migration inhibition test and complement fixation. Br. J. Dermatol., *93:* 539–544, 1975.

49. Whitley, R. Herpes simplex viruses. *In:* B. N. Fields, D. M. Knipe, and P. M. Holey (eds.), Virology, Vol. 2, pp. 2297–2342. Philadelphia, PA: Lippincott-Raven Publishers, 1996.

50. Advani, S., Sibley, G., Song, P., Hallahan, D., Kataoka, Y., Roizman, B., and Weichselbaum, R. Enhancement of replication of genetically engineered herpes simplex viruses by ionizing radiation: a new paradigm for destruction of therapeutically intractable tumors. Gene Ther., *5:* 160–165, 1998.

51. Brown, S. M., Ritchie, D. A., and Subak-Sharpe, J. H. Genetic studies with herpes simplex virus type 1. The isolation of temperature-sensitive mutants, their arrangement into complementation groups and recombination analysis leading to a linkage map. J. Gen. Virol., *18:* 329–346, 1973.

52. Ejercito, P. M., Kieff, E. D., and Roizman, B. Characterization of herpes simplex virus strains differing in their effects on social behaviour of infected cells. J. Gen. Virol., *2:* 357–364, 1968.

53. Dubin, G., Basu, S., Mallory, D., Basu, M., Tal-Singer, R., and Friedman, H. Characterization of domains of herpes simplex virus type 1 glycoprotein E involved in Fc binding activity for immunoglobulin G aggregates. J. Virol., *68:* 2478–2485, 1994.

54. Eisenberg, R., Ponce de Leon, M., Friedman, H., Fries, L., Frank, M., Hastings, J., and Cohen, G. Complement component C3b binds directly to purified glycoprotein C of herpes simplex virus types 1 and 2. Microb. Pathog., *3:* 423–435, 1987.

55. Wiertz, E., Mukherjee, S., and Ploegh, H. Viruses use stealth technology to escape from the host immune system. Mol. Med. Today, *3:* 116–123, 1997.

56. Toda, M., Martuza, R., Kojima, H., and Rabkin, S. *In situ* cancer vaccination: an IL-12 defective vector/replication-competent herpes simplex virus combination induces local and systemic antitumor activity. J. Immunol., *160:* 4457–4464, 1998.

57. Andreansky, S., He, B., van Cott, J., McGhee, J., Markert, J. M., Gillespie, G. Y., Roizman, B., and Whitley, R. J. Treatment of intracranial gliomas in immunocompetent mice using herpes simplex viruses that express murine interleukins. Gene Ther., *5:* 121–130, 1998.

58. Fahy, G. T., Hooper, D. C., and Easty, D. L. Antigen presentation of herpes simplex virus by corneal epithelium-an *in vitro* and *in vivo* study. Br. J. Ophthalmol., *77:* 440–444, 1993.

59. Chase, M., Chung, R. Y., and Chiocca, E. A. An oncolytic viral mutant that delivers the *CYP2B1* transgene and augments cyclophosphamide chemotherapy. Nat. Biotechnol., *16:* 444–448, 1998.

60. Oligino, T., Poliani, P. L., Wang, Y., Tsai, S. Y., O'Malley, B. W., Fink, D. J., and Glorioso, J. C. Drug-inducible transgene expression in brain using a herpes simplex virus vector. Gene Ther., *5:* 491–496, 1998.

APPENDIX III

Gene Therapy (2007), 1–14

www.nature.com/gt

ORIGINAL ARTICLE

Targeted release of oncolytic measles virus by blood outgrowth endothelial cells in situ *inhibits orthotopic gliomas*

J Wei[1,5,6], J Wahl[1,5], T Nakamura[2,7], D Stiller[3], T Mertens[4], K-M Debatin[1] and C Beltinger[1]
[1]*University Children's Hospital, Ulm, Germany;* [2]*Molecular Medicine Program, Mayo Clinic College of Medicine, Rochester, MN, USA;* [3]*Boehringer Ingelheim Pharma, Biberach an der Riß, Germany and* [4]*Department of Virology, University Hospital, Ulm, Germany*

Malignant gliomas remain largely incurable despite intensive efforts to develop novel therapies. Replicating oncolytic viruses have shown great promise, among them attenuated measles viruses of the Edmonston B strain (MV-Edm). However, host immune response and the infiltrative nature of gliomas limit their efficacy. We show that human blood outgrowth endothelial cells (BOECs), readily expandable from peripheral blood, are easily infected by MV-Edm and allow replication of MV-Edm while surviving long enough after infection to serve as vehicles for MV-Edm (BOEC/MV-Edm). After intravenous and peritumoral injection, BOEC/MV-Edm deliver the viruses selectively to irradiated orthotopic U87 gliomas in mice. At the tumor, MV-Edm produced by the BOECs infect glioma cells. Subsequent spread from tumor cell to tumor cell leads to focal infection and cytopathic effects that decrease tumor size and, in the case of peritumoral injection, prolong survival of mice. Since MV-Edm within BOECs are not readily neutralized and because BOEC/MV-Edm search and destroy glioma cells, BOEC/MV-Edm constitute a promising novel approach for glioma therapy.
Gene Therapy advance online publication, 27 September 2007; doi:10.1038/sj.gt.3303027

Keywords: *oncolytic measles virus; endothelial progenitors; brain tumor therapy*

Introduction

Nearly all patients with malignant gliomas die from their disease and prognosis has improved only little over decades. The efficacy of locoregional therapies such as a surgical resection, irradiation, radioimmunotherapy and gene therapy is modest at best. One major reason is the limited delivery of the therapeutic moiety to the glioma cells. This is exemplified by the failure of gene therapy, which, when directly aimed against glioma cells, is hampered by low gene transfer efficacy requiring a complete bystander effect impossible to achieve. A second major reason for the failure of existing local therapies is the infiltrative growth of malignant glioma leading to the formation of glioma cell clusters isolated within normal brain tissue. These are inaccessible without risking destruction of normal brain tissue. Systemic therapy is also inefficient in glioma patients despite recent advances. This is in part due to the blood–brain barrier, which, although impaired, remains partially functional in malignant gliomas and hinders their systemic therapy by drugs, DNA or viruses.

Replicating oncolytic viruses are emerging as a promising modality for the treatment of malignant gliomas and other malignancies. They promise to overcome the problem of limited delivery of the therapeutic agent since, in principle, the successful infection of only a few tumor cells should suffice for subsequent spread to most tumor cells. A variety of replicating oncolytic viruses are being investigated. A recent addition to this arsenal is attenuated measles virus of the Edmonston B vaccine strain (MV-Edm; reviewed in Nakamura and Russell[1] and Fielding[2]). MV-Edm infects cells by preferentially binding to CD46[3,4] rather than to CD150, as wild-type MV does. The higher density of CD46 on malignant cells, including malignant gliomas,[5] compared to non-malignant cells contributes to the preferential killing of tumor cells by MV-Edm.[6] Once MV-Edm has infected tumor cells it spreads to noninfected tumor bystander cells by cell-to-cell contact.[7,8] MV-Edm-infected tumor cells form syncytia[9] induced by the F-protein of the virus, eventually leading to cell death that includes programmed cell death.[10] MV-Edm has been shown in animal models to have oncolytic activity against human lymphoma,[9] multiple myeloma,[11] ovarian cancer,[12,13] malignant glioma,[5] fibrosarcoma[14] and against cutaneous T-cell lymphoma in patients.[15]

As for other replicating oncolytic viruses, host immune response and cellular barriers limit infection by and intratumoral spread of MV-Edm, respectively. MV is

Correspondence: Professor C Beltinger, University Children's Hospital, Eythstrasse 24, Ulm 89075, Germany.
E-mail: christian.beltinger@uniklinik-ulm.de
[5]These authors have contributed equally to this work.
[6]Current address: Division of Clinical Pharmacology, Section of Gastroenterology, Medizinische Klinik Innenstadt, University of Munich, Ziemssenstr. 1, 80336 Munich, Germany.
[7]Current address: Department of Molecular Genetics, Medical Institute of Bioregulation, Kyushu University, 3–1–1 Maidashi, Fukuoka 812-8582, Japan.
Received 1 November 2006; revised 2 July 2007; accepted 14 August 2007

readily neutralized by serum antibodies from humans immune to measles, which is true for most adults. Although cancer patients are usually immunocompromised and the brain may be an 'immune-privileged' site, an immune response against MV-Edm may still be mounted, limiting infection of gliomas by MV-Edm. As the spread of MV-Edm depends on tumor-cell-to-tumor-cell contact, noninfectable cells such as most non-malignant cells will impede the spread of MV-Edm. This problem is accentuated in malignant gliomas because of their propensity for infiltrative growth.

Various cellular vehicles can be envisioned to deliver therapeutic agents to experimental brain tumors. These include neural progenitors derived from the patient, from cadavers or fetuses, or generated from embryonic stem cells. However, clinical, logistical, immunological and ethical considerations will limit their use (reviewed in Jarmy *et al.*[16]). In contrast, bone marrow-derived cells, known to target experimental tumors including gliomas,[17–19] are more easy to procure. Blood outgrowth endothelial cells (BOECs), in particular, are readily obtained from human peripheral blood.[20] They can be massively expanded *ex vivo* and lend themselves to genetic manipulation. BOECs are progenitor cells with a microvascular endothelial phenotype[20,21] expressing VEGFR2, VEGFR1, vWF, CD31, VE-cadherin, $a_v\beta_3$, $a_v\beta_5$ and CD105. They do not or only marginally express CD133, c-kit, CD45, CXCR4, ESL (E-selectin ligand), CD162, cutaneous lymphocyte-associated Ag, CD49d, CD11a and CD11b. The expression of CD34 varies. BOECs take up acetylated low-density lipoprotein and build vessel-like structures on Matrigel. BOECs have been shown to seek experimental tumors, invade them and incorporate into tumor structures.[21] However, when armed with the cytosine deaminase gene and administered intravenously (i.v.), they did not prolong the life of mice bearing disseminated metastases of Lewis lung carcinoma.[21] A major reason for this failure was the temporary and spatially limited bystander effect on tumor cells, the limitation being caused by suicide of the BOECs upon prodrug administration.

We reasoned that combining the tumor-seeking and protective ability of BOECs with the sustained and far reaching oncolytic 'lateral effect' of attenuated measles virus might control experimental brain tumors. We show in this study that MV-Edm within BOECs are protected against MV-neutralizing serum antibodies and are carried in mice through normal brain tissue to orthotopic malignant glioma cells, infect them, decrease tumor size and increase survival.

Results

BOECs express CD46 and can be infected by MV-Edm while being resistant to MV-Edm-mediated cell death

To employ BOECs as tumor-targeting cellular vehicles for MV-Edm, we first had to verify whether BOECs can be infected by MV-Edm. Expression of CD46, the preferred receptor for MV-Edm, on BOECs was strong and comparable with U87 glioma cells, A549 lung carcinoma cells and the myelomonocytic leukemia cell line K562, and was markedly stronger than on monocytes (Figure 1a).

We then determined whether MV-Edm infect and replicate within BOECs. Indeed, the virus titer ($TCID_{50}$) of lysates of BOECs infected with MV-Edm increased 139-fold as compared to the virus inoculum within 3 days after infection (Figure 1b). Human monocytes, another potential cellular vehicle for MV, also supported MV replication, whereas replication in human lymphocytes was limited (Figure 1b). Despite efficient replication, the majority of BOECs did not succumb to MV 3 days after infection (Figure 1c), in contrast to monocytes. Thus, BOECs, but not monocytes or lymphocytes, support replication of MV for several days without dying.

While BOECs initially resisted MV-induced cell death, human cancer cell lines, such as A549 lung carcinoma and U87 glioma cells, were readily killed by MV-Edm (Figure 1d).

Infection with MV-Edm may change homing-associated surface molecules of BOECs. However, no change in the expression of VEGFR2 (KDR), CXCR4, VE-Cadherin, $a_v\beta_5$, CD11a, CD11b, CD49d, CD162 and cutaneous lymphocyte-associated Ag was detected 1 and 24 h after infection (data not shown).

Taken together, BOECs could be infected by MV-Edm without being quickly killed or downregulating homing-associated surface molecules. This suggests that they are suitable cellular vehicles for MV-Edm.

BOECs do not carry loosely adsorbed MV-Edm-eGFP on their surface after infection with MV-Edm-eGFP

We investigated whether MV-Edm added to BOECs *in vitro* just adhere to the BOECs' surface and subsequently become released to infect surrounding cells. To this end, Vero indicator cells were incubated with cell-free washes of BOEC/MV-Edm-eGFP. While BOECs were clearly infected with MV-Edm-eGFP, as seen by the green fluorescence of BOECs (Figure 2, left panel), no infectious MV-Edm-eGFP could be detached by washing and trypsinizing after infection as no Vero cells became infected (Figure 2, right panel).

MV-Edm spread from BOECs to neighboring U87 glioma cells and exert a strong bystander effect

It is crucial for any therapeutic vehicle to effectively release its payload to the target cells. As determined by fluorescence microscopy, MV-Edm-eGFP spread rapidly from single BOEC/MV-Edm cells to surrounding U87 cells (Figures 3Aa–c) and then to more distant U87 cells (Figures 3Ad–f). The few GFP-positive foci of U87 cells that were not adjacent to the BOEC/MV-Edm may have originated from MV-Edm-eGFP released into the culture medium by dying tumor cells. The spread of MV-Edm-eGFP induced multinuclear syncytia of U87 cells (Figures 3Ag and h) and caused their death (Figure 3B). Low numbers of BOEC/MV-Edm sufficed to cause a strong bystander effect on U87 glioma cells (Figure 3B). These data show that MV-Edm efficiently spread from BOECs to tumor cells and kill them.

MV-Edm protected within BOECs from measles antibodies infect bystander tumor cells in the presence of measles immune serum

Clinical application of MV-Edm as an oncolytic virus faces the potential hurdle of pre-existing measles antibodies in

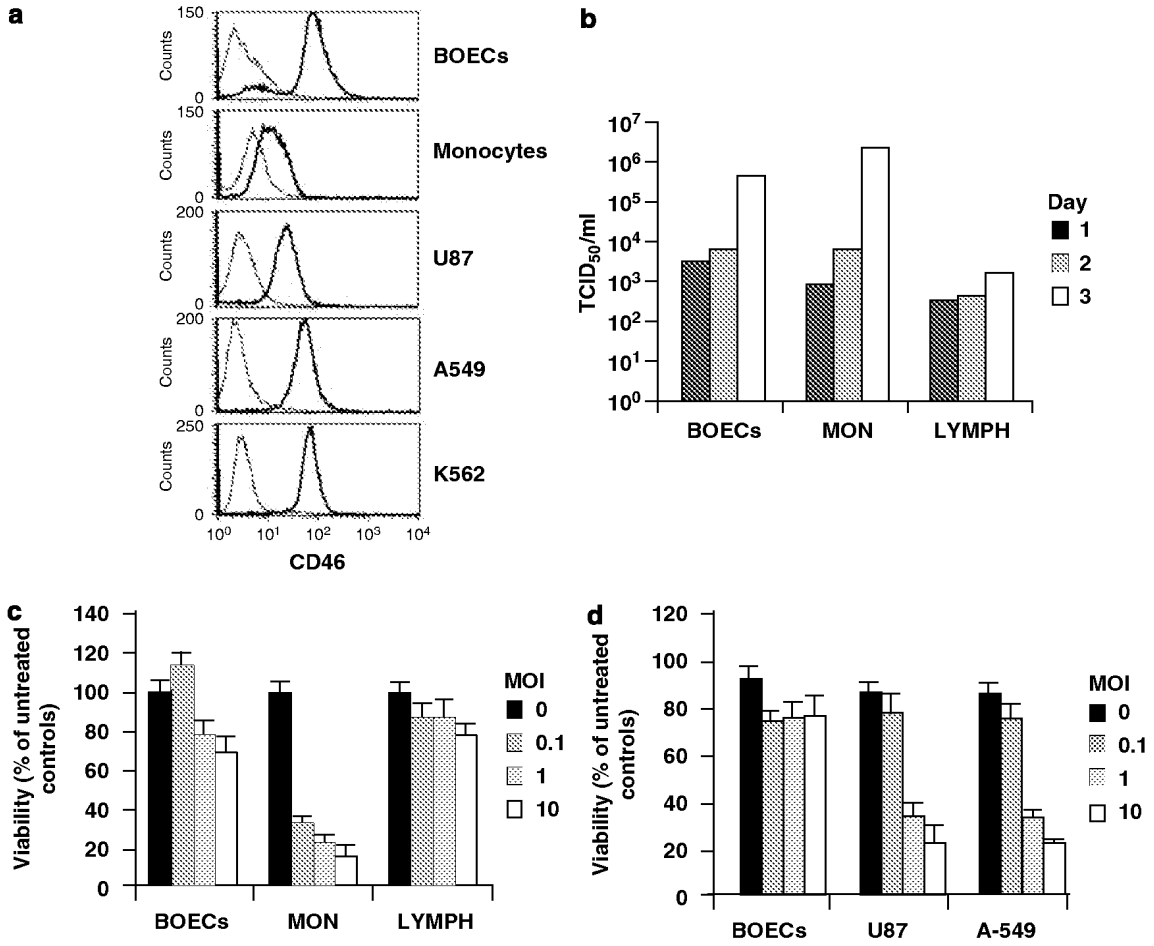

Figure 1 BOECs (blood outgrowth endothelial cells) allow efficient replication of MV-Edm, while being transiently resistant to measles viruses of the Edmonston B strain (MV-Edm)-induced cell death. (**a**) BOECs strongly express CD46, as do human U87 glioma, A549 lung carcinoma and K562 myelomonocytic leukemia cells. Cell surface expression of CD46 was determined by fluorescence-activated cell sorting analysis using anti-CD46 and isotype-matched control antibodies (bold and thin lines, respectively). Similar results were obtained in two independent experiments. (**b**) MV-Edm efficiently replicate within BOECs. BOECs, human monocytes (MON) and human lymphocytes (LYMPH) were infected with MV-Edm at a MOI of 2. At the time points indicated, MV-Edm was procured from cell lysates and Vero indicator cells were infected. Shown is the $TCID_{50}$ per ml of cell lysate supernatant. (**c**) BOECs are initially resistant to MV-Edm-induced cell death. BOECs, human monocytes and human lymphocytes were seeded in 96-well plates (2×10^3 BOECs, 2×10^4 monocytes and 2×10^5 lymphocytes per well) and infected with MV-Edm at increasing MOIs. Cell viability was determined 3 days after infection by the MTT (3-(4, 5-dimethyl-2-thiazolyl)-2,5-diphenyl-2*H*-tetrazolium bromide) assay. Results are means of six duplicates and are expressed as percentage of untreated controls. (**d**) U87 glioma cells are susceptible to MV-Edm-induced cell death. BOECs, U87 glioma cells and A549 lung carcinoma cells were seeded at 2×10^3 cells per well in 96-well plates. Cell viability was determined by MTT assay 3 days after infection by MV-Edm with increasing MOIs. Results are means of six duplicates and are expressed as percentage of untreated controls. Similar results were obtained in two independent experiments.

most patients. Indeed, infection of U87 by MV-Edm was almost completely abrogated by human MV immune serum (Figure 4Aa), which rescued the viability of U87 cells (Figure 4Ac, upper panels). Of note, just 1% immune serum sufficed to prevent MV-Edm-induced cell death (Figure 4Ac). In contrast, MV antibody-negative serum did not prevent infection (Figure 4Ab) and cell death (Figure 4Ac, lower panels) of U87 cells by MV-Edm.

We reasoned that BOECs should protect MV-Edm from neutralization by human measles antibodies. To simulate the situation that would occur in immune hosts immediately after i.v. injection of BOEC/MV-Edm, we first exposed BOEC/MV-Edm to human measles immune serum for a short period of time (30 min) before adding them to U87 cells. As shown in Figure 4B, 48 h later MV-Edm had spread to surrounding U87 cells and formed syncytia, even when BOEC/MV-Edm had been preincubated with measles immune serum at concentrations as high as 90% (Figure 4B, right panel). In contrast, when MV-Edm was exposed to immune serum, the infectious capability of MV-Edm on tumor cells was neutralized (Figure 4B, left panel).

Next we wanted to know whether the protection of MV-Edm provided by the BOECs would allow the spread of MV-Edm during continuous exposure to human measles immune serum. After a 30 min preincubation with measles immune serum, BOEC/MV-Edm were added to U87 glioma cells in the presence of 90% measles immune serum. Indeed, despite the continuous presence of measles antibodies, MV-Edm-eGFP spread from a single BOEC/MV-Edm-eGFP (Figure 4Cb, arrow) to surrounding U87 cells and to more distant tumor cells, eventually causing the formation of a syncytium (Figure 4Cd). This suggests that the spread of MV-Edm from

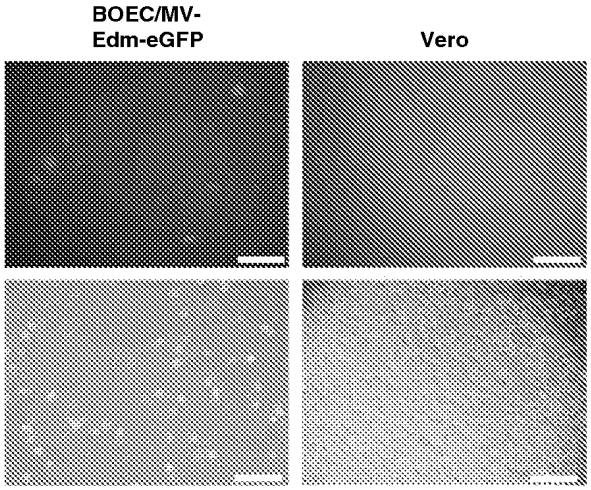

Figure 2 BOECs do not carry adsorbed MV-Edm-eGFP on their surface shortly after infection with MV-Edm-eGFP. BOECs were infected with MV-Edm-eGFP at a MOI of 2 for 3 h in OptiMEM and washed with phosphate-buffered saline. After incubation for 1 h in growth medium, BOECs were trypsinized and resuspended in OptiMEM. The cell suspension was centrifuged and the cell-free supernatant was added to Vero cells. The infected BOEC/MV-Edm-eGFP were replated in complete growth medium. The left panels show adherent BOEC/MV-Edm-eGFP 48 h after infection; the right panel, Vero cells after 72 h of incubation with supernatant. Scale bars represent 100 μm. BOECs, blood outgrowth endothelial cells; MV-Edm, measles viruses of the Edmonston B strain.

BOECs to cancer cells and from cancer cells to cancer cells is protected against human measles antibodies because spread proceeds by cell-to-cell contact.

Intratumoral administration of BOEC/MV-Edm significantly prolongs the life of mice with orthotopic U87 gliomas

To determine whether BOEC/MV-Edm exert a tumor inhibitory effect *in vivo*, we injected BOEC/MV-Edm stereotactically into U87 gliomas growing in the striatum of mice. Survival of mice was significantly prolonged compared to controls, which received intratumoral injections of phosphate-buffered saline (PBS) (Figure 5, red and black lines, respectively). The therapeutic efficacy of BOEC/MV-Edm was similar to MV-Edm injected intratumorally (blue line). Since noninfected BOECs do not kill tumor cells[21] this indicates that MV-Edm spread from BOEC/MV-Edm to tumor cells and killed them.

I.v. injected BOECs home to orthotopic U87 gliomas and, when armed with MV-Edm, decrease tumor size

We first confirmed that BOECs target orthotopic gliomas. Since irradiation has been shown to promote homing of hematopoietic progenitors toward gliomas,[19] cranial irradiation was employed prior to i.v. injection of BOECs. Because the autofluorescence of U87 gliomas complicates the interpretation of fluorescent signals, BOECs were labeled *ex vivo* with BrdU. Anti-BrdU staining showed i.v. injected BOECs within the gliomas but not in surrounding normal brain tissue (Figures 6Aa–c).

Next, we determined whether BOEC/MV-Edm given i.v. prolong the life of mice with orthotopic U87 gliomas. After five i.v. injections of BOEC/MV-Edm (denoted by arrows in Figure 6B), there was only a slight, albeit statistically significant, survival advantage (Figure 6B, red line) compared to control mice treated with uninfected BOECs or PBS (green and black lines, respectively). Mice treated with cell-free MV-Edm i.v. (blue line) survived significantly longer than both the control and the BOEC/MV-Edm-treated groups.

Magnetic resonance imaging (MRI) images of fixed brains of mice that died on day 28 revealed significantly smaller tumors in mice treated with BOEC/MV-Edm when compared to nontreated mice (Figure 6C). When tumor volumes were calculated from the MRI images, the volume of gliomas treated with BOEC/MV-Edm was clearly smaller than that of untreated gliomas (Figure 6C).

Peritumorally injected BOEC/MV-Edm migrate to orthotopic U87 gliomas

Given the infiltrative nature of gliomas leading to small clusters of glioma cells that initially lack vessels, an efficient cellular vehicle has to search for glioma cells navigating through normal brain tissue. Since a robust infiltrative human glioma mouse model is lacking, we investigated cell migration by injecting BrdU-labeled BOEC/MV-Edm into normal brain tissue surrounding U87 gliomas. Two days after BOEC injection, BOECs were visualized by anti-BrdU staining. While the majority of BOECs remained at the injection site (Figure 7Aa), numerous BOECs migrated toward the tumor (Figure 7Ab) and accumulated there (Figure 7Ac). To determine the presence of measles virus in the glioma, adjacent sections were stained separately with anti-measles hemagglutinin antibody and anti-BrdU, thus avoiding the pitfalls of immunohistochemical double staining. BrdU-positive BOECs were seen at sites where MV were detected (compare the MV-containing cells in Figure 7Bc with the BOECs in Figure 7Bd). This indicates that the peritumorally injected BOEC/MV-Edm carried MV-Edm to the tumor mass.

We then investigated whether BOECs target orthotopic gliomas in mice passively immunized against measles virus. Intraperitoneal injection of human measles antibodies generated levels of measles-specific immunoglobin G (IgG) antibodies in the blood known to prevent measles in humans (ELISA index greater than 1.1). Such preventive levels were found at 1 h, increased at 6 h and were still present 28 h after injection (data not shown). The presence of antibodies against measles virus did not preclude that many BOEC/MV-Edm injected peritumorally migrated into the tumor (Figures 7Ca–c). Only very few BOEC/MV-Edm migrated into the normal brain tissue (Figures 7Ca–c).

To address the specificity of homing of BOECs, we injected BrdU-labeled human fibroblasts peritumorally into glioma-bearing mice (Figure 7Da). The fibroblasts did not migrate into the gliomas (Figure 7Db) nor into the surrounding normal brain tissue (Figure 7Dc). Thus, the ability of BOECs to target gliomas is specific.

Peritumorally injected BOEC/MV-Edm significantly prolong survival of mice with orthotopic U87 gliomas by focal infection

Having shown the tumor searching capability of BOEC/MV-Edm navigating through the brain, we wanted to clarify whether peritumorally applied BOEC/MV-Edm prolong survival of mice with orthotopic U87 gliomas.

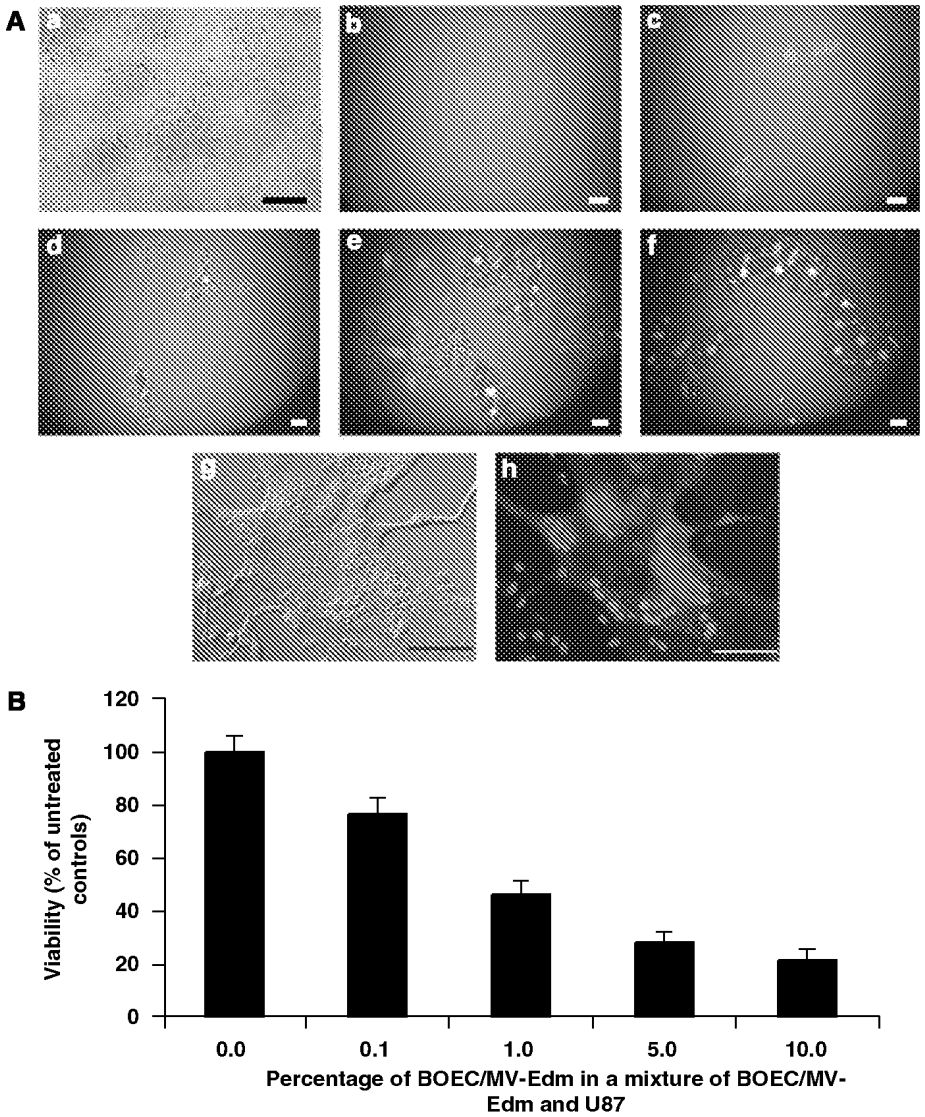

Figure 3 MV-Edm spread from BOEC/MV-Edm to surrounding U87 glioma cells and exert a strong bystander effect. BOECs were infected with MV-Edm-eGFP at a MOI of 2 for 24 h (BOEC/MV-Edm-eGFP) and added to U87 cells seeded at 2×10^3 cells per well in collagen I-coated 96-well plates in pentaplicates. (**A**) MV-Edm-eGFP spread from BOEC/MV-Edm-eGFP to U87 cells. BOEC/MV-Edm-eGFP were added to U87 cells (a; phase contrast). Spread of MV-Edm-eGFP was monitored by fluorescence microscopy at time points 2 h (b), 24 h (c), 48 h (d), 72 h (e) and 96 h (f) after the addition of MV-Edm-eGFP. A syncytium of U87 cells induced by a single BOEC/MV-Edm-eGFP is seen at 72 h after the addition of BOEC/MV-Edm-eGFP (g and h). Nuclei were stained by Hoechst 33258. Scale bars = 200 μm (a–f) and 100 μm (g and h). (**B**) BOEC/MV-Edm exert a strong bystander effect on U87 glioma cells *in vitro*. BOEC/MV-Edm-eGFP were added to U87 cells at shares indicated and viability was determined by MTT assay after 4 days. Results are expressed as percentage of untreated controls. Means and standard deviations of pentaplicates are shown. Similar results were obtained in three independent experiments. MV-Edm, measles viruses of the Edmonston B strain; BOECs, blood outgrowth endothelial cells.

After three sequential peritumoral injections at alternating sites (Figure 8A), mice treated with BOEC/MV-Edm (Figure 8B, red line) survived significantly longer than those injected with BOECs (green line) or with PBS (black line). Importantly, mice treated with BOEC/MV-Edm survived longer than MV-Edm-treated mice (blue line). This shows that tumor control is enhanced when the immobile MV-Edm are delivered by tumor targeting BOECs to the tumor.

The extent of intratumoral spread of MV-Edm after peritumoral injection of BOEC/MV-Edm was investigated in a subset of mice at the time of death. Syncytium formation by MV-Edm and persistent infection by MV-Edm without formation of syncytia was clearly focal, with large areas of unaffected tumor tissue surrounding islands of affected tissue (Figure 8C).

Discussion

Inefficient delivery of therapeutic modalities and isolation of glioma cells due to infiltrative growth are major hurdles toward improving the poor prognosis of malignant gliomas. We show that replicating oncolytic

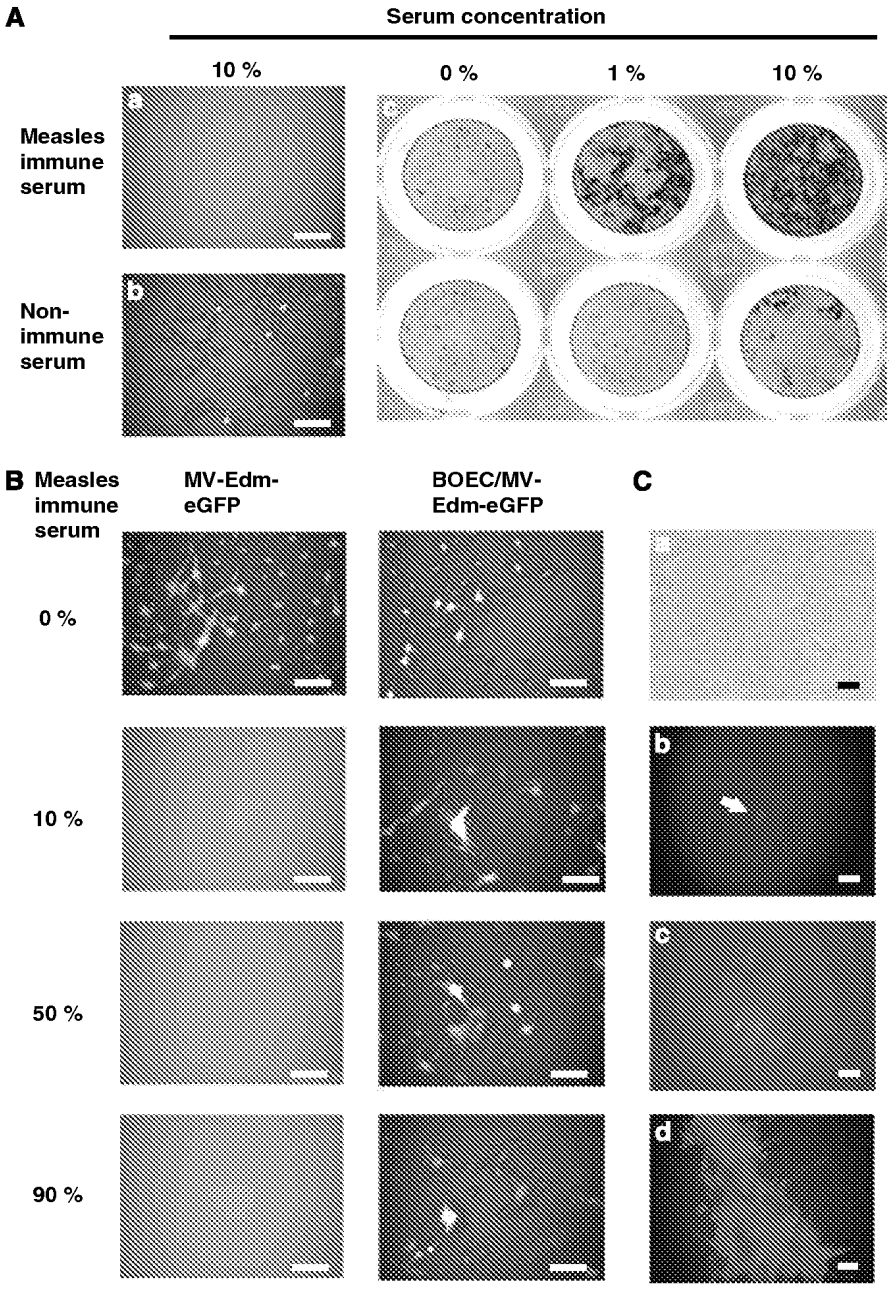

Figure 4 MV-Edm protected within BOECs from human measles immune serum spread to and kill bystander tumor cells. (**A**) Human measles immune serum prevents MV-Edm-eGFP from infecting and killing U87 cells. MV-Edm-eGFP were incubated with human measles immune serum or with human nonimmune serum at concentrations of 0, 1 and 10% for 30 min at 37 °C and then added at a MOI of 5 to U87 cells seeded at 2×10^3 cells per well on 96-well plates. The spread of MV-Edm-eGFP and syncytia formation was monitored by fluorescence microscopy at 72 h after infection (a and b, scale bars = 500 μm). Cell viability was determined by crystal violet staining at 96 h after infection (c). (**B**) BOECs protect MV-Edm from exposure to human measles immune serum, thus allowing their spread to U87 cells. BOEC/MV-Edm-eGFP and MV-Edm-eGFP were incubated with measles immune serum for 30 min at concentrations indicated before being added to U87 cells. MV-Edm-eGFP at a MOI of 5 (left panel) or 2×10^2 BOEC/MV-Edm-eGFP cells (right panel) were added to 2×10^3 U87 cells per well in a 96-well plate. Spread of MV-Edm-eGFP and syncytia formation was observed by fluorescence microscopy at 48 h after infection (scale bars = 500 μm). (**C**) MV-Edm can spread from BOECs to U87 cells in the continuous presence of human measles immune serum. 2×10^2 BOEC/MV-Edm-eGFP preincubated for 30 min with 90% measles immune serum were transferred to 2×10^3 U87 cells per well in a 96-well plate containing medium with 90% measles immune serum (a, phase contrast, scale bar = 25 μm). The spread of MV-Edm-eGFP and syncytia formation was monitored by fluorescence microscopy at 18 h (b), 48 h (c) and 72 h (d). Scale bar = 100 μm for (b–d). MV-Edm, measles viruses of the Edmonston B strain; BOECs, blood outgrowth endothelial cells.

MV-Edm carried within BOECs to malignant gliomas may be one approach to overcome these hurdles. BOECs protected MV-Edm from human measles serum antibodies, homed to brain tumors and carried MV-Edm through normal brain tissue to the tumors. Subsequently, MV-Edm released from BOECs infected brain tumor cells causing shrinkage of tumors, which prolonged the life of tumor-bearing mice.

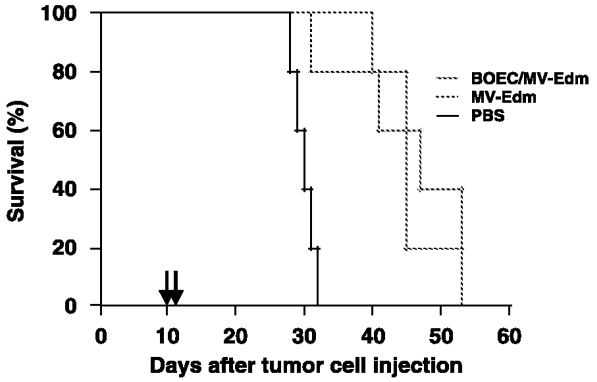

Figure 5 Intratumorally injected BOEC/MV-Edm significantly prolong the life of mice with orthotopic U87 gliomas. 5×10^5 U87 glioma cells were stereotactically injected into the right striatum of 10- to 12-week-old male $Rag2^{-/-}c\gamma c^{-/-}$ mice. Ten days later, mice were randomized into three groups ($n = 5$ for each group). The treatment groups received two intratumoral injections (denoted by arrows) spaced 1 day apart of either 2×10^5 BOEC/MV-Edm or 3×10^5 PFU MV-Edm, while the control group received PBS. Survival was determined and plotted for Kaplan–Meier survival analysis and analyzed by log-rank test. Compared to PBS (black line), survival of both BOEC/MV-Edm (red line) and MV-Edm (blue line) was prolonged ($P = 0.0088$ and 0.0018, respectively). BOECs, blood outgrowth endothelial cells; MV-Edm, measles viruses of the Edmonston B strain; PBS, phosphate-buffered saline.

For this approach to be successful, several prerequisites have to be met in sequence: easy procurement of BOECs, efficient infection of BOECs by MV-Edm, replication of MV-Edm within the BOECs, resistance of BOECs to MV-Edm-induced early cell death, protection of MV-Edm against MV-neutralizing serum activity, efficient homing and specific migration of MV-Edm-infected BOECs to glioma cells, proficient infection of glioma cells by MV-Edm from BOECs, intratumoral spread of MV-Edm within the glioma and finally killing of the infected glioma cells.

The ease of BOEC generation as well as determinants of efficacy concerning their use in gene therapy of peripheral metastases has been established previously.[20,21]

MV-Edm infected and efficiently replicated within BOECs without killing them during the first few days after infection. This predisposes BOECs to be carriers for MV-Edm as compared to other blood-derived cells such as monocytes, which were rapidly killed by replicating MV-Edm, and lymphocytes, which did not allow MV-Edm to replicate sufficiently. BOECs were resistant to MV-Edm-induced cell death despite the strong expression of CD46, known not only to function as the entry receptor for MV but also to determine the degree of cell death.[6] The multitude of antiapoptotic mechanisms operative in endothelial cells most likely accounts for this resistance. These mechanisms include VEGF-induced PI3K-mediated signaling, nuclear factor-κB activation and strong expression of Bcl-2, survivin and XIAP, and of antioxidative enzymes such as MnSOD, catalase and glutathione peroxidase (reviewed in Jarmy *et al.*[16]).

Many cell types infected with MV-Edm are killed by complement-mediated lysis, which is facilitated by downregulation of CD46, an inhibitor of complement-mediated lysis, after MV-Edm infection.[22] Of note, BOEC/MV-Edm were not killed when subjected to human measles immune serum containing complement. CD46 may not have been downregulated yet and MV proteins may not have appeared yet on the surface of infected BOECs during the time of transit to the tumor. Furthermore, the degree of downregulation of CD46 may be limited in BOECs. Further studies will elucidate the mechanisms involved.

Homing of BOEC/MV-Edm into gliomas also occurred when measles virus antibodies were present at levels sufficient to protect humans from measles. It remains to be shown whether BOEC/MV-Edm are susceptible to T cell-mediated destruction. The low number of T cells in cancer patients secondary to disease and previous chemotherapy may reduce this potential problem. T cells may also exert a beneficial effect by reacting against MV-Edm-infected tumor cells, thus enhancing the oncolytic effect of MV-Edm.

Specific and efficient homing of BOEC/MV-Edm to gliomas is crucial for their therapeutic efficacy. Intravenously injected BOECs homed into irradiated orthotopic U87 malignant gliomas, but did not sequester into normal brain tissue. More importantly, when BOEC/MV-Edm were injected peritumorally to simulate the situation in the patient, where BOEC/MV-Edm have to reach isolated glioma cells not yet connected to blood vessels, BOEC/MV-Edm navigated through normal brain tissue to the glioma mass. Migration appeared to be directional, because far more BOEC/MV-Edm were seen within the glioma than in the normal brain tissue surrounding the injection site and since human fibroblasts injected in the same manner did not target gliomas. It is important to note that infection with MV-Edm did not preclude migration of peritumorally injected BOECs, even in mice immune against measles virus.

Cranial irradiation was employed assuming that it would increase migration of BOECs to gliomas as has been described for hematopoietic stem cells. However, we could not demonstrate increased infiltration of BOECs into irradiated tumor spheroids;[23] thus the role of irradiation in the homing of BOECs remains to be elucidated.

Once at the glioma cells, MV-Edm residing within the BOECs have to infect the glioma cells. This was indeed the case, despite the heterologous nature of BOECs and glioma cells. We have no evidence that infection of surrounding cells occurred by MV-Edm-eGFP that remained loosely adsorbed on the surface of BOECs following their infection with MV-Edm-eGFP *ex vivo*. However, it remains possible that some MV-Edm-eGFP strongly tethered to the BOECs surface may have contributed to the infection of tumor bystander cells.

After infection of glioma cells surrounding the BOEC/MV-Edm, the virus spread to more distal glioma cells and killed them. *In vitro*, a few BOEC/MV-Edm sufficed to infect a far larger number of glioma cells and to kill most of them. *In vivo*, glioma cells were infected and killed by intratumorally injected BOEC/MV-Edm leading to a significant survival benefit of glioma-bearing mice indistinguishable from those receiving intratumorally injected MV-Edm. Of note, despite the presence of MV-neutralizing serum antibodies *in vitro*, MV-Edm spread from BOECs to surrounding and then to more distant glioma cells inducing syncytia. This shows that U87 glioma cells can be controlled by BOEC/MV-Edm in the face of natural MV-neutralizing activity. As a corollary, spread by tumor-cell-to-tumor-cell contact, as

has been described for MV-Edm in other tumors,[7,8] appears to be the relevant route MV-Edm can spread in U87 gliomas.

We show that i.v. injected BOEC/MV-Edm home specifically to orthotopic U87 gliomas and that BOEC/MV-Edm decrease the size of the tumors, as detected by MRI. However, because the responses were partial (with some tumors continuing to grow into the brain stem, as in Figure 6Ce), the survival benefit was minute. In contrast, i.v. injected cell-free MV prolonged survival more pronounced than i.v. injected BOEC/MV-Edm. It is known that some i.v. injected BOECs are sequestered in the lung and the spleen.[21] Sequestration of i.v. injected MV-Edm may be less, which could explain their increased efficacy. In addition, the blood–brain barrier is less permeable for large cells such as BOECs than for viruses with their smaller size. This may also have led to increased extravasation of MV-Edm into the cerebrospinal fluid and thus to increased infection of tumors abutting the ventricle.

I.v. injection of MV-Edm will not be feasible in most patients, given their immunity against measles. BOEC/MV-Edm are not affected by measles antibodies; however, they show limited efficacy against gliomas when given i.v. Thus, intracranial injection of BOEC/MV-Edm is an obvious route to ensure high-level and consistent delivery. We injected BOEC/MV-Edm peritumorally to mimic the clinical situation, where BOECs would have to

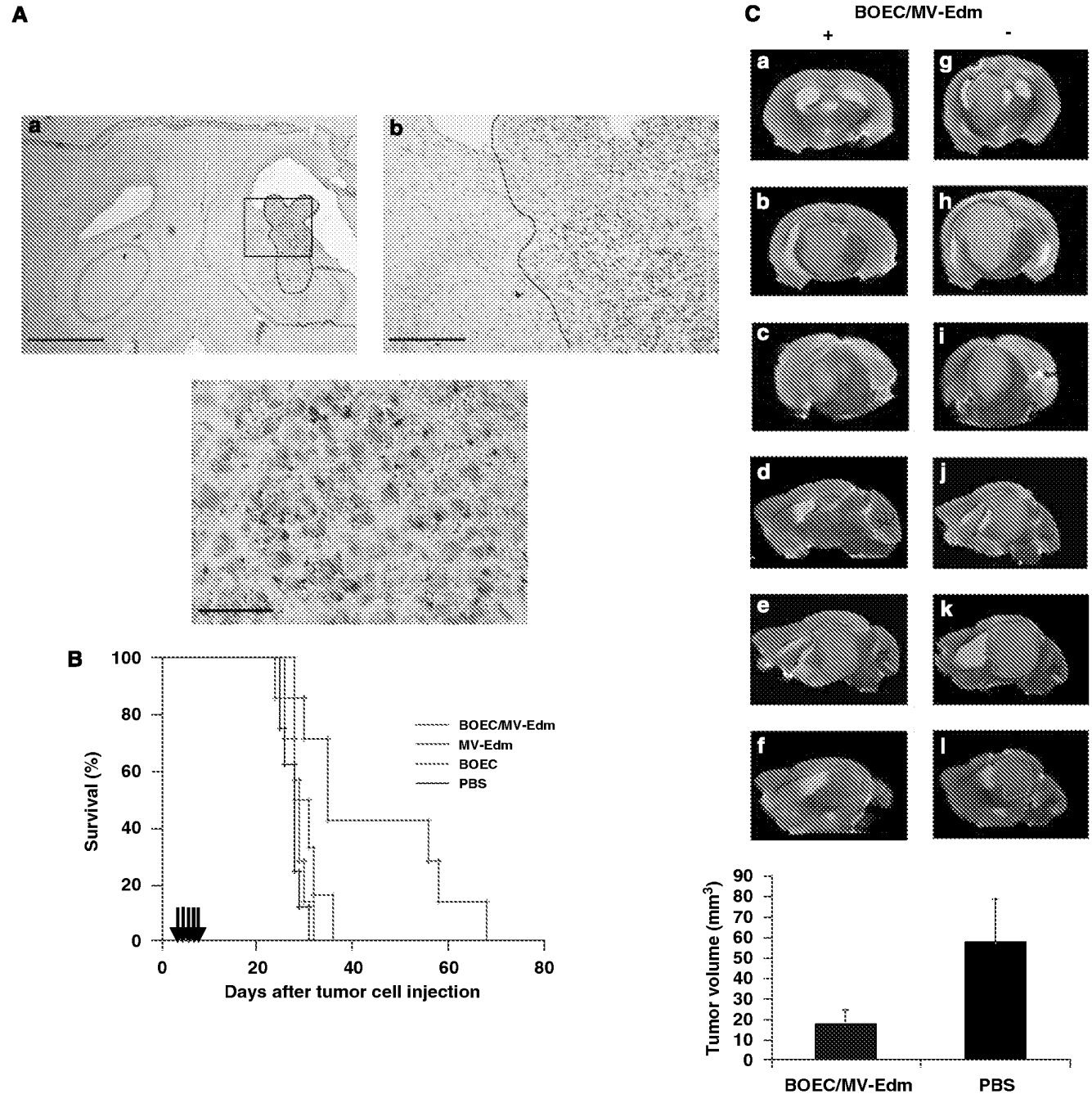

migrate to isolated clusters of glioma cells. BOEC/MV-Edm navigated through normal brain tissue, infected glioma cells and killed them, thus significantly prolonging the life of glioma-bearing mice. Therefore, BOEC/MV-Edm have the search-and-destroy capability to target infiltrative gliomas. Surprisingly, there was a survival benefit of peritumorally injected MV-Edm. Thus, some of the MV must have found their way into the tumor despite their immobility. This most likely occurred by convection of the small MV-Edm to the tumor by increased hydrostatic pressure due to the large carrier volume applied during the injections of MV-Edm. This factitious convection-enhanced delivery of MV-Edm was nevertheless inferior to delivery via the actively tumor searching BOECs, since there was a clear trend toward increased survival for BOEC/MV-Edm. Again, in the measles immune glioma patient, cell-free MV-Edm may be subjected to neutralization, in contrast to MV-Edm protected within BOECs, adding to the superiority of BOEC/MV-Edm over MV-Edm when applied intracranially.

For glioma abutting or growing into the ventricles (as in Figure 6Aa), intrathecal injection of BOEC/MV-Edm may be the most efficient route of delivery.

While tumor size decreased and survival was prolonged upon administration of BOEC/MV-Edm, no cures were achieved since responses were partial, as shown by MRI. Intratumoral heterogeneity of response was reflected on the cellular level. After peritumoral injection, BOEC/MV-Edm infiltrated and infected large parts of the tumors. At the time of death, however, the distribution of syncytia and MV-Edm-infected cells was focal. There are several explanations for this finding. First, proliferation of uninfected tumor cells must have outpaced the spread of MV, in line with recent findings in experimental ovarian carcinoma.[24] It remains to be determined whether attenuation of the spread of MV-Edm contributes to this. Second, the presence of foci of persistent MV-Edm infection without cytopathic effect suggests resistance of tumor cells to MV-Edm-induced cell death. Finally, the migratory function of BOECV/MV-Edm within the tumor must have subsided, most likely because MV-Edm finally overcame the resistance of BOECs to early cell death. Elucidating the mechanisms of intratumoral virus spread and of MV-Edm-induced cell death, and modulating them, such as by arming MV-Edm with additional tumor cytotoxic effectors,[11,25,26] will address the challenge of increasing the efficacy of BOEC/MV-Edm for therapy of gliomas and other tumors.

Several oncolytic viruses in diverse cellular vehicles have been successful in preclinical studies. These encompass herpes simplex virus-1 in human teratocarcinoma cells,[27] retrovirus in outgrowth endothelial cells,[28] retrovirus on antigen-specifc T cells[29] and modified vaccinia virus in cytokine-induced killer cells.[30] Their relative merit for glioma therapy has yet to be defined. The nonintegrating MV do not carry the risk of insertional mutagenesis, unlike retroviruses. Not all the positive features of BOECs are shared by the other cellular vehicles that have been used to carry oncolytic viruses to experimental tumors. Tumor antigen-specific T cells, for example, are complex to generate,[29] a feature they share with neural progenitors that target experimental brain tumors,[31] and may lack the ability to navigate through normal brain tissue. The latter may also apply to cytokine-induced killer cells.[30]

In conclusion, BOEC/MV-Edm warrant to be included in future studies of cellular vehicles carrying oncolytic viruses for the therapy of gliomas.

Materials and methods

Cell culture

Tissue culture media and supplements were obtained from Life Technologies (Eggenstein, Germany) unless stated otherwise. BOECs were isolated from human adult peripheral blood, propagated as described[16] and cultured in ECBM-2 medium (PromoCell, Heidelberg, Germany) supplemented with SupplementPack (PromoCell) and 10% fetal calf serum (FCS) (Biochrom, Berlin, Germany). Human mononuclear cells were isolated from peripheral blood cells and separated into monocytes and lymphocytes by adherence to plastic. Monocytes were maintained in Dulbecco's modified Eagle's medium (DMEM) supplemented with 10% FCS and 15% human serum. Lymphocytes were cultivated in RPMI supplemented with 10% FCS, 50 μM 2-mercaptoethanol, 1 mM pyruvate and 30 U ml^{-1} interleukin-2 (Pepro Tech, Rocky Hill, NJ, USA). U87, K-562 cells and Vero cells were

Figure 6 I.v. applied BOECs target orthotopic U87 gliomas and, when carrying MV-Edm, decrease tumor size. 5×10^5 U87 glioma cells were injected stereotactically into the right striatum of 8- to 12-week-old male $Rag2^{-/-}c\gamma c^{-/-}$ mice. (**A**) BOECs home to U87 gliomas in the brain when given by tail vein injection. Fourteen days after tumor cell injection, the brain of U87 glioma-bearing mice was γ-irradiated with a dose of 6 Gy. Three days later, the mice received tail vein injection of BOECs pulsed with BrdU (BOEC-BrdU, $n = 3$). Organs were procured 1 day later, cryosectioned, immunohistochemically stained using anti-BrdU antibody to detect BOEC-BrdU and counterstained with hematoxylin. A U87 glioma outlined in red is seen in the right striatum (a, scale bar = 1 mm). Higher magnification of the black frame in (a) shows BrdU-positive (red-stained) BOECs in the glioma, but not in the surrounding normal brain tissue (b, scale bar = 200 μm). Higher magnification of the yellow frame in (b) demonstrates accumulation of BOECs in the glioma (c, scale bar = 50 μm). (**B**) I.v. injected BOEC/MV-Edm just slightly prolong the life of mice with orthotopic U87 gliomas. Four days after tumor cell injection, mice received cranial γ-irradiation with a dose of 6 Gy and were randomized into four groups on day 6 followed by daily i.v. injections for 5 days (indicated by arrows). The treatment groups received BOEC/MV-Edm or MV-Edm and the control groups BOECs or PBS. Compared to control mice treated with PBS (black line) or BOECs (green line), survival of mice injected with BOEC/MV-Edm (red line) was slightly prolonged ($P = 0.0498$), whereas mice treated with MV-Edm (blue line) had a more pronounced survival benefit ($P = 0.0035$). Statistical testing was by log-rank test. (**C**) I.v. injected BOEC/MV-Edm decrease the size of orthotopic gliomas. Three mice treated with BOEC/MV-Edm and three untreated control mice died on day 28. The brains of these mice were procured, fixed in 4% paraformaldehyde and subjected to serial MRI. The upper panel shows corresponding axial planes in an anterior to posterior order (a–c and g–i) and sagittal planes in a left to right order (d–f and j–l) of two representative mice that either received or did not receive BOEC/MV-Edm (+ or −). The gliomas are outlined in red. Smaller size of the gliomas treated with BOEC/MV-Edm is discernible as absence or smaller area of tumor on corresponding planes. The lower panel depicts the means and standard deviations of the tumor volumes calculated from the MRI scans. I.v. intravenously; BOECs, blood outgrowth endothelial cells; MV-Edm, measles viruses of the Edmonston B strain; PBS, phosphate-buffered saline; MRI, magnetic resonance imaging.

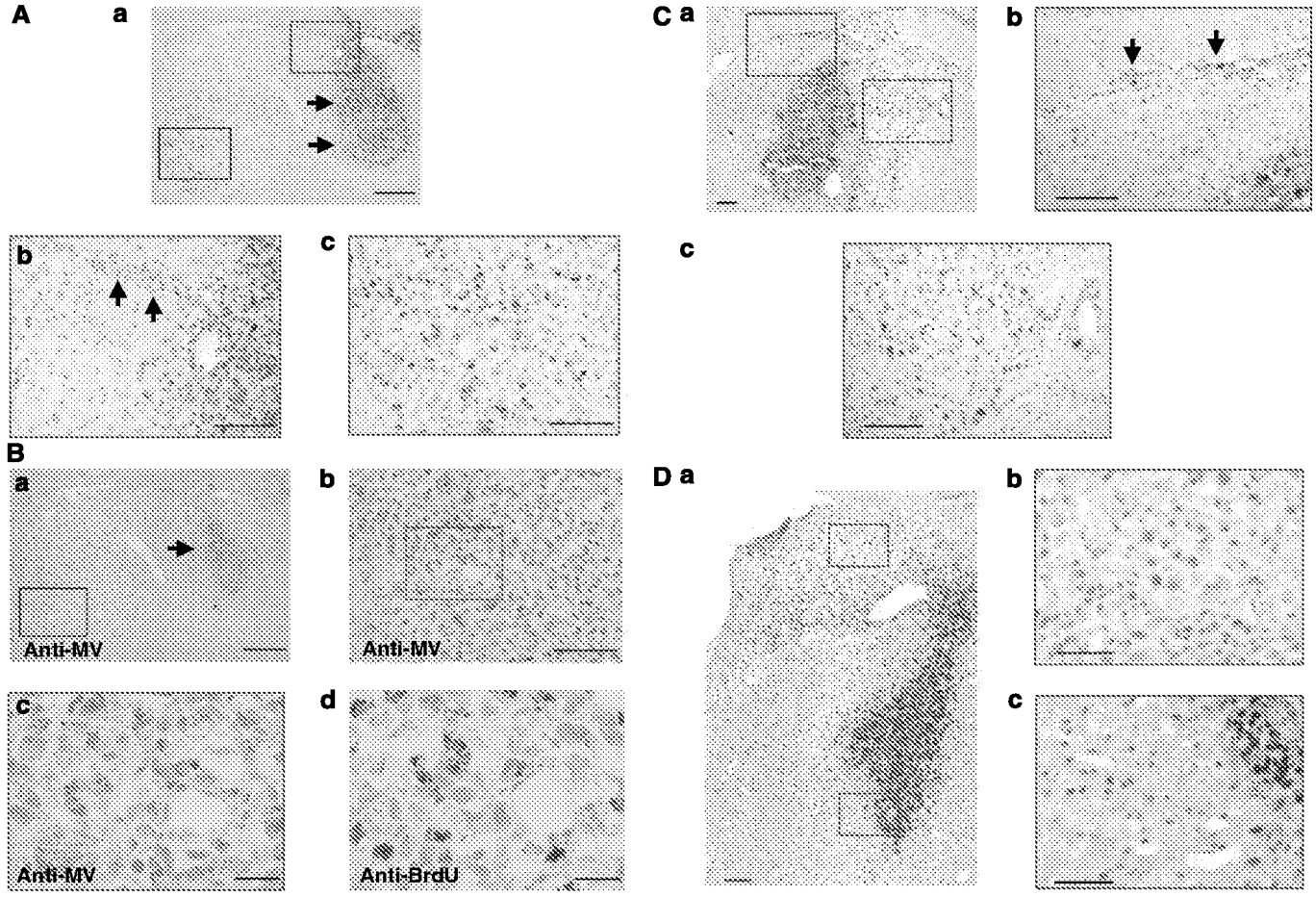

Figure 7 Peritumorally injected BOEC/MV-Edm specifically target orthotopic U87 gliomas in nonimmune mice and in mice passively immunized against measles. 5×10^5 U87 glioma cells were stereotactically injected into the right striatum of 8- to 10-week-old male $Rag2^{-/-}c\gamma c^{-/-}$ mice. Ten days after tumor cell injection, mice received 6 Gy of γ-irradiation to the brain. Three days later, BOECs pulsed with BrdU and infected with MV-Edm were injected peritumorally into mice that were not immunized (**A**, **B**; $n=3$) or immunized by intraperitoneal injection of 500 µl human measles immune serum 18 h prior to injection of BOEC/MV-Edm (**C**; $n=3$). (**A**) BOEC/MV-Edm navigate within the brain of nonimmunized mice to U87 gliomas. Brains were procured 2 days later and cryosectioned horizontally. BOECs were detected by anti-BrdU immunohistochemical staining. Counterstaining was by hematoxylin. In (a) (scale bar = 1 mm), BrdU-positive BOECs (red-stained nuclei) are seen deposited at the end of the injection canal (arrows) lateral of the hypercellular glioma. Higher magnification of the red-framed area in (a) shows a stream of BrdU-positive BOECs migrating (arrows) toward the tumor (b, scale bar = 100 µm). Higher magnification of the blue frame in (a) depicts BrdU-positive cells accumulating within the tumor (c, scale bar = 100 µm). (**B**) The distribution of intratumoral MV-Edm mirrors the intratumoral spread of BOEC/MV-Edm. Adjacent cryosections were stained by anti-BrdU for BOEC/MV-Edm and by anti-measles hemagglutinin for MV-Edm. Low magnification (a, scale bar = 250 µm) shows MV-Edm-containing cells stained red at the injection site (indicated by an arrow). Higher magnification of the blue-framed area reveals MV-positive cells within the tumor (b, scale bar = 100 µm), which are clearly delineated at higher magnification of the red-framed area (c, scale bar = 25 µm). A section adjacent to (c) shows BrdU-positive BOECs (d, scale bar = 25 µm). (**C**) BOEC/MV-Edm navigate to U87 gliomas in passively immunized mice. In these coronal sections, BrdU-positive BOECs (red) are seen at the injection site and in the tumor (a, scale bar = 100 µm). Higher magnification of the blue-framed area in (a) shows BrdU-positive BOECs following a sheath of tumor cells (arrow) without migrating into the normal brain tissue (b, scale bar = 100 µm). Higher magnification of the red frame in (a) delineates BrdU-positive cells spreading within the main tumor mass (c, scale bar = 100 µm). (**D**) Human fibroblasts injected peritumorally do not migrate to U87 gliomas. Human foreskin fibroblasts were injected peritumorally into U87-bearing, cranially irradiated mice. Two days later the brains were procured, stained by anti-BrdU and counterstained by hematoxylin (a, scale bar = 100 µm). Higher magnification of the red- and blue-framed areas shows no migration of the fibroblasts into the glioma (b, scale bar = 50 µm) or the normal brain (c, scale bar = 50 µm), respectively. BOECs, blood outgrowth endothelial cells; MV-Edm, measles viruses of the Edmonston B strain.

obtained from ATCC (Manassas, VA, USA) and A549 was obtained from the German Collection of Microorganisms and Cell Cultures (Braunschweig, Germany). K-562 cells were maintained in RPMI and all other tumor cell lines were grown in DMEM. Cell culture media for cell lines were supplemented with 10% FCS, 2 mM glutamine, 2 mM nonessential amino acids, 100 U ml^{-1} penicillin and 100 µg ml^{-1} streptomycin.

Virus production and infection

The construction of MV-Edm-eGFP has been described elsewhere.[32] MV-Edm and MV-Edm-eGFP were propagated by Vero cells with a MOI of 0.02 in 2 ml OptiMEM (Life Technologies) at 37 °C for 3 h. The medium was changed to DMEM supplemented with 5% FCS and cells were incubated at 37 °C for 1 day before being transferred to 32 °C for another day. Cells were harvested

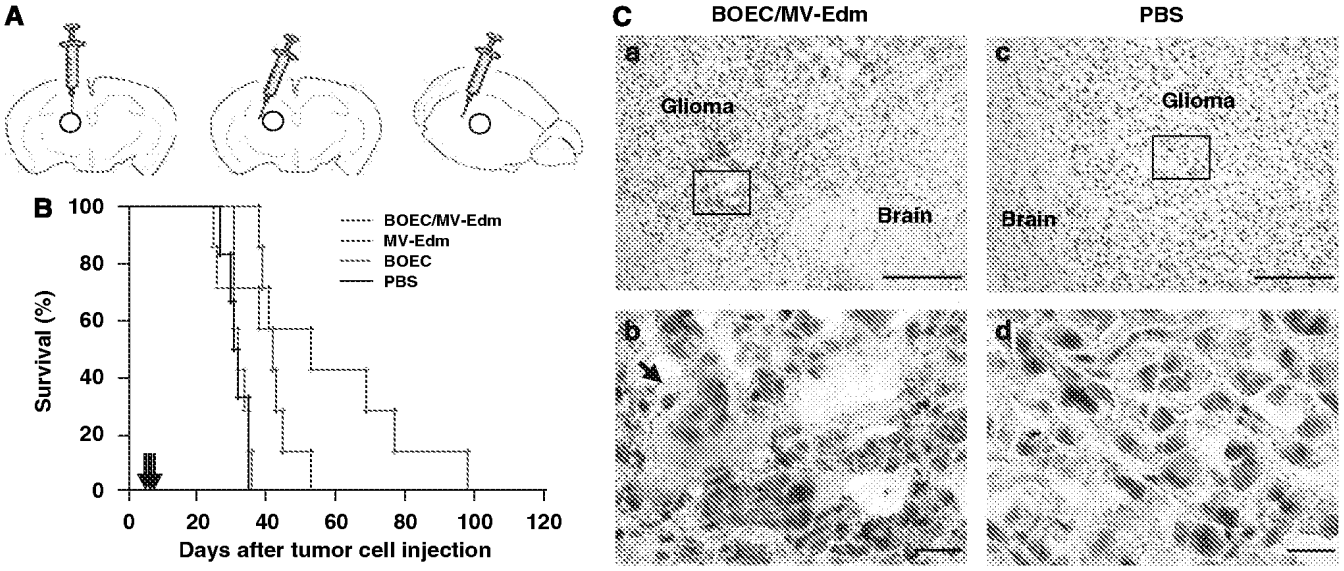

Figure 8 Peritumorally injected BOEC/MV-Edm significantly prolong survival of mice with orthotopic U87 gliomas by focal infection. 5×10^5 U87 glioma cells were stereotactically injected into the right striatum of 8- to 10-week-old male $Rag2^{-/-}c\gamma c^{-/-}$ mice. Four days after tumor cell injection, the mice received 6 Gy of cranial γ-irradiation. On day 6, the mice were randomized into four groups and received daily peritumoral injections for 3 days at alternating sites. (**A**) Schematic of peritumoral injections. Injections were placed 1 mm superior, 0.5 mm lateral and 0.5 mm posterior to the tumor mass. (**B**) Mice treated with peritumoral injections of BOEC/MV-Edm survive longer. The treatment groups received BOEC/MV-Edm ($n=7$) or MV-Edm ($n=7$) and the control groups BOECs ($n=7$) or PBS ($n=6$). Arrows denote injections. Survival of the mice was determined and plotted for Kaplan–Meier survival analysis. Mice treated with BOEC/MV-Edm (red line) survived longer than control mice receiving BOECs (green line, $P=0.0018$), PBS (black line, $P=0.0031$) or MV-Edm (blue line, $P=0.174$). Statistical testing was performed by log-rank test. (**C**) Persistent infection by MV-Edm and formation of syncytia is focal. Brains of mice that had received BOEC/MV-Edm ($n=3$) or PBS ($n=3$) were analyzed by immunohistochemistry for expression of MV hemagglutinin when they had to be killed. The images of a representative BOEC/MV-Edm-treated mouse that was killed on day 69 (a and b) and of a PBS-treated mouse killed on day 30 (c and d) are shown. Higher magnification of the area framed in (a) reveals red-stained MV-Edm-infected tumor surrounding a syncytium (b, arrow), whereas no MV-Edm can be detected in tumors treated with PBS (c and d). Scale Bars = 200 μm (a and c) and 20 μm (b and d). BOECs, blood outgrowth endothelial cells; MV-Edm, measles viruses of the Edmonston B strain; PBS, phosphate-buffered saline.

and viral particles released by two cycles of snap freezing in liquid nitrogen and subsequent thawing. Viral titers were determined by 50% end-point dilution assays ($TCID_{50}$) on Vero cells.

Infection by MV-Edm or MV-Edm-eGFP in vitro

Tumor cells or BOECs were seeded on tissue culture flasks or plates. The medium was removed and the cells were infected with MV-Edm in OptiMEM for 3 h at 37 °C. The medium was then replaced with appropriate tissue culture media. BOECs infected with MV-Edm are called BOEC/MV-Edm and those infected with MV-Edm-eGFP are called BOEC/MV-Edm-eGFP.

Lymphocytes were infected in suspension for 3 h at 37 °C. After centrifugation the medium was replaced with the appropriate culture medium described above.

MV-Edm replication

BOECs and monocytes were seeded at 2×10^5 cells per well (six-well plate) and infected the following day with MV-Edm at a MOI of 2 for 3 h. Lymphocytes were infected in suspension at a MOI of 2 for 3 h and than seeded at 2×10^5 cells per well. At 24, 48 and 72 h after infection, the cells were scraped into 1 ml OptiMEM (Invitrogen, Karlsruhe, Germany) and the cell-associated viruses were released by two freeze–thaw cycles. Viral titers were determined as $TCID_{50}$ on Vero cells.

Determination of bystander infection by MV-Edm bound to the surface of BOECs

2×10^5 BOECs per well in a six-well collagen I-coated plate were infected with MV-Edm-eGFP at a MOI of 2 in OptiMEM for 3 h at 37 °C. BOECs were washed with PBS and the medium was changed to ECBM-2 with 10% FCS. After 1 h, BOECs were washed twice with PBS, trypsinized for 5 min, resuspended in OptiMEM and separated from the supernatant by centrifugation. The cell-free supernatant was used to infect 2×10^5 Vero cells per well in six-well plates. The infected BOECs were replated in growth medium to follow their expression of eGFP. Vero cells were monitored for eGFP expression 24, 48 and 72 h after infection.

Determination of viability in vitro

Prior to determination of viability, cell culture plates were ultraviolet irradiated to inactivate MV. Viability of cells was determined by MTT (3-(4,5-dimethyl-2-thiazolyl)-2, 5-diphenyl-2*H*-tetrazolium bromide) assay as described.[33] To determine viability by crystal violet staining, cells were incubated in 0.75% crystal violet ethanol solution at room temperature for 15 min, washed, dried and photographed.

Bystander effect assays

BOECs infected with MV-Edm were added to U87 glioma cells seeded at 2×10^3 cells per well in DMEM

on collagen I-coated 96-well plates at ratios of 0, 0.1, 1.0 and 10.0% for 4 days. Cell death was determined by the MTT assay.

MV neutralization assays

Serum was obtained from a healthy donor with immunity against measles as defined by high levels of measles-specific IgG antibodies using an appropriate ELISA. Nonimmune serum (as determined by ELISA) was obtained from nonimmune humans. Sera were centrifuged at 14 000 r.p.m. for 10 min at 4 °C before use. 5×10^4 PFU MV-Edm-eGFP were incubated with MV immune serum or with nonimmune serum at concentrations of 0.0, 1.0 and 10.0% in OptiMEM at 37 °C for 30 min. MV-Edm-eGFP at a MOI of 5 in 50 µl OptiMEM were added to 2×10^3 U87 glioma cells per well growing in collagen I-coated 96-well plates 2 h after infection, the infectious medium was removed, cells were washed once with PBS and then cultivated in supplemented DMEM. Cell viability was determined by crystal violet staining as described above. The spread of MV-Edm-eGFP and syncytia formation was monitored by fluorescence microscopy.

MV protection by BOECs in vitro

To investigate protection by BOECs of MV-Edm against the neutralizing effect of measles immune serum, BOECs were infected with MV-Edm-eGFP at a MOI of 2 in OptiMEM for 3 h at 37 °C and then maintained in supplemented ECBM-2 medium. Twenty-four hours after infection, BOEC/MV-Edm-eGFP were harvested and MV-Edm-eGFP were incubated in OptiMEM containing 0.0, 10.0, 50.0 and 90.0% measles immune serum at 37 °C for 30 min. Hundred BOEC/MV-Edm-eGFP or 1×10^4 MV-Edm-eGFP per well were then added to U87 glioma cells seeded at 2×10^3 cells per well on collagen I-coated 96-well plates. Two hours after the addition of BOEC/MV-Edm-eGFP or MV-Edm-eGFP, U87 cells were washed once with PBS followed by incubation in supplemented DMEM.

To investigate the spread of MV-Edm from BOECs to U87 cells in the presence of measles immune serum, BOEC/MV-Edm were preincubated with 90% measles immune serum as above and then cocultivated with U87 cells in the presence of 90% measles immune serum in supplemented DMEM for 4 days.

Fluorescence-activated cell sorting analysis

Cells were incubated with phycoerythrin-conjugated monoclonal antibodies against CD11a, CD11b, CD49d, CD162 and CXCR4 (all from BD Biosciences Pharmingen, Heidelberg, Germany), with fluorescein isothiocyanate-conjugated monoclonal antibodies against cutaneous lymphocyte-associated Ag (BD Biosciences Pharmingen), VE-cadherin (Bender MedSystems, Vienna, Austria) and with unconjugated antibodies against VEGFR2 (Sigma, Munich, Germany), CD46 and integrin $a_v\beta_5$ (both from BD Biosciences Pharmingen) followed by fluorescein isothiocyanate-conjugated goat anti-mouse secondary antibody (DAKO, Hamburg, Germany). All incubations were performed for 30 min at 4 °C. Isotype-matched antibodies (BD Biosciences Pharmingen) served as controls. Analyses were performed using a FACScan flow cytometer and CellQuest software (BD Biosciences).

Immunohistochemistry

Organs were perfused with PBS and 4% paraformaldehyde, further fixed for 2 h in 4% paraformaldehyde, cryoprotected in 20% sucrose/PBS (Roth, Karlsruhe, Germany), embedded in optimal cutting temperature compound (Sakura Finetek, Zoeterwoude, The Netherlands) at −80°C and serially cut into 7-µm-thick sections. Slides were microwaved in 0.01 M citrate acid solution (pH 6.0) twice for 5 min and incubated with 1% bovine serum albumin (Serva, Heidelberg, Germany). To detect BrdU-incorporating cells, slides were incubated with anti-BrdU monoclonal antibody (1:20; Roche, Mannheim, Germany) followed by alkaline phosphatase-conjugated anti-mouse IgG (Roche) and visualized by Fast Red (DAKO). To detect MV-Edm-infected cells, slides were blocked with MOM mouse Ig blocking reagent (Vector Laboratories Inc. Burlingame, CA, USA) and then incubated with mouse anti-measles hemagglutinin monoclonal antibody (Chemicon, Temecula, CA, USA) followed by alkaline phosphatase-conjugated anti-mouse IgG (DAKO) and visualized by Fast Red (DAKO). Hematoxylin was used for subsequent counterstaining.

Animal studies

Intracranial xenografting of human glioma cells. 5×10^5 U87 glioma cells in 5 µl DMEM were stereotactically injected into the right striatum of $Rag2^{-/-}c\gamma c^{-/-}$ mice. Mice were anesthetized with xylazine and ketamine during the procedure. All animal work was carried out in accordance with state guidelines for animal care and use.

In vivo *homing.* Fourteen days after injection of U87 cells, when tumors had formed, the mice received 6 Gy of cranial γ-irradiation (^{137}Cs; Gammacell 40, Nordion, Kanata, Canada). Three days later, 1×10^5 BOECs pulsed with BrdU at a concentration of 10 µM for 5 days were injected into the tail vein once ($n = 3$). Tumor-bearing mice not receiving BOECs were used as controls ($n = 3$). One day later, brains were procured, fixed in 4% paraformaldehyde (PFA), cryosectioned and examined by immunohistochemistry for BrdU-incorporating cells as described above.

Transfer of antibodies against measles virus into mice. Serum was isolated from a healthy donor with immunity against measles as determined by high levels of measles-specific IgG antibodies (index 7.247) using an ELISA (Enzygnost Anti-MeaslesVirus/IgG, DADE Behring GmbH, Marburg, Germany). The serum was inactivated at 56 °C for 30 min, centrifuged at 14 000 r.p.m. for 10 min and proven to completely neutralize MV-Edm *in vitro* (data not shown).

To determine the duration of protection against measles, 500, 750 and 1000 µl of measles immune serum was injected intraperitoneally into two mice for each dose and blood was drawn at 1, 6, 18 and 28 h. The levels of measles-specific human IgG antibodies were determined by ELISA (Enzygnost Anti-Measles-Virus/IgG, DADE Behring GmbH), previously validated to perform correctly after dilution in mouse serum.

Intracranial migration of BOECs and fibroblasts. Mice with striatal U87 gliomas received 6 Gy of cranial γ-irradiation. Two days later, mice were immunized with

500 μl human measles immune serum injected intraperitoneally or were not immunized. Eighteen hours later, 2×10^5 BOECs pulsed with BrdU and infected with MV-Edm were injected peritumorally ($n = 4$ for the immunized and nonimmunized group). A nonimmunized control group with irradiated gliomas received human foreskin fibroblasts pulsed with BrdU ($n = 4$). Two days after BOEC injection, mouse brains were procured, fixed in 4% PFA, cryosectioned and examined by immunohistochemistry for BrdU incorporation and for the presence of MV-Edm.

In vivo *survival studies*. To determine the efficacy of intratumoral injections, mice with established striatal gliomas generated by the growth of 5×10^5 U87 cells for 10 days received daily intratumoral injections given for 2 days. Tumors of the treatment groups were injected with 3×10^5 PFU MV-Edm in 5 μl OptiMEM ($n = 5$) or with 2×10^5 BOEC/MV-Edm harvested 1 h after infection with MV-Edm at a MOI of 1.5 ($n = 5$). Tumors of the control group ($n = 5$) were injected with 5 μl PBS.

To investigate the effects of intravenous injections, mice with established striatal U87 gliomas generated by the growth of 5×10^5 human U87 glioma cells for 4 days were subjected to 6 Gy of cranial γ-irradiation. Two days later, mice were randomized into three groups to receive daily tail vein injections for 5 days. The treatment groups were injected with 4×10^5 PFU MV-Edm in 200 μl PBS ($n = 7$) or with 2×10^5 BOEC/MV-Edm harvested 1 h after infection with MV-Edm at an MOI of 2 ($n = 6$). The control group was injected with 200 μl PBS ($n = 8$).

To determine the efficacy of peritumoral injections, mice with striatal U87 gliomas established by the growth of 5×10^5 human U87 glioma cells for 4 days received 6 Gy of cranial γ-irradiation. Two days later, daily peritumoral injections of BOEC/MV-Edm were given for 3 days. Each day, injections were applied to a different peritumoral location, that is approximately 1 mm superior, 0.5 mm lateral and 0.5 mm posterior to the glioma. The treatment groups received 3×10^5 PFU MV-Edm in 5 μl OptiMEM ($n = 7$) or 2×10^5 BOEC/MV-Edm harvested 1 h after infection with MV-Edm at an MOI of 1.5 ($n = 7$). Control groups received 2×10^5 BOECs ($n = 7$) or 5 μl PBS ($n = 6$).

Animals were followed until they were moribund, at which time they were killed.

MRI scanning procedure and image analysis

MRI was performed with formalin-fixed mouse brains on a 4.7-T BRUKER Biospec scanner (Bruker Biospin MRI, Ettlingen, Germany) by generating high-resolution T_2-weighted spin echo images. Twenty sagittal and 20 axial slices were acquired covering the entire brain (slice thickness: 0.5 mm). Images were analyzed using ParaVision software (Bruker Biospin MRI). Borderlines of tumors were delineated using a tracking function, the volume of tumor tissue was calculated for each slice and then added from all slices to obtain the total tumor volume.

Statistical analysis

Survival data were analyzed by Kaplan–Meier estimator analysis and compared using the log-rank test. $P < 0.05$ were considered significant.

Acknowledgements

We thank L Liu for statistical analysis. This work was supported in part by a grant from the Deutsche Forschungsgemeinschaft (to CB).

References

1 Nakamura T, Russell SJ. Oncolytic measles viruses for cancer therapy. *Expert Opin Biol Ther* 2004; **4**: 1685–1692.
2 Fielding AK. Measles as a potential oncolytic virus. *Rev Med Virol* 2005; **15**: 135–142.
3 Dorig RE, Marcil A, Chopra A, Richardson CD. The human CD46 molecule is a receptor for measles virus (Edmonston strain). *Cell* 1993; **75**: 295–305.
4 Naniche D, Varior-Krishnan G, Cervoni F, Wild TF, Rossi B, Rabourdin-Combe C *et al.* Human membrane cofactor protein (CD46) acts as a cellular receptor for measles virus. *J Virol* 1993; **67**: 6025–6032.
5 Phuong LK, Allen C, Peng KW, Giannini C, Greiner S, TenEyck CJ *et al.* Use of a vaccine strain of measles virus genetically engineered to produce carcinoembryonic antigen as a novel therapeutic agent against glioblastoma multiforme. *Cancer Res* 2003; **63**: 2462–2469.
6 Anderson BD, Nakamura T, Russell SJ, Peng KW. High CD46 receptor density determines preferential killing of tumor cells by oncolytic measles virus. *Cancer Res* 2004; **64**: 4919–4926.
7 Firsching R, Buchholz CJ, Schneider U, Cattaneo R, ter Meulen V, Schneider-Schaulies J. Measles virus spread by cell–cell contacts: uncoupling of contact-mediated receptor (CD46) downregulation from virus uptake. *J Virol* 1999; **73**: 5265–5273.
8 Duprex WP, McQuaid S, Roscic-Mrkic B, Cattaneo R, McCallister C, Rima BK. *In vitro* and *in vivo* infection of neural cells by a recombinant measles virus expressing enhanced green fluorescent protein. *J Virol* 2000; **74**: 7972–7979.
9 Grote D, Russell SJ, Cornu TI, Cattaneo R, Vile R, Poland GA *et al.* Live attenuated measles virus induces regression of human lymphoma xenografts in immunodeficient mice. *Blood* 2001; **97**: 3746–3754.
10 Esolen LM, Park SW, Hardwick JM, Griffin DE. Apoptosis as a cause of death in measles virus-infected cells. *J Virol* 1995; **69**: 3955–3958.
11 Dingli D, Peng KW, Harvey ME, Greipp PR, O'Connor MK, Cattaneo R *et al.* Image-guided radiovirotherapy for multiple myeloma using a recombinant measles virus expressing the thyroidal sodium iodide symporter. *Blood* 2004; **103**: 1641–1646.
12 Peng KW, TenEyck CJ, Galanis E, Kalli KR, Hartmann LC, Russell SJ. Intraperitoneal therapy of ovarian cancer using an engineered measles virus. *Cancer Res* 2002; **62**: 4656–4662.
13 Hasegawa K, Pham L, O'Connor MK, Federspiel MJ, Russell SJ, Peng KW. Dual therapy of ovarian cancer using measles viruses expressing carcinoembryonic antigen and sodium iodide symporter. *Clin Cancer Res* 2006; **12**: 1868–1875.
14 Springfeld C, von Messling V, Frenzke M, Ungerechts G, Buchholz CJ, Cattaneo R. Oncolytic efficacy and enhanced safety of measles virus activated by tumor-secreted matrix metalloproteinases. *Cancer Res* 2006; **66**: 7694–7700.
15 Heinzerling L, Kunzi V, Oberholzer PA, Kundig T, Naim H, Dummer R. Oncolytic measles virus in cutaneous T-cell lymphomas mounts antitumor immune responses *in vivo* and targets interferon-resistant tumor cells. *Blood* 2005; **106**: 2287–2294.
16 Jarmy G, Wei J, Debatin KM, Beltinger C. Apoptosis-inducing cellular vehicles for cancer gene therapy: endothelial and neural progenitors. In: Srivastava R (ed). *Apoptosis, Cell Signaling and Human Diseases: Molecular Mechanisms*. Humana Press Inc.: Totowa, 2006, pp 279–302.

17 Ferrari N, Glod J, Lee J, Kobiler D, Fine HA. Bone marrow-derived, endothelial progenitor-like cells as angiogenesis-selective gene-targeting vectors. *Gene Therapy* 2003; **10**: 647–656.
18 Tabatabai G, Bahr O, Mohle R, Eyupoglu IY, Boehmler AM, Wischhusen J *et al.* Lessons from the bone marrow: how malignant glioma cells attract adult haematopoietic progenitor cells. *Brain* 2005; **128**: 2200–2211.
19 Tabatabai G, Frank B, Mohle R, Weller M, Wick W. Irradiation and hypoxia promote homing of haematopoietic progenitor cells towards gliomas by TGF-beta-dependent HIF-1alpha-mediated induction of CXCL12. *Brain* 2006; **129**: 2426–2435.
20 Lin Y, Weisdorf DJ, Solovey A, Hebbel RP. Origins of circulating endothelial cells and endothelial outgrowth from blood. *J Clin Invest* 2000; **105**: 71–77.
21 Wei J, Jarmy G, Genuneit J, Debatin KM, Beltinger C. Human blood late outgrowth endothelial cells for gene therapy of cancer: determinants of efficacy. *Gene Therapy* 2006; **14**: 344–356.
22 Schnorr JJ, Dunster LM, Nanan R, Schneider-Schaulies J, Schneider-Schaulies S, ter Meulen V. Measles virus-induced down-regulation of CD46 is associated with enhanced sensitivity to complement-mediated lysis of infected cells. *Eur J Immunol* 1995; **25**: 976–984.
23 Wei J, Zhou S, Bachem MG, Debatin KM, Beltinger C. Infiltration of blood outgrowth endothelial cells into tumor spheroids: role of matrix metalloproteinases and irradiation. *Anticancer Res* 2007; **27**: 1415–1421.
24 Peng KW, Hadac EM, Anderson BD, Myers R, Harvey M, Greiner SM *et al.* Pharmacokinetics of oncolytic measles virotherapy: eventual equilibrium between virus and tumor in an ovarian cancer xenograft model. *Cancer Gene Ther* 2006; **13**: 732–738.
25 Grote D, Cattaneo R, Fielding AK. Neutrophils contribute to the measles virus-induced antitumor effect: enhancement by granulocyte macrophage colony-stimulating factor expression. *Cancer Res* 2003; **63**: 6463–6468.
26 Hallak LK, Merchan JR, Storgard CM, Loftus JC, Russell SJ. Targeted measles virus vector displaying echistatin infects endothelial cells via alpha(v)beta3 and leads to tumor regression. *Cancer Res* 2005; **65**: 5292–5300.
27 Coukos G, Makrigiannakis A, Kang EH, Caparelli D, Benjamin I, Kaiser LR *et al.* Use of carrier cells to deliver a replication-selective herpes simplex virus-1 mutant for the intraperitoneal therapy of epithelial ovarian cancer. *Clin Cancer Res* 1999; **5**: 1523–1537.
28 Jevremovic D, Gulati R, Hennig I, Diaz RM, Cole C, Kleppe L *et al.* Use of blood outgrowth endothelial cells as virus-producing vectors for gene delivery to tumors. *Am J Physiol Heart Circ Physiol* 2004; **287**: H494–H500.
29 Cole C, Qiao J, Kottke T, Diaz RM, Ahmed A, Sanchez-Perez L *et al.* Tumor-targeted, systemic delivery of therapeutic viral vectors using hitchhiking on antigen-specific T cells. *Nat Med* 2005; **11**: 1073–1081.
30 Thorne SH, Negrin RS, Contag CH. Synergistic antitumor effects of immune cell-viral biotherapy. *Science* 2006; **311**: 1780–1784.
31 Aboody KS, Brown A, Rainov NG, Bower KA, Liu S, Yang W *et al.* Neural stem cells display extensive tropism for pathology in adult brain: evidence from intracranial gliomas. *Proc Natl Acad Sci USA* 2000; **97**: 12846–12851.
32 Duprex WP, McQuaid S, Hangartner L, Billeter MA, Rima BK. Observation of measles virus cell-to-cell spread in astrocytoma cells by using a green fluorescent protein-expressing recombinant virus. *J Virol* 1999; **73**: 9568–9575.
33 Beltinger C, Fulda S, Walczak H, Debatin KM. TRAIL enhances thymidine kinase/ganciclovir gene therapy of neuroblastoma cells. *Cancer Gene Ther* 2002; **9**: 372–381.

APPENDIX IV

HUMAN GENE THERAPY 18:627–641 (July 2007)

DOI: 10.1089/hum.2007.034

Human Mesenchymal Stem Cells Lack Tumor Tropism but Enhance the Antitumor Activity of Oncolytic Adenoviruses in Orthotopic Lung and Breast Tumors

TANJA HAKKARAINEN,[1,2] MERJA SÄRKIOJA,[1,2] PETRI LEHENKARI,[3,4] SUSANNA MIETTINEN,[5,6] TIMO YLIKOMI,[5–7] RIITTA SUURONEN,[6] RENEE A. DESMOND,[8] ANNA KANERVA,[1,2,9] and AKSELI HEMMINKI[1,2]

ABSTRACT

Systemic adenoviral delivery into tumors is inefficient because of liver sequestration of intravenously administered virus. One potential solution for improving bioavailability is the use of carrier cells such as human mesenchymal stem cells (MSCs), which have been suggested to have inherent tumor tropism. Here we investigated the capacity of capsid-modified adenoviruses to infect and replicate in MSCs. Further, biodistribution and tumor-killing efficacy of MSCs loaded with oncolytic adenoviruses were evaluated in orthotopic murine models of lung and breast cancer. *In vitro*, heparan sulfate proteoglycan- and $\alpha_v\beta$ integrin-targeted viruses enhanced gene delivery to bone marrow- and adipose tissue-derived MSCs up to 11,000-fold over adenovirus serotype 5 (Ad5). Infectivity-enhanced oncolytic adenoviruses showed notably higher rates of cytolysis of *in vitro*-passaged MSCs in comparison with wild-type virus. *In vivo*, intravenously injected MSCs homed primarily to the lungs, and virus was released into advanced orthotopic breast and lung tumors for therapeutic efficacy and increased survival. When the same dose of virus was injected intravenously without MSCs, only transduction of the liver was seen. These results suggest that MSCs loaded with oncolytic adenoviruses might be a useful approach for improving the bioavailability of systemically administered oncolytic adenoviruses.

OVERVIEW SUMMARY

Human mesenchymal stem cells (MSCs) have been suggested to have inherent tumor tropism and could thus be exploited as efficient viral carriers in virotherapy. Her we show that infectivity of MSCs can be significantly enhanced via targeting of adenoviruses to alternative receptors and that MSCs are capable of supporting viral replication and release of infectivity enhanced oncolytic adenoviruses both *in vitro* and *in vivo*. In addition, intravenously administered MSCs loaded with oncolytic adenoviruses prolong survival of orthotopic lung tumor-bearing mice, and deliver antitumor efficacy in an orthotopic model of advanced breast cancer. These results suggest that MSCs could be a potentially powerful tool for improving the bioavailability of and delivering oncolytic viruses into human tumors in the context of human trials.

INTRODUCTION

ONCOLYTIC ADENOVIRUSES are promising experimental tools for therapy of tumors resistant to available modalities. The use of these viruses is based on their ability to destroy tumor

[1]Cancer Gene Therapy Group, Molecular Cancer Biology Program and Haartman Institute, University of Helsinki, 00014 Helsinki, Finland.
[2]Department of Oncology and HUSLAB, Helsinki University Central Hospital, 00029 Helsinki, Finland.
[3]Clinical Research Center, Department of Surgery, University of Oulu, 90014 Oulu, Finland.
[4]Department of Anatomy and Cell Biology, University of Oulu, 90014 Oulu, Finland.
[5]Department of Cell Biology, Medical School, University of Tampere, 33014 Tampere, Finland.
[6]Regea Institute of Regenerative Medicine, University of Tampere and Tampere University Hospital, 33014 Tampere, Finland.
[7]Department of Clinical Chemistry, Tampere University Hospital, 33521 Tampere, Finland.
[8]Comprehensive Cancer Center, Biostatistics and Bioinformatics Unit, University of Alabama at Birmingham, Birmingham, AL 35294-3300.
[9]Department of Obstetrics and Gynecology, Helsinki University Central Hospital, 00029 Helsinki, Finland.

cells by viral replication, that is, oncolysis (Bauerschmitz *et al.*, 2002). After oncolysis, newly produced viruses will be released to surrounding tumor tissue. Thus, the input dose of the oncolytic viruses is multiplied rapidly because of viral replication, which increases tumor penetration and the subsequent therapeutic potency. However, replication needs to be limited to tumor tissue in order to minimize adverse side effects. In the adenovirus genome, the *E1* region contains several genes that regulate initialization of viral replication (Russell, 2000). There are two main approaches that have been shown to be promising strategies for restriction of viral replication. The first is based on partial deletions in the *E1* region that are *trans*-complemented in tumor cells. For example, deleting 24 bp from constant region 2 of *E1A* limits replication to cells in which the p16/Rb pathway is dysregulated, which includes the majority of human cancer cells (Sherr, 1996; Fueyo *et al.*, 2000; Heise *et al.*, 2000). In the second approach, tumor-specific promoters are employed to control *E1A* expression (Bauerschmitz *et al.*, 2002). In addition, the two approaches can be combined for further specificity, although loss of efficacy can result from some combinations (Nettelbeck *et al.*, 2002; Bauerschmitz *et al.*, 2006).

To infect cells, most serotypes of adenovirus bind first to coxsackievirus–adenovirus receptor (CAR), which is expressed ubiquitously on most tissues (Law and Davidson, 2005). Second, adenovirus binds to cellular $\alpha_v\beta$-class integrins, which triggers the internalization of the virus. Unfortunately, CAR is often expressed to a variable degree in many or most tumor types (Li *et al.*, 1999; Bauerschmitz *et al.*, 2002; Kanerva *et al.*, 2002), which can lead to decreased infection efficacy and oncolytic potency. To improve the specificity and/or efficacy of oncolytic adenoviruses, they can be modified to bind alternative receptors highly expressed on cancer cells. Several studies have shown that oncolytic adenoviruses can be targeted to, for example, $\alpha_v\beta$ integrins, adenovirus serotype 3 (Ad3) receptor, polyanionic heparan sulfate proteoglycans (HSPGs), and epidermal growth factor receptor (EGFR) (Hemminki *et al.*, 2001; Suzuki *et al.*, 2001; Kanerva *et al.*, 2003; Ranki *et al.*, 2007a).

Although the infectivity and specificity of adenoviruses can be enhanced, there are still several obstacles that may hinder the systemic bioavailability of adenoviruses. Intravenous delivery would be attractive, because most patients in need of experimental treatments feature disseminated disease. Despite retargeting, the majority of systemically administered adenovirus accumulates in the liver. More specifically, hepatic Kupffer cells clear viruses rapidly from blood, which decreases dramatically the amount of available therapeutic virus (Alemany *et al.*, 2000). Data suggest that blood factors including vitamin K-dependent coagulation zymogens (e.g., factor IX [FIX] and factor X [FX]) and complement protein C4BP are involved in transduction of hepatocytes by adenovirus, which may be an important determinant of liver tropism and toxicity (Shayakhmetov *et al.*, 2005; Parker *et al.*, 2006). In addition, innate and adaptive immune responses may eliminate therapeutic viruses (Bessis *et al.*, 2004) In fact, it has been reported that more than 50% of the adult population have variable levels of preexisting neutralizing antibodies against adenoviruses (Harvey *et al.*, 1999). Further, advanced solid tumor masses are intricate and complex, comprising, for example, hypoxic, necrotic, and stromal areas, which may prevent the access of the viruses into all regions of the tumor.

One potential solution for circumventing some of these problems might be to engineer cells as viral carriers. Previously, certain types of cells have been used for sustained local production of retroviruses, cytokines, and human endostatin (Savelkoul *et al.*, 1994; Sandmair *et al.*, 2000; Joki *et al.*, 2001). However, these cells lack the capability to home into target tissue, are typically allogeneic, and therefore require encapsulation to avoid immune responses.

Human mesenchymal stem cells (MSCs) have been the focus for various therapeutic purposes. MSCs are bone marrow- or fat tissue-originating precursor cells, which can differentiate into adipocytes, chondrocytes, osteoblasts, myoblasts, and tenocytes (Prockop, 1997). There are also some MSCs present in blood, from where they are recruited to repair injured tissues (Prockop, 1997; Studeny *et al.*, 2004). It has been hypothesized that the tumor environment resembles injured tissue and therefore circulating MSCs would home into tumor tissue (Dvorak, 1986; Studeny *et al.*, 2002, 2004). In fact, studies have shown that genetically modified MSCs are capable of homing into tumors and show antineoplastic activity *in vivo* in xenograft murine glioma, melanoma, and ovarian and breast cancer models (Studeny *et al.*, 2002, 2004; Nakamizo *et al.*, 2005; Komarova *et al.*, 2006).

The aim of this project was to use human MSCs as carriers for oncolytic adenoviruses, thereby combining cellular tropism for tumors with the antitumor effect provided by oncolytic adenoviruses. Specifically, we investigated the capacity of capsid-modified adenoviruses to infect and replicate in MSCs. Further, biodistribution, tumor-homing ability, and tumor-killing efficacy of systemically delivered, virus-loaded MSCs in orthotopic lung and breast cancer tumor models were evaluated.

MATERIALS AND METHODS

Cells

Bone marrow-derived human mesenchymal stem cells were isolated as described previously (Leskela *et al.*, 2003). Half the medium (α-modified essential medium [GIBCO, Paisley, UK] supplemented with 10% fetal bovine serum [FBS], 2 m*M* L-glutamine, 20 m*M* HEPES, and a 10-ml/liter concentration of antibiotic solution [penicillin, 10,000 U/ml; streptomycin, 10 mg/ml] [Sigma, St. Louis, MO]) was replaced two times per week. Adipose stem cells were obtained from human subcutaneous and intraperitoneal adipose tissue. Fat tissue was washed with sterile phosphate-buffered saline (PBS) and digested with collagenase type I (1.5 mg/ml; GIBCO) in Dulbecco's modified Eagle's medium–Ham's nutrient mixture F-12 (DMEM–F12) (1:1, v/v; Sigma) supplemented with penicillin (100 U/ml), streptomycin (100 μg/ml), and amphotericin B (0.25 μg/ml) (1% antibiotic–antimycotic; GIBCO) for 45–90 min at 37°C with gentle agitation. The digested tissue was centrifuged and the supernatant with mature adipocytes was removed. The cellular pellet was resuspended in sterile H_2O to lyse the red blood cells and the stem cell fraction was collected by centrifugation. The cellular pellet was resuspended in DMEM–F12 supplemented with 10% FBS and 1% antibi-

otic–antimycotic and filtrated through a 100-μm mesh filter to remove debris. The collected adipose stem cells were plated on 25-cm^3 tissue culture flasks. Growth medium was replaced partly two times per week. For the *in vitro* and *in vivo* experiments cells were trypsinized, counted, and plated before reaching confluence. Green fluorescent protein (GFP)-expressing large cell lung carcinoma line LNM35/EGFP (from T. Takahashi, Honda Research Institute, Japan) and breast cancer cell line M4A4-LM3 (Goodison *et al.*, 2005) were cultured in RPMI supplemented with 10% fetal bovine serum, 2 m*M* L-glutamine, and a 10-ml/liter concentration of antibiotic solution (penicillin, 10,000 U/ml; streptomycin, 10 mg/ml) (Sigma). MSCs, LNM35/EGFP cells, and M4A4-LM3 cells were cultured at 37°C in a humidified atmosphere of 5% CO_2.

Recombinant viruses

Viruses used in this study are listed in Table 1. Nonreplicating adenoviruses and oncolytic adenoviruses were propagated in 293 and A549 cells, respectively. Viruses were purified by standard cesium chloride gradient techniques, and quality control was performed by polymerase chain reaction (PCR). Viral particles (VP) were determined by spectrophotometry and infectious units are expressed as the median tissue culture infective dose ($TCID_{50}$).

Flow cytometry

For flow cytometric analysis, cells (2×10^5) were incubated for 20 min at 4°C with the following primary antibodies at 1:200 dilution: anti-CAR (clone RmcB; Upstate Cell Signaling Solutions/Millipore, Lake Placid, NY), anti-HSPG (clone F58-10E4; Seikagaku, Falmouth, MA), anti-$\alpha_v\beta_3$ integrin (clone LM609; Chemicon International/Millipore, Temecula, CA), anti-$\alpha_v\beta_5$ integrin (clone P1F6; Chemicon International/Millipore), or anti-CD46 (clone E4.3; BD Biosciences, San Jose, CA). Cells were washed with fluorescence-activated cell-sorting (FACS) buffer (phosphate-buffered saline containing 2% FBS) and incubated with a 1:200 dilution of phycoerythrin (PE)-labeled secondary antibody (goat anti-mouse polyclonal antibody; BD Biosciences) for 30 min at 4°C. Cells were washed with FACS buffer and analyzed by flow cytometry (FACSCalibur; BD Biosciences) to determine receptor expression levels. Nonstained cells were used as a negative control.

Transduction efficacy assay

Adipose tissue- and bone marrow-derived MSCs were infected with Ad5luc1, Ad5(GL), Ad5/3luc1, Ad5lucRGD, Ad5.pK7(GL), or Ad5.RGD.pK7(GL) for 2 hr, using 50, 100, 500, and 1000 VP/cell. Luciferase activity was determined 48 hr postinfection with a luciferase assay system (Promega, Madison, WI) according to the manufacturer's protocol. Values are presented as relative to syngeneic control viruses [Ad5luc1 and Ad5(GL)], which have been given a value of 1.

Cell viability assay

Adipose tissue- and bone marrow-derived MSCs were infected with Ad300wt, Ad5Δ24E3+, Ad5/3-Δ24, Ad5-Δ24RGD, or Ad5.pK7-Δ24, using 0.1, 1, 10, 100, 1000, and 10,000 VP/cell. Growth medium was changed every third day. Cell viability

Table 1. Replication-Deficient and Oncolytic Adenoviruses Used in This Study

Virus	*E1A*	*Transgene*	*Capsid modification*	*Target receptor*
Ad5luc1 (Dmitriev *et al.*, 1998)	Deleted	*luciferase*	—	CAR
Ad5(GL) (Wu *et al.*, 2002)	Deleted	*GFP* and *luciferase*	—	CAR
Ad5/3luc2 (Kanerva *et al.*, 2002)	Deleted	*luciferase*	Serotype 3 knob	Unknown and CD46
Ad5lucRGD (Dmitriev *et al.*, 1998)	Deleted	*luciferase*	RGD-4C motif in the H1 loop	$\alpha_v\beta$ integrins and CAR
Ad5.pK7(GL) (Wu *et al.*, 2002)	Deleted	*GFP* and *luciferase*	Seven polylysines at the COOH terminus	Heparan sulfates and CAR
Ad5.pK7LacZ		lacZ	Seven polylysines at the COOH terminus	Heparan sulfates and CAR
Ad5.RGD.pK7(GL) (Wu *et al.*, 2002)	Deleted	*GFP* and *luciferase*	RGD-4C motif in the H1 loop and seven polylysines at the COOH terminus	$\alpha_v\beta$ integrins, heparan sulfates, and CAR
Ad300wt	Intact	—	—	CAR
Ad5Δ24D3+ (Suzuki *et al.*, 2001)	24-bp deletion	—	—	CAR
Ad5/3-Δ24 (Kanerva *et al.*, 2003)	24-bp deletion	—	Serotype 3 knob	Unknown and CD46
Ad5-Δ24RGD (Suzuki *et al.*, 2001)	24-bp deletion	—	RGD-4C motif in the H1 loop	$\alpha_v\beta$ integrins and CAR
Ad5.pK7-Δ24 (Ranki *et al.*, 2007a)	24-bp deletion	—	Seven polylysines at the COOH terminus	Heparan sulfates and CAR

Abbreviation: CAR, coxsackievirus–adenovirus receptor.

was determined 10 days postinfection with CellTiter 96 AQ_{ueous} One Solution cell proliferation assay [also called the 3-(4,5-dimethylthiazol-2-yl)-5-(3-carboxymethoxyphenyl)-2-(4-sulfophenyl)-2*H*-tetrazolium [MTS] assay; Promega).

In vivo *studies*

Female 3- to 4-week-old NMRI nude mice were obtained from Taconic (Ejby, Denmark). The orthotopic lung tumor model used in these studies has been described in more detail by Särkioja *et al.* (2006). Tumor growth was monitored by detecting GFP with the IVIS imaging system 100 series (Xenogen, Alameda, CA). To facilitate imaging in the *in vivo* experiments, a mixture of replication-deficient luciferase-expressing virus and therapeutic virus was used. The dose of intravenously injected virus was equal to the dose used for infecting MSCs. Bone marrow-derived MSCs were used for *in vivo* experiments. In the systemic delivery study, 5 days after cancer cell inoculation, each mouse received intravenously either virus only [1.4×10^8 VP of Ad5.pK7(GL) + 7×10^7 VP of Ad5.pK7-Δ24], 7×10^5 MSCs preinfected with replication-deficient adenovirus [Ad5.pK7(GL) at 200 VP/cell + Ad5pK7LacZ at 100 VP/cell] or 7×10^5 MSCs preinfected with oncolytic adenoviruses [Ad5.pK7(GL) at 200 VP/cell + Ad5.pK7-Δ24 at 100 VP/cell]. To visualize viral distribution, luciferin (4.5 mg/mouse) was injected intraperitoneally followed by bioluminescence imaging. Mice were imaged 15 min after MSC administration and again 3, 7, and 10 days later. For kinetic studies, orthotopic lung tumor-bearing mice received treatments as described above and bioluminescence imaging was performed at 15 min, 8 hr, and 24 hr. Images were captured after removal of the skin and again after removal of the abdominal wall and ribs. To track the MSCs *in vivo*, cells were labeled before intravenous injection with Vybrant CM-DiI cell-labeling solution according to the manufacturer's protocol (Invitrogen Molecular Probes, Eugene, OR). Tumor-free and lung or breast tumor-bearing mice were killed 24 hr later and tissues were fixed with 4% paraformaldehyde and embedded into paraffin. Histological sections were examined under a fluorescence microscope. In the survival experiment, tumor-bearing mice received intravenously either MSCs (7×10^5 cells per mouse, $n = 5$), virus [1.4×10^8 VP of Ad5.pK7(GL) + 7×10^7 VP of Ad5.pK7-Δ24, $n = 10$], MSCs infected with nonreplicating adenovirus [Ad5.pK7(GL) at 200 VP/cell + Ad5pK7LacZ at 100 VP/cell, 7×10^5 cells per mouse, $n = 6$], or MSCs infected with oncolytic adenoviruses [Ad5.pK7(GL) at 200 VP/cell of + Ad5.pK7-Δ24 at 100 VP/cell, 7×10^5 cells per mouse, $n = 10$] 7, 11, and 15 days after cancer cell inoculation. The health of the mice was monitored daily and mice were killed according to humane end-point guidelines.

The orthotopic breast cancer model used in these studies has been described in more detail by Ranki *et al.* (2007a). Briefly, 2 million M4A4-LM3 cells were injected into both the right and left second lowest mammary fat pads. Tumors were allowed to develop until they reached a diameter of approximately 0.4 cm. Tumor-bearing mice received intravenously either saline ($n = 12$ tumors in 6 mice), MSCs ($n = 10$ tumors in 5 mice), virus ($n = 12$ tumors in 6 mice), MSCs infected with nonreplicating adenovirus ($n = 8$ tumors in 4 mice), or MSCs infected with oncolytic adenoviruses ($n = 8$ tumors in 4 mice) 14, 19, 24, and 35 days after cancer cell inoculation. Tumors were measured in two dimensions with calipers and tumor volumes were calculated according to the following formula: length × width^2 × 0.5. Data are expressed as percentage of the tumor volume at the initiation of therapy, which was set as 100%. To determine the number of functional viral particles in tumor tissue, breast cancer tumors treated with MSCs plus oncolytic adenovirus ($n = 8$) or virus only ($n = 8$) were harvested, mechanically homogenized, and subjected to three freeze–thaw cycles. Cell remnants were centrifuged and collected supernatants were used in the $TCID_{50}$ assay. Data are expressed as plaque-forming units per gram of tumor tissue. All animal experiments were approved by the Experimental Animal Committee of the University of Helsinki (Helsinki, Finland) and the provincial government of southern Finland.

Statistical analysis

Analysis of transduction efficacy and viral replication data was performed by one-way analysis of variance (ANOVA) with Bonferroni's post-hoc test. Survival analysis was conducted with PROC LIFETEST (SAS version 9.1; SAS Institute, Cary, NC), using a Weibull distribution. The distribution of event times was assessed by evaluation of log–log survivor plots of the data. Our main interest was to determine whether MSCs could improve the efficacy of oncolytic virus and therefore the parameter estimates of the effect of treatment versus virus only were evaluated by χ^2 test. Analysis of the tumor size data was performed with a repeated measures growth model with PROC MIXED (SAS version 9.1). Tumor size data were log transformed for normality. The effects of treatment group, time, and the interaction of treatment group and time were evaluated by F tests. Curvature in the growth curves was tested for by a quadratic term for time. The site of tumor (left vs. right) was included as an additional covariate. The *a priori* planned comparisons of differences in predicted treatment means of all groups to the MSCs loaded with oncolytic adenovirus group were computed by t statistics averaged over all time points and on day 36. Analysis of $TCID_{50}$ data was performed with an unpaired t test with Welch's correction. For all analyses $p < 0.05$ was deemed statistically significant.

RESULTS

Infectivity of MSCs can be significantly enhanced with capsid-modified adenoviruses

To study adenoviral infectivity, bone marrow- and fat tissue-derived human MSCs were transduced with Ad3 receptor-, $\alpha_v\beta$ integrin-, and HSPG-targeted luciferase-expressing replication-deficient adenoviruses (Fig. 1). When compared with control virus, infection with HSPG-targeted virus significantly enhanced transduction efficiencies up to 11,000-, 1200-, and 140-fold (all $p < 0.001$), whereas targeting to $\alpha_v\beta$ integrins enhanced transduction up to 1100-, 1100-, and 40-fold ($p < 0.001$, $p < 0.01$, and $p < 0.05$, respectively) in adipose tissue-derived MSCs (Fig. 1A–C). Similarly, in bone marrow-derived MSCs, HSPG targeting significantly increased gene transfer rates 900- and 400-fold (both $p < 0.001$) and $\alpha_v\beta$ integrin targeting 190- and 120-fold over control virus (both $p < 0.001$) (Fig. 1D and

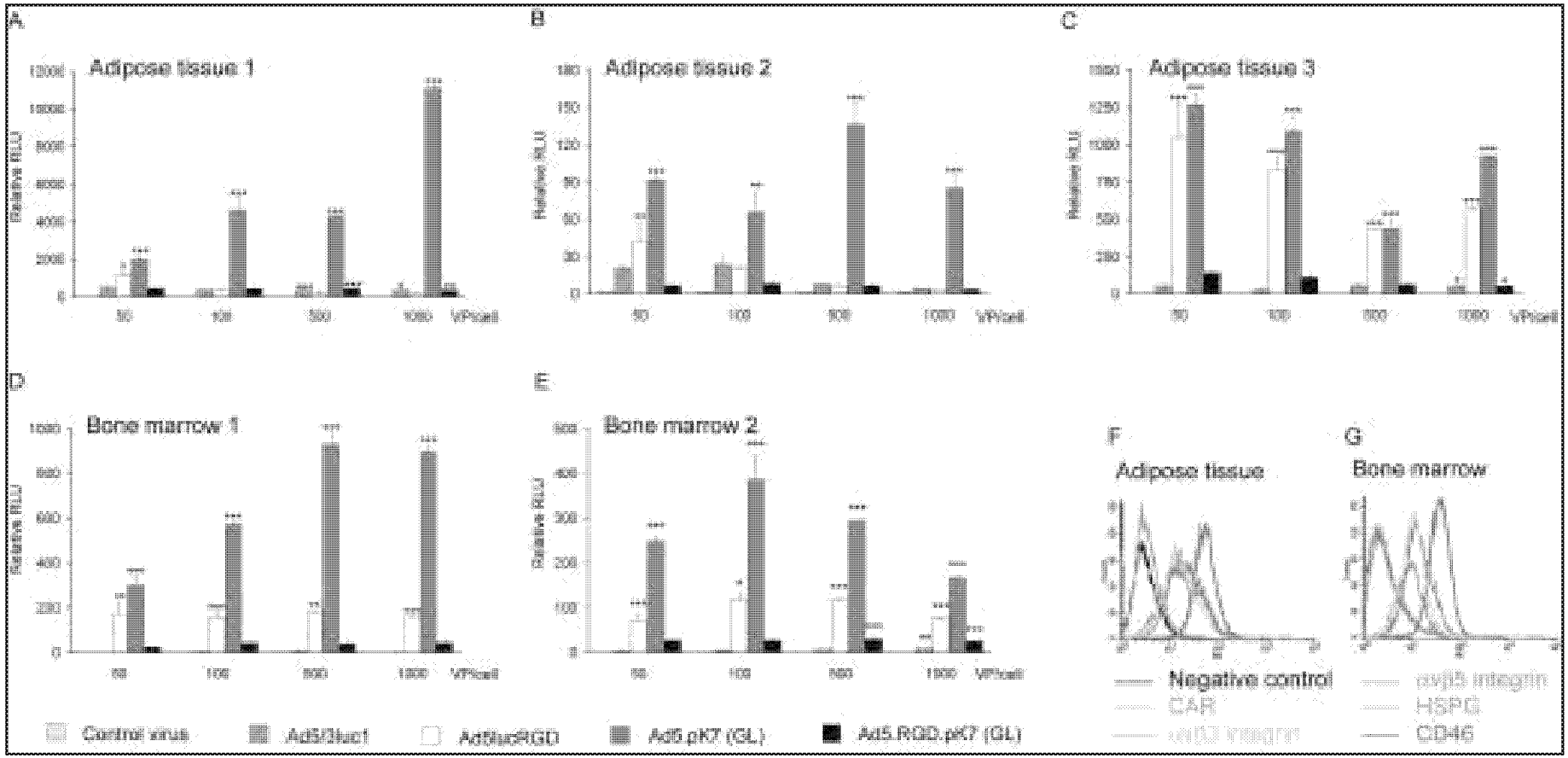

FIG. 1. Transduction efficiency of modified adenoviruses in human MSCs. Adipose tissue-derived (**A–C**) and bone marrow-derived (**D** and **E**) MSCs were infected with Ad5/3luc1, Ad5lucRGD, Ad5.pK7(GL), Ad5.RGD.pK7(GL), or the respective syngeneic Ad5 control virus. Luciferase activity was determined 48 hr after infection. Values are presented relative to control viruses [Ad5(GL) or Ad5luc1], which have been given a value of 1. Error bars indicate the standard error of the mean. RLU, relative light units; VP, viral particles. $***p < 0.001$; $**p < 0.01$; $*p < 0.05$. (**F** and **G**) Flow cytometric analysis of putative virus receptor expression levels. Adipose tissue-derived (**F**) and bone marrow-derived (**G**) MSCs were stained with antibodies to detect CAR (green), $\alpha_v\beta_3$ integrin (gray), $\alpha_v\beta_5$ integrin (orange), heparan sulfate proteoglycans (blue), or CD46 (red). Unstained cells were used as a negative control (black).

E). Also, minor infectivity enhancement was seen with Ad3 receptor-targeted virus in adipose tissue MSCs (Fig. 1A–C), but not in bone marrow MSCs (Fig. 1D and E).

To determine the expression levels of proposed target receptors including CAR, $\alpha_v\beta_3$ integrin, $\alpha_v\beta_5$ integrin, HSPG, and CD46 (one of the proposed receptors for Ad3 [Sirena *et al.*, 2004; Shen *et al.*, 2006]), antibody-stained cells were analyzed by flow cytometry (Fig. 1F and G). Both types of MSCs were CAR negative, but moderately expressed both $\alpha_v\beta$ integrins and HSPG. Surprisingly, both cell types stained strongly for CD46, despite only minor infectivity enhancement with Ad5/3luc1.

Capsid-modified oncolytic adenoviruses replicate in MSCs

To determine whether oncolytic viruses can be released from *in vitro*-passaged MSCs, cells were infected with a panel of capsid-modified oncolytic adenoviruses harboring a 24-bp deletion in *E1A*, and cell viability was analyzed by MTS assay (Fig. 2). In comparison with wild-type virus and untargeted oncolytic adenovirus, HSPG-targeted virus showed significantly higher cytolysis rates both in adipose tissue-derived cells (Fig. 2A and B) and bone marrow-derived cells (Fig. 2C and D) ($p < 0.001$ for all comparisons when 1–1000 VP/cell was used). Similarly, $\alpha_v\beta$ integrin targeting significantly enhanced cytolysis when compared with control viruses (Fig. 2A–D) ($p < 0.001$ for all comparisons when 10–1000 VP/cell was used). Although Ad3 receptor targeting did not improve transduction efficiency remarkably, it did enhance cytolysis significantly, especially in adipose tissue-derived cells, when compared with control viruses ($p < 0.001$ for all comparisons when 10–1000 VP/cell was used). Control viruses without capsid modification resulted in cytolysis only with the highest viral doses.

MSCs home to lungs in vivo

To test whether MSCs could support viral replication and release in the context of orthotopic lung tumors, tumor-bearing

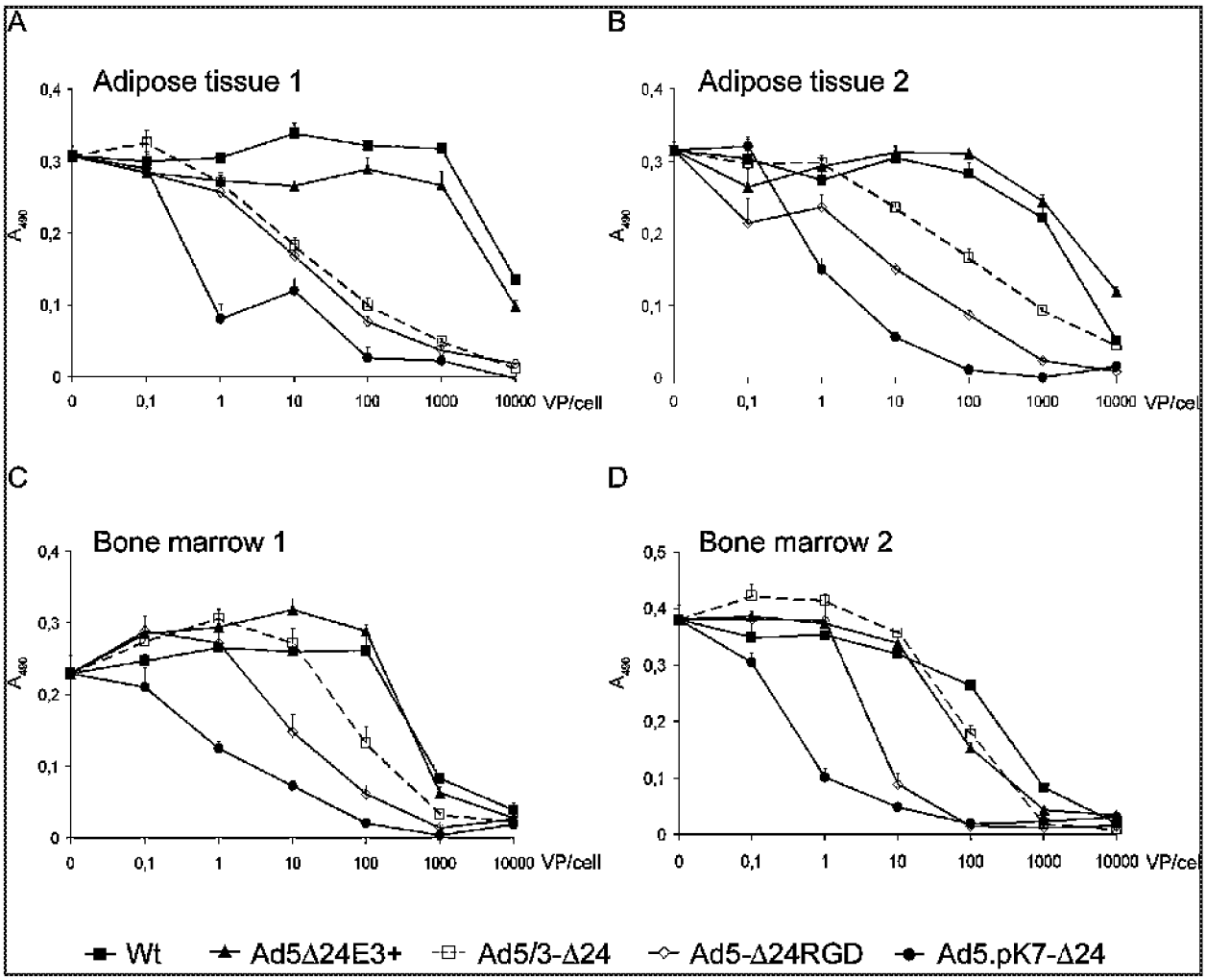

FIG. 2. Replication of infectivity-enhanced oncolytic adenoviruses and consequent cytolysis of MSCs. Adipose tissue-derived (**A** and **B**) and bone marrow-derived (**C** and **D**) MSCs were infected and cell viability was determined 10 days later. Error bars indicate the standard error of the mean.

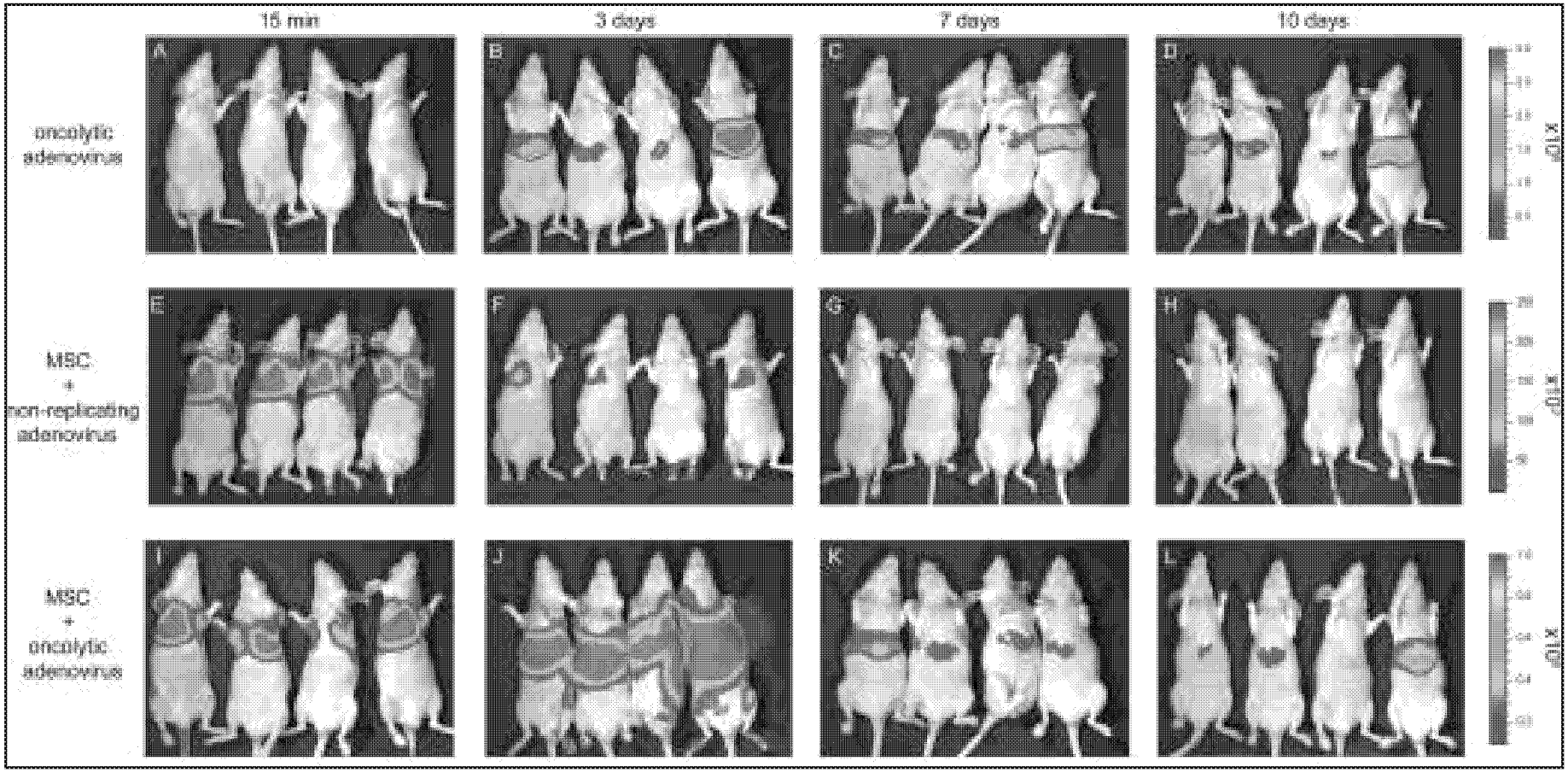

FIG. 3. Systemic delivery of MSCs loaded with oncolytic adenoviruses in orthotopic lung tumor model. Two million LNM35/EGFP cells were injected into the left lung of nude mice. Five days later mice received intravenous virus (**A–D**), MSCs infected with replication-deficient adenovirus (**E–H**), or MSCs infected with oncolytic adenovirus (**I–L**). To visualize the viral distribution, luciferin was injected intraperitoneally followed by bioluminescence imaging 15 min, 3 days, 7 days, and 10 days later. Please note lower emission scale in the middle row.

mice received a single dose of intravenous oncolytic adenovirus (Fig. 3A–D) or MSCs infected either with replication-deficient (Fig. 3E–H) or oncolytic adenovirus (Fig. 3I–L). Because a mixture of luciferase-expressing virus and therapeutic virus was used, we were able to monitor biodistribution of the virus-loaded MSCs and kinetics of viral release. Our previous studies have shown consistent correlation between noninvasive external detection of luciferase and the presence of both luciferase protein and viral particles in tissues (Särkioja *et al.*, 2006; Guse *et al.*, 2007; Ranki *et al.*, 2007a,b). Therefore, to reduce the number of animals needed, we chose to use the noninvasive bioimaging system instead of conventional luciferase quantification from tissue extracts. Fifteen minutes after injection, a luciferase signal was detected from the lungs of all MSC-treated mice (Fig. 3E and I). Approximately 10-fold higher expression was achieved when MSCs were preinfected with oncolytic adenoviruses in comparison with replication-deficient adenoviruses (Fig. 4A). No signal was obtained from mice treated only with virus, because of lack of sufficient time for luciferase production (Fig. 3A).

Three days later, a weak luciferase signal was detected from the lungs of the mice that received MSCs preinfected with replication-deficient adenovirus (Figs. 3F and 4A). In contrast, mice treated with oncolytic adenovirus-loaded MSCs displayed a strong luciferase signal in the liver (Figs. 3J and 4A), suggesting release of the virus from MSCs and subsequent liver transduction. As expected, a similar but 60 times weaker luciferase signal was captured from livers of mice treated with virus only (Figs. 3B and 4A). Because virus-only treatment gave a weaker liver luciferase signal than MSCs carrying oncolytic virus, viruses probably amplified in MSCs before release, or in lung tumors subsequent to release. Both 7 and 10 days after the injections, mice treated with virus only (Fig. 3C and D and Fig. 4A) or with oncolytic adenovirus-loaded MSCs (Fig. 3K and L and Fig. 4A) showed detectable luciferase expression in liver whereas no luciferase signal was obtained from mice treated with replication-deficient adenovirus-loaded MSCs (Fig. 3G and H and Fig. 4A).

For more precise study of the kinetics of viral release from virus-loaded MSCs, lung tumor-bearing mice were treated intravenously either with virus only or with MSCs loaded with oncolytic adenovirus, followed by bioluminescence imaging 15 min, 8 hr, and 24 hr later (Fig. 4B–K). To unequivocally distinguish the luciferase signal from different organs, the abdominal skin was removed before the first set of imaging (Fig. 4B, D, F, H, and J) and the abdominal wall and ribs (Fig. 4C, E, G, I, and K) were removed before the second set. After injection of cells, a strong lung-specific luciferase signal was soon detected from mice treated with oncolytic adenovirus-loaded MSCs (Fig. 4F and G). Luciferase expression was also seen preferentially in the lungs at the 8-hr time point, whereas mice treated only with virus displayed a luciferase signal preferentially from the liver throughout the experiment (Fig. 4H and I and Fig. 4B–E, respectively). When virus-loaded MSC-treated mice were imaged 24 hr after injection of cells, a strong luciferase signal was still obtained from the lungs but some luciferase expression emerged also from the liver (Fig. 4J and K). Because mice were dead by the time luciferase analysis was performed after removal of the abdominal wall and ribs, luciferase signals quickly declined, probably because of rapid postmortem ATP degradation. When DiI-labeled MSCs were injected intravenously into tumor-free mice (Fig. 5A and B) and into lung tumor-bearing mice (Fig. 5C and D) or breast tumor-bearing mice (Fig. 5E and F), a strong fluorescence signal was obtained symmetrically from both lungs, suggesting accumulation preferentially in the lungs instead of specificity for tumors. No MSCs could be found in breast tumors.

Intravenously delivered MSCs loaded with oncolytic adenoviruses prolong survival of mice with orthotopic lung cancer

To test whether MSC carriers could increase the therapeutic potency of oncolytic adenoviruses, a survival experiment was carried out in an aggressive orthotopic lung tumor model (Fig. 6A). Tumor-bearing mice received three doses of virus, MSCs, MSCs preinfected with replication-deficient adenovirus, or MSCs preinfected with oncolytic adenovirus. The median survival times were 23, 25, 27, and 28 days, respectively. However, a subpopulation of mice treated with MSCs loaded with oncolytic viruses benefited from the treatment, and statistical analysis revealed a significant survival advantage in comparison with mice treated only with virus ($p = 0.0031$). Despite the extremely aggressive nature of the model (resembling most clinical cases), one mouse treated with MSCs loaded with oncolytic adenoviruses survived until the end of experiment (day 111).

MSCs loaded with oncolytic viruses deliver antitumor effect in orthotopic murine model of advanced breast cancer

To study whether oncolytic adenovirus-loaded MSCs could yield efficacy in another animal model, an orthotopic murine model of advanced breast cancer was used (Fig. 6B). MSCs loaded with oncolytic adenovirus significantly inhibited tumor growth when compared with control-treated mice ($p < 0.001$). To explore the presence of virus, tumors were analyzed by $TCID_{50}$ assay (Fig. 6C). In comparison with the group treated only with virus, more than 10 times more virus was found when MSC carriers were used ($p = 0.0347$).

DISCUSSION

Although serotype 5-based adenoviruses are the most widely used tools in cancer gene therapy, there are obstacles that limit their efficacious intravenous use. For example, the immune system can prevent effective readministration, and hepatic uptake by Kupffer and other macrophage lineage cells can result in decreased bioavailability (Harvey *et al.*, 1999; Alemany *et al.*, 2000; Bessis *et al.*, 2004). Second, CAR is often variably expressed on tumor cells, which hinders adequate gene delivery (Bauerschmitz *et al.*, 2002).

Both unmodified and genetically engineered MSCs have been used for various cell-based therapeutic approaches, including bone regeneration for treatment of osteogenesis imperfecta, regeneration of heart muscle after myocardial infarction, and for treatment of Parkinson's disease (Chamberlain *et al.*, 2004; Amado *et al.*, 2005; Lu *et al.*, 2005; Miyahara *et al.*, 2006). In addition, a number of studies have confirmed the immune-privileged nature of MSCs, and their ability to avoid al-

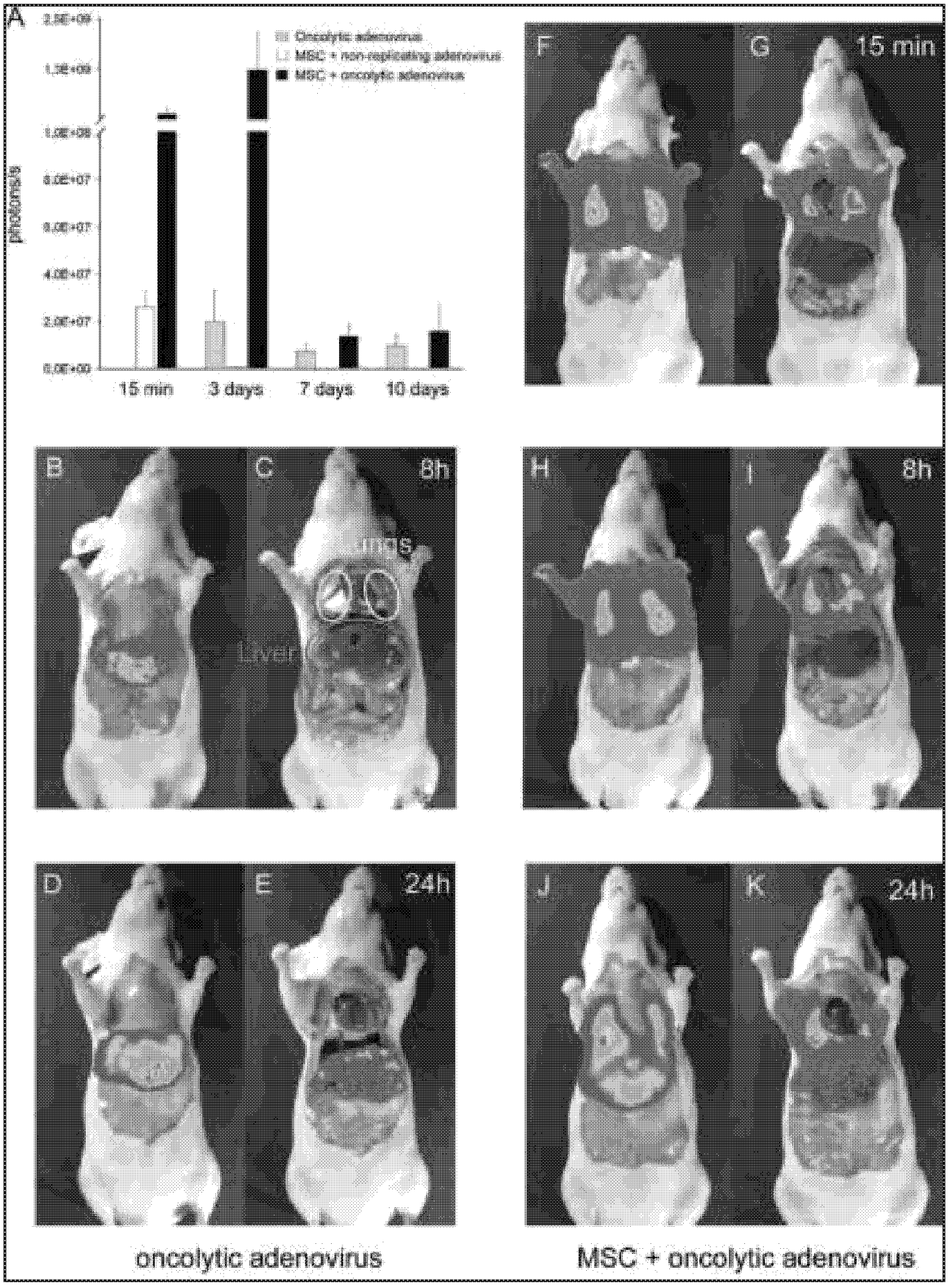

FIG. 4. Quantification of viral delivery and kinetics of viral release from systemically delivered MSCs *in vivo*. Luciferase signals obtained after systemic delivery of MSCs loaded with oncolytic adenovirus into lung tumor-bearing mice (see Fig. 3) are presented as numeric values (**A**). For kinetic studies, orthotopic lung tumor-bearing mice received intravenously either oncolytic virus alone (**B–E**) or MSCs infected with oncolytic adenovirus (**F–K**). Bioluminescence imaging was performed after removal of skin (**B**, **D**, **F**, **H**, and **J**) or after removal of the abdominal wall and ribs (**C**, **E**, **G**, **I**, and **K**) 15 min, 8 hr, and 24 hr after viral administration.

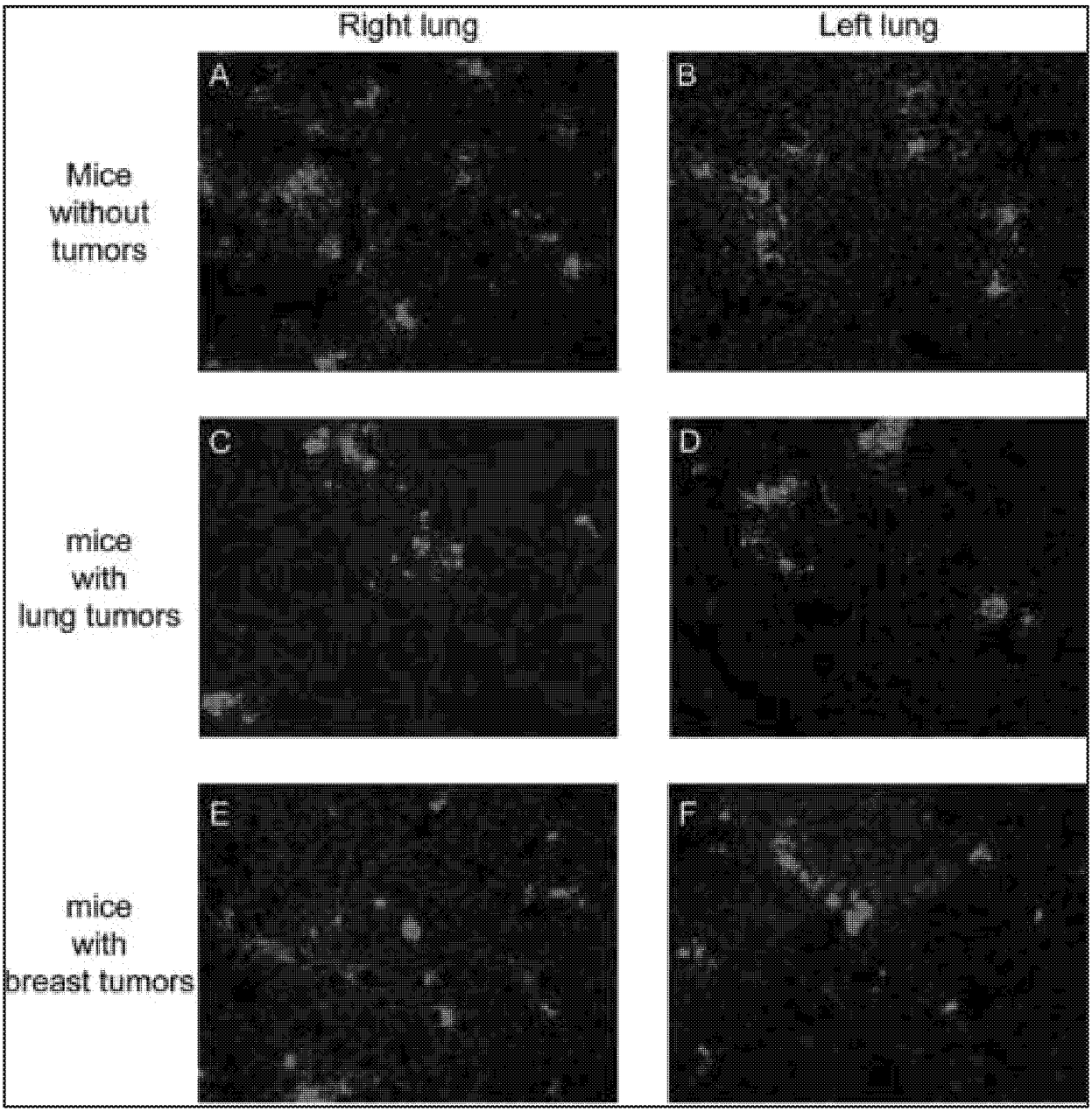

FIG. 5. MSC homing to lungs *in vivo*. DiI-labeled MSCs were injected intravenously into mock-treated mice (**A** and **B**), lung tumor-bearing mice (**C** and **D**), and breast tumor-bearing mice (**E** and **F**). Lungs were harvested 24 hr later and histological sections were examined by fluorescence microscopy. Regardless of the tumor burden status or site, DiI-labeled MSCs were detected mainly in the lungs 24 hr after injection.

FIG. 6. Therapeutic efficacy of MSCs loaded with oncolytic adenovirus. (**A**) Orthotopic lung tumor-bearing mice received intravenously either MSCs ($n = 5$), virus ($n = 10$), MSCs infected with nonreplicating adenovirus ($n = 6$), or MSCs infected with oncolytic adenoviruses ($n = 10$) on days 7, 11, and 15. Treatment with MSCs loaded with oncolytic adenoviruses significantly prolonged the survival of the mice in comparison with virus only (**$p = 0.0031$). (**B**) Orthotopic breast tumor-bearing mice received intravenously either saline ($n = 12$ tumors in 6 mice), MSCs ($n = 10$ tumors in 5 mice), virus ($n = 12$ tumors in 6 mice), MSCs infected with nonreplicating adenovirus ($n = 8$ tumors in 4 mice), or MSCs infected with oncolytic adenoviruses ($n = 8$ tumors in 4 mice) 14, 19, 24, and 35 days after cancer cell inoculation. Tumor growth was significantly inhibited with oncolytic virus-loaded MSCs when compared with mock and virus only-treated groups (***, both $p < 0.0001$), or to MSCs preinfected with replication-deficient adenovirus ($p = 0.0002$). (**C**) Virus present in orthotopic breast cancer tumors were determined from homogenized tumor lysates ($n = 8$) using $TCID_{50}$ assay. When compared with virus-only-treated tumors, MSCs significantly enhanced viral delivery ($p = 0.0347$).

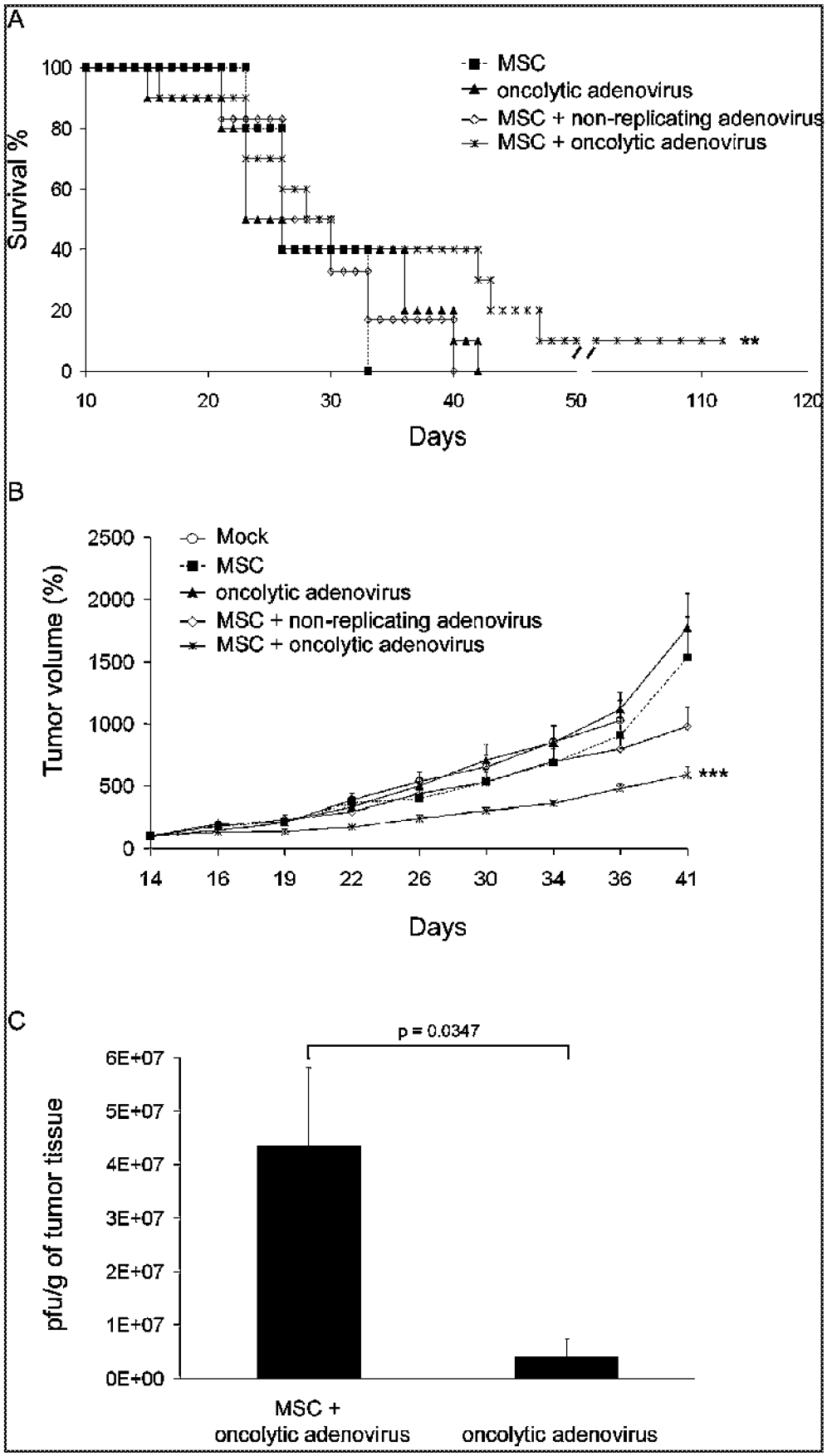
A
Survival %
100
80
60
40
20
0
10
20
30
40
50
110
120
Days
MSC
oncolytic adenovirus
MSC + non-replicating adenovirus
MSC + oncolytic adenovirus
**
B
Tumor volume (%)
2500
2000
1500
1000
500
0
14
16
19
22
26
30
34
36
41
Days
Mock
MSC
oncolytic adenovirus
MSC + non-replicating adenovirus
MSC + oncolytic adenovirus
***
C
pfu/g of tumor tissue
6E+07
5E+07
4E+07
3E+07
2E+07
1E+07
0E+00
p = 0.0347
MSC +
oncolytic adenovirus
oncolytic adenovirus

logeneic rejection in humans and animal models, which broadens the potential for their therapeutic use (Le Blanc *et al.*, 2004; Aggarwal and Pittenger, 2005). Modified MSCs have already been used preclinically as anticancer therapeutics for glioma, metastatic melanoma, and ovarian cancer (Studeny *et al.*, 2002, 2004; Nakamura *et al.*, 2004; Nakamizo *et al.*, 2005; Komarova *et al.*, 2006).

Unfortunately, genetic manipulation of MSCs with gene transfer vectors is potentially challenging. For instance, infectivity of MSCs with serotype 5 adenoviruses has been shown to be quite inadequate because of low CAR expression levels on MSCs (Conget and Minguell, 2000; Studeny *et al.*, 2002; Mizuguchi *et al.*, 2005). To compensate, MSCs have been infected with relatively high viral doses or capsid-modified viruses (Olmsted-Davis *et al.*, 2002; Pereboeva *et al.*, 2003; Knaan-Shanzer *et al.*, 2005; Mizuguchi *et al.*, 2005; Komarova *et al.*, 2006). On the basis of our results, transduction of MSCs can be increased up to 1100- and 11,000-fold by using $\alpha_v\beta$ integrin- or HSPG-targeted adenoviruses, respectively. Thus, substantially smaller viral doses are needed for gene transfer. Interestingly, both types of MSCs showed high expression levels of CD46, a proposed Ad3 receptor, although an Ad3 receptor-targeted virus did not notably enhance transduction. These findings are in accordance with data suggesting that CD46 is not the only receptor for adenovirus serotype 3 (Gaggar *et al.*, 2003; Tuve *et al.*, 2006), especially regarding the 5/3 chimera used here, which features the long and bent shaft from Ad5 (the Ad3 receptor shaft is short and rigid) and just the knob from Ad3 receptor.

To use MSCs as carriers for oncolytic adenoviruses, MSCs must support viral replication and release. Preliminary data from Komarova and coworkers suggest that 5/3-modified wild-type adenoviruses can indeed replicate in MSCs (Komarova *et al.*, 2006). However, they did not use a tumor-selective virus or employ systemic delivery. To study the capacity of infectivity-enhanced tumor-specific oncolytic viruses to be released from MSCs, we used MSCs from various tissues and a panel of viruses currently undergoing clinical development for the treatment of human cancers (Raki *et al.*, 2006). We found that viral cytolysis closely correlated with gene transfer; MSCs were able to support the viral replication of capsid-modified adenoviruses whereas the replication rates of viruses with Ad5 capsids remained low. These results parallel earlier studies showing close correlation between infectivity, replication, and subsequent oncolysis (Suzuki *et al.*, 2001; Kanerva *et al.*, 2003; Kuhnel *et al.*, 2004; Reddy *et al.*, 2006).

Although viral release from MSCs was evident, the rate of cytolysis was notably lower than previously seen in the context of various cancer cells. The 24-bp deletion in the constant region 2 of *E1A* has been shown to result in preferential replication in p16/Rb pathway-deficient cells (Fueyo *et al.*, 2000; Heise *et al.*, 2000). However, rapidly proliferating normal cells feature phosphorylation of retinoblastoma protein (Rb), which would be expected to allow replication of Δ24-type viruses, explaining the replication seen here (Heise *et al.*, 2000). Although MSCs do not replicate rapidly *in vitro*, they can be expanded and therefore most cells are expected to be in a state of slow proliferation when passaged *in vitro*. We speculate that together with the effective infection accomplished *in vitro*, this is what allowed the release of oncolytic viruses from MSCs. However, it is likely that a much smaller proportion of MSCs would proliferate in humans, that infection would be less efficient, and therefore that normal dormant MSCs might not be subject to cytolysis. Although these findings emphasize the need for careful monitoring of toxicity in clinical trials with these agents, potential toxicity to replicating cells is not unprecedented. Instead, hundreds of millions of patients have been treated with chemotherapy and radiation therapy, both of which target cells mainly on the basis of replicativity and therefore this mode of potential toxicity would be familiar to oncologists.

We did not detect differences in the relative attractiveness of bone marrow- or adipose tissue-derived MSCs as both seemed to allow effective release of oncolytic virions. In fact, it has been suggested that there might be similarities between adipose- and bone marrow-derived MSCs both on biological and molecular levels (Izadpanah *et al.*, 2006; Kern *et al.*, 2006; Talens-Visconti *et al.*, 2006).

To test whether virus-loaded MSCs could efficiently deliver viruses into tumors for improved therapeutic potency, a set of experiments was performed with orthotopic lung and breast cancer models. Because of its superiority *in vitro*, the HSPG-targeted Ad5.pK7-Δ24 was used. Our previous studies with these orthotopic tumor models have shown that the biodistribution pattern of HSPG-targeted adenovirus is similar to that of Ad5. Although some virus can be detected in tumors after intravenous injection, the vast majority are found in the liver, spleen, and lungs (Sarkioja *et al.*, 2006; Ranki *et al.*, 2007a,b). Here, we were able to demonstrate that virus-loaded MSCs homed efficiently to the lungs of mice bearing orthotopic pulmonary tumors. Also, an increase in luciferase signal versus that of MSCs with nonreplicating virus suggested multiplication of the input viral dose, which might further increase the therapeutic potential of the approach. The kinetics studies revealed that viral release from MSC carriers was relatively rapid, because 24 hr after MSC injection (i.e., 72 hr after infection) a proportion of the released virus was already detectable in the liver.

The survival of lung tumor-bearing mice was significantly prolonged when they received therapeutic virus with an intravenously delivered MSC-based carrier. In addition, oncolytic adenovirus-loaded MSCs resulted in enhanced viral delivery and antitumor effect in an orthotopic murine model of advanced breast cancer. These results suggest that although MSCs did not specifically home to tumors, they were able to release therapeutic virus for subsequent transduction of tumors. In essence, MSCs allowed multiplication of the input virus dose in the context of an extended release system.

Our results in this highly aggressive lung cancer model, which closely models the human disease (Särkioja *et al.*, 2006), are in accordance with the data of Studeny and co-workers, who studied a lung metastatic melanoma tumor model (Studeny *et al.*, 2002, 2004). Although they did not load MSCs with oncolytic viruses, they were able to see accumulation of the MSCs in lungs of mice, and interferon production resulted in therapeutic benefit. Further, the capacity of MSCs to release replication-competent adenoviruses for therapeutic benefit is supported by the data by Komarova and coworkers, although they did not use a selectively oncolytic virus. To avoid biodistribution complexities, they delivered MSCs intraperitoneally to mice with intraperitoneal ovarian cancer (Komarova *et al.*, 2006). Further studies are required to clarify how viral infection and replication affect MSCs at the molecular and biologi-

cal levels. Given the immune-privileged nature of MSCs (Le Blanc *et al.*, 2004; Aggarwal and Pittenger, 2005), it is possible that allogeneic MSCs could be used without rejection. Further, it might be interesting to study the capacity of MSC carriers to avoid preexisting immune responses such as neutralizing antibodies against adenoviruses.

In summary, infectivity of MSCs can be significantly enhanced via targeting of viruses to $\alpha_v\beta$ integrins and HSPG. Furthermore, MSCs are capable of supporting replication and viral release of infectivity-enhanced oncolytic adenoviruses both *in vitro* and *in vivo*. In addition, intravenously administered MSCs loaded with oncolytic adenoviruses prolong the survival of orthotopic lung tumor-bearing mice, and deliver antitumor efficacy in an orthotopic model of advanced breast cancer. These results suggest that MSCs could be a potentially powerful tool for improving the bioavailability and delivery of oncolytic viruses into human tumors in the context of human trials.

ACKNOWLEDGMENTS

This study was supported by the Academy of Finland, the Finnish Cultural Foundation, EU FP6 THERADPOX and APOTHERAPY, HUCH Research Funds (EVO), the Sigrid Juselius Foundation, the Emil Aaltonen Foundation, the Finnish Cancer Society, the University of Helsinki, the Schering Research Foundation, the Finnish Oncology Association, by Competitive Research Funding of the Pirkanmaa Hospital District, and the Employment and Economic Development Centre for Pirkanmaa. Akseli Hemminki is K. Albin Johansson Research Professor of the Foundation for the Finnish Cancer Institute. The authors thank Eerika Karli (Rational Drug Design Program and Haartman Institute, University of Helsinki, Finland) for technical assistance and Takashi Takahashi (Honda Research Institute, Japan) for LNM35/EGFP cells.

AUTHOR DISCLOSURE STATEMENT

No competing financial interests exist.

REFERENCES

AGGARWAL, S., and PITTENGER, M.F. (2005). Human mesenchymal stem cells modulate allogeneic immune cell responses. Blood **105,** 1815–1822.

ALEMANY, R., SUZUKI, K., and CURIEL, D.T. (2000). Blood clearance rates of adenovirus type 5 in mice. J. Gen. Virol. **81,** 2605–2609.

AMADO, L.C., SALIARIS, A.P., SCHULERI, K.H., ST JOHN, M., XIE, J.S., CATTANEO, S., DURAND, D.J., FITTON, T., KUANG, J.Q., STEWART, G., LEHRKE, S., BAUMGARTNER, W.W., MARTIN, B.J., HELDMAN, A.W., and HARE, J.M. (2005). Cardiac repair with intramyocardial injection of allogeneic mesenchymal stem cells after myocardial infarction. Proc. Natl. Acad. Sci. U.S.A. **102,** 11474–11479.

BAUERSCHMITZ, G.J., BARKER, S.D., and HEMMINKI, A. (2002). Adenoviral gene therapy for cancer: From vectors to targeted and replication competent agents [review]. Int. J. Oncol. **21,** 1161–1174.

BAUERSCHMITZ, G.J., GUSE, K., KANERVA, A., MENZEL, A., HERRMANN, I., DESMOND, R.A., YAMAMOTO, M., NETTELBECK, D.M., HAKKARAINEN, T., DALL, P., CURIEL, D.T., and HEMMINKI, A. (2006). Triple-targeted oncolytic adenoviruses featuring the *cox2* promoter, *E1A* transcomplementation, and serotype chimerism for enhanced selectivity for ovarian cancer cells. Mol. Ther. **14,** 164–174.

BESSIS, N., GARCIACOZAR, F.J., and BOISSIER, M.C. (2004). Immune responses to gene therapy vectors: Influence on vector function and effector mechanisms. Gene Ther. **11**(Suppl. 1), S10–S17.

CHAMBERLAIN, J.R., SCHWARZE, U., WANG, P.R., HIRATA, R.K., HANKENSON, K.D., PACE, J.M., UNDERWOOD, R.A., SONG, K.M., SUSSMAN, M., BYERS, P.H., and RUSSELL, D.W. (2004). Gene targeting in stem cells from individuals with osteogenesis imperfecta. Science **303,** 1198–1201.

CONGET, P.A., and MINGUELL, J.J. (2000). Adenoviral-mediated gene transfer into *ex vivo* expanded human bone marrow mesenchymal progenitor cells. Exp. Hematol. **28,** 382–390.

DMITRIEV, I., KRASNYKH, V., MILLER, C.R., WANG, M., KASHENTSEVA, E., MIKHEEVA, G., BELOUSOVA, N., and CURIEL, D.T. (1998). An adenovirus vector with genetically modified fibers demonstrates expanded tropism via utilization of a coxsackievirus and adenovirus receptor-independent cell entry mechanism. J. Virol. **72,** 9706–9713.

DVORAK, H.F. (1986). Tumors: Wounds that do not heal. Similarities between tumor stroma generation and wound healing. N. Engl. J. Med. **315,** 1650–1659.

FUEYO, J., GOMEZ-MANZANO, C., ALEMANY, R., LEE, P.S., McDONNELL, T.J., MITLIANGA, P., SHI, Y.X., LEVIN, V.A., YUNG, W.K., and KYRITSIS, A.P. (2000). A mutant oncolytic adenovirus targeting the Rb pathway produces anti-glioma effect *in vivo*. Oncogene **19,** 2–12.

GAGGAR, A., SHAYAKHMETOV, D.M., and LIEBER, A. (2003). CD46 is a cellular receptor for group B adenoviruses. Nat. Med. **9,** 1408–1412.

GOODISON, S., VIARS, C., and URQUIDI, V. (2005). Molecular cytogenetic analysis of a human breast metastasis model: Identification of phenotype-specific chromosomal rearrangements. Cancer Genet. Cytogenet. **156,** 37–48.

GUSE, K., DIAS, J.D., BAUERSCHMITZ, G.J., HAKKARAINEN, T., AAVIK, E., RANKI, T., PISTO, T., SARKIOJA, M., DESMOND, R.A., KANERVA, A., and HEMMINKI, A. (2007). Luciferase imaging for evaluation of oncolytic adenovirus replication *in vivo*. Gene Ther. **14,** 902–911.

HARVEY, B.-G., HACKETT, N.R., EL-SAWY, T., ROSENGART, T.K., HIRSCHOWITZ, E.A., LIEBERMAN, M.D., LESSER, M.L., and CRYSTAL, R.G. (1999). Variability of human systemic humoral immune responses to adenovirus gene transfer vectors administered to different organs. J. Virol. **73,** 6729–6742.

HEISE, C., HERMISTON, T., JOHNSON, L., BROOKS, G., SAMPSON-JOHANNES, A., WILLIAMS, A., HAWKINS, L., and KIRN, D. (2000). An adenovirus E1A mutant that demonstrates potent and selective systemic anti-tumoral efficacy. Nat. Med. **6,** 1134–1139.

HEMMINKI, A., DMITRIEV, I., LIU, B., DESMOND, R.A., ALEMANY, R., and CURIEL, D.T. (2001). Targeting oncolytic adenoviral agents to the epidermal growth factor pathway with a secretory fusion molecule. Cancer Res. **61,** 6377–6381.

IZADPANAH, R., TRYGG, C., PATEL, B., KRIEDT, C., DUFOUR, J., GIMBLE, J.M., and BUNNELL, B.A. (2006). Biologic properties of mesenchymal stem cells derived from bone marrow and adipose tissue. J. Cell Biochem. **99,** 1285–1297.

JOKI, T., MACHLUF, M., ATALA, A., ZHU, J., SEYFRIED, N.T., DUNN, I.F., ABE, T., CARROLL, R.S., and BLACK, P.M. (2001). Continuous release of endostatin from microencapsulated engineered cells for tumor therapy. Nat. Biotechnol. **19,** 35–39.

KANERVA, A., MIKHEEVA, G.V., KRASNYKH, V., COOLIDGE, C.J., LAM, J.T., MAHASRESHTI, P.J., BARKER, S.D., STRAUGHN, M., BARNES, M.N., ALVAREZ, R.D., HEMMINKI,

A., and CURIEL, D.T. (2002). Targeting adenovirus to the serotype 3 receptor increases gene transfer efficiency to ovarian cancer cells. Clin. Cancer Res. **8,** 275–280.

KANERVA, A., ZINN, K.R., CHAUDHURI, T.R., LAM, J.T., SUZUKI, K., UIL, T.G., HAKKARAINEN, T., BAUERSCHMITZ, G.J., WANG, M., LIU, B., CAO, Z., ALVAREZ, R.D., CURIEL, D.T., and HEMMINKI, A. (2003). Enhanced therapeutic efficacy for ovarian cancer with a serotype 3 receptor-targeted oncolytic adenovirus. Mol. Ther. **8,** 449–458.

KERN, S., EICHLER, H., STOEVE, J., KLUTER, H., and BIEBACK, K. (2006). Comparative analysis of mesenchymal stem cells from bone marrow, umbilical cord blood, or adipose tissue. Stem Cells **24,** 1294–1301.

KNAAN-SHANZER, S., VAN DE WATERING, M.J.M., VAN DER VELDE, I., GONCALVES, M.A.F.V., VALERIO, D., and DE VRIES, A.A.F. (2005). Endowing human adenovirus serotype 5 vectors with fiber domains of species B greatly enhances gene transfer into human mesenchymal stem cells. Stem Cells **23,** 1598–1607.

KOMAROVA, S., KAWAKAMI, Y., STOFF-KHALILI, M.A., CURIEL, D.T., and PEREBOEVA, L. (2006). Mesenchymal progenitor cells as cellular vehicles for delivery of oncolytic adenoviruses. Mol. Cancer Ther. **5,** 755–766.

KUHNEL, F., SCHULTE, B., WIRTH, T., WOLLER, N., SCHAFERS, S., ZENDER, L., MANNS, M., and KUBICKA, S. (2004). Protein transduction domains fused to virus receptors improve cellular virus uptake and enhance oncolysis by tumor-specific replicating vectors. J. Virol. **78,** 13743–13754.

LAW, L.K., and DAVIDSON, B.L. (2005). What does it take to bind CAR? Mol. Ther. **12,** 599–609.

LE BLANC, K., RASMUSSON, I., SUNDBERG, B., GOTHERSTROM, C., HASSAN, M., UZUNEL, M., and RINGDEN, O. (2004). Treatment of severe acute graft-versus-host disease with third party haploidentical mesenchymal stem cells. Lancet **363,** 1439–1441.

LESKELA, H.V., RISTELI, J., NISKANEN, S., KOIVUNEN, J., IVASKA, K.K., and LEHENKARI, P. (2003). Osteoblast recruitment from stem cells does not decrease by age at late adulthood. Biochem. Biophys. Res. Commun. **311,** 1008–1013.

LI, Y., PONG, R.C., BERGELSON, J.M., HALL, M.C., SAGALOWSKY, A.I., TSENG, C.P., WANG, Z., and HSIEH, J.T. (1999). Loss of adenoviral receptor expression in human bladder cancer cells: A potential impact on the efficacy of gene therapy. Cancer Res. **59,** 325–330.

LU, L., ZHAO, C., LIU, Y., SUN, X., DUAN, C., JI, M., ZHAO, H., XU, Q., and YANG, H. (2005). Therapeutic benefit of TH-engineered mesenchymal stem cells for Parkinson's disease. Brain Res. Brain Res. Protoc. **15,** 46–51.

MIYAHARA, Y., NAGAYA, N., KATAOKA, M., YANAGAWA, B., TANAKA, K., HAO, H., ISHINO, K., ISHIDA, H., SHIMIZU, T., KANGAWA, K., SANO, S., OKANO, T., KITAMURA, S., and MORI, H. (2006). Monolayered mesenchymal stem cells repair scarred myocardium after myocardial infarction. Nat. Med. **12,** 459–465.

MIZUGUCHI, H., SASAKI, T., KAWABATA, K., SAKURAI, F., and HAYAKAWA, T. (2005). Fiber-modified adenovirus vectors mediate efficient gene transfer into undifferentiated and adipogenic-differentiated human mesenchymal stem cells. Biochem. Biophys Res. Commun. **332,** 1101–1106.

NAKAMIZO, A., MARINI, F., AMANO, T., KHAN, A., STUDENY, M., GUMIN, J., CHEN, J., HENTSCHEL, S., VECIL, G., DEMBINSKI, J., ANDREEFF, M., and LANG, F.F. (2005). Human bone marrow-derived mesenchymal stem cells in the treatment of gliomas. Cancer Res. **65,** 3307–3318.

NAKAMURA, K., ITO, Y., KAWANO, Y., KUROZUMI, K., KOBUNE, M., TSUDA, H., BIZEN, A., HONMOU, O., NIITSU, Y., and HAMADA, H. (2004). Antitumor effect of genetically engineered mesenchymal stem cells in a rat glioma model. Gene Ther. **11,** 1155–1164.

NETTELBECK, D.M., RIVERA, A.A., BALAGUE, C., ALEMANY, R., and CURIEL, D.T. (2002). Novel oncolytic adenoviruses targeted to melanoma: Specific viral replication and cytolysis by expression of E1A mutants from the tyrosinase enhancer/promoter. Cancer Res. **62,** 4663–4670.

OLMSTED-DAVIS, E.A., GUGALA, Z., GANNON, F.H., YOTNDA, P., McALHANY, R.E., LINDSEY, R.W., and DAVIS, A.R. (2002). Use of a chimeric adenovirus vector enhances BMP2 production and bone formation. Hum. Gene Ther. **13,** 1337–1347.

PARKER, A.L., WADDINGTON, S.N., NICOL, C.G., SHAYAKHMETOV, D.M., BUCKLEY, S.M., DENBY, L., KEMBALL-COOK, G., NI, S., LIEBER, A., McVEY, J.H., NICKLIN, S.A., and BAKER, A.H. (2006). Multiple vitamin K-dependent coagulation zymogens promote adenovirus-mediated gene delivery to hepatocytes. Blood **108,** 2554–2561.

PEREBOEVA, L., KOMAROVA, S., MIKHEEVA, G., KRASNYKH, V., and CURIEL, D.T. (2003). Approaches to utilize mesenchymal progenitor cells as cellular vehicles. Stem Cells **21,** 389–404.

PROCKOP, D.J. (1997). Marrow stromal cells as stem cells for nonhematopoietic tissues. Science **276,** 71–74.

RAKI, M., REIN, D.T., KANERVA, A., and HEMMINKI, A. (2006). Gene transfer approaches for gynecological diseases. Mol. Ther. **14,** 154–163.

RANKI, T., KANERVA, A., RISTIMAKI, A., HAKKARAINEN, T., SARKIOJA, M., KANGASNIEMI, L., RAKI, M., LAAKKONEN, P., GOODISON, S., and HEMMINKI, A. (2007a). A heparan sulfate-targeted conditionally replicative adenovirus, Ad5.pk7-Δ24, for the treatment of advanced breast cancer. Gene Ther, **14,** 58–67.

RANKI, T., SARKIOJA, M., HAKKARAINEN, T., SMITTEN, K., KANERVA, A., and HEMMINKI, A. (2007b). Systemic efficacy of oncolytic adenoviruses in imagable orthotopic models of hormone refractory metastatic breast cancer. Int. J. Cancer **121,** 2919–2928.

REDDY, P.S., GANESH, S., and YU, D.-C. (2006). Enhanced gene transfer and oncolysis of head and neck cancer and melanoma cells by fiber chimeric oncolytic adenoviruses. Clin. Cancer Res. **12,** 2869–2878.

RUSSELL, W.C. (2000). Update on adenovirus and its vectors. J. Gen. Virol. **81,** 2573–2604.

SANDMAIR, A.M., LOIMAS, S., PURANEN, P., IMMONEN, A., KOSSILA, M., PURANEN, M., HURSKAINEN, H., TYYNELA, K., TURUNEN, M., VANNINEN, R., LEHTOLAINEN, P., PALJARVI, L., JOHANSSON, R., VAPALAHTI, M., and YLA-HERTTUALA, S. (2000). Thymidine kinase gene therapy for human malignant glioma, using replication-deficient retroviruses or adenoviruses. Hum. Gene Ther. **11,** 2197–2205.

SÄRKIOJA, M., KANERVA, A., SALO, J., KANGASNIEMI, L., ERIKSSON, M., RAKI, M., RANKI, T., HAKKARAINEN, T., and HEMMINKI, A. (2006). Noninvasive imaging for evaluation of the systemic delivery of capsid-modified adenoviruses in an orthotopic model of advanced lung cancer. Cancer **107,** 1578–1588.

SAVELKOUL, H.F., VAN OMMEN, R., VOSSEN, A.C., BREEDLAND, E.G., COFFMAN, R.L., and VAN OUDENAREN, A. (1994). Modulation of systemic cytokine levels by implantation of alginate encapsulated cells. J. Immunol. Methods **170,** 185–196.

SHAYAKHMETOV, D.M., GAGGAR, A., NI, S., LI, Z.Y., and LIEBER, A. (2005). Adenovirus binding to blood factors results in liver cell infection and hepatotoxicity. J. Virol. **79,** 7478–7491.

SHEN, B.H., BAUZON, M., and HERMISTON, T.W. (2006). The effect of hypoxia on the uptake, replication and lytic potential of group B adenovirus type 3 (Ad3) and type 11p (Ad11p). Gene Ther. **13,** 986–990.

SHERR, C.J. (1996). Cancer cell cycles. Science **274,** 1672–1677.

SIRENA, D., LILIENFELD, B., EISENHUT, M., KALIN, S., BOUCKE, K., BEERLI, R.R., VOGT, L., RUEDL, C., BACH-

MANN, M.F., GREBER, U.F., and HEMMI, S. (2004). The human membrane cofactor CD46 is a receptor for species B adenovirus serotype 3. J. Virol. **78,** 4454–4462.

STUDENY, M., MARINI, F.C., CHAMPLIN, R.E., ZOMPETTA, C., FIDLER, I.J., and ANDREEFF, M. (2002). Bone marrow-derived mesenchymal stem cells as vehicles for interferon-β delivery into tumors. Cancer Res. **62,** 3603–3608.

STUDENY, M., MARINI, F.C., DEMBINSKI, J.L., ZOMPETTA, C., CABREIRA-HANSEN, M., BEKELE, B.N., CHAMPLIN, R.E., and ANDREEFF, M. (2004). Mesenchymal stem cells: Potential precursors for tumor stroma and targeted-delivery vehicles for anticancer agents. J. Natl. Cancer Inst. **96,** 1593–1603.

SUZUKI, K., FUEYO, J., KRASNYKH, V., REYNOLDS, P.N., CURIEL, D.T., and ALEMANY, R. (2001). A conditionally replicative adenovirus with enhanced infectivity shows improved oncolytic potency. Clin. Cancer Res. **7,** 120–126.

TALENS-VISCONTI, R., BONORA, A., JOVER, R., MIRABET, V., CARBONELL, F., CASTELL, J.V., and GOMEZ-LECHON, M.J. (2006). Hepatogenic differentiation of human mesenchymal stem cells from adipose tissue in comparison with bone marrow mesenchymal stem cells. World J. Gastroenterol. **12,** 5834–5845.

TUVE, S., WANG, H., WARE, C., LIU, Y., GAGGAR, A., BERNT, K., SHAYAKHMETOV, D., LI, Z., STRAUSS, R., STONE, D., and LIEBER, A. (2006). A new group B adenovirus receptor is expressed at high levels on human stem and tumor cells. J. Virol. **80,** 12109–12120.

WU, H., SEKI, T., DMITRIEV, I., UIL, T., KASHENTSEVA, E., HAN, T., and CURIEL, D.T. (2002). Double modification of adenovirus fiber with RGD and polylysine motifs improves coxsackievirus–adenovirus receptor-independent gene transfer efficiency. Hum. Gene Ther. **13,** 1647–1653.

Address reprint requests to:
Dr. Akseli Hemminki
P.O. Box 63
University of Helsinki
00014 Helsinki, Finland

E-mail: akseli.hemminki@helsinki.fi

Received for publication March 13, 2007; accepted after revision May 27, 2007.

Published online: June 25, 2007.